2014-09-24

Terrain Assessment for High Speed Navigation of Unmanned Ground Vehicles

El-Kabbany, Ahmed

UNIVERSITY OF CALGARY

Terrain Assessment for High Speed Navigation of Unmanned Ground Vehicles

by

Ahmed El-Kabbany

A THESIS

SUBMITTED TO THE FACULTY OF GRADUATE STUDIES

IN PARTIAL FULFILMENT OF THE REQUIREMENTS FOR THE

DEGREE OF DOCTOR OF PHILOSOPHY

Mechanical and Manufacturing Engineering

CALGARY, ALBERTA

September, 2014

Abstract

This thesis proposes a novel terrain assessment technique that is based on an analytical analysis of the vehicle-terrain dynamic interaction. Two geometric characteristics of the terrain: roughness and slope, are addressed in this thesis. Based on such characteristics, two indices are developed in this thesis to assess the Unmanned Ground Vehicle's (UGV's) traversability of the terrain quantitatively: *Roughness Index* (*RI*) and *Stability Index* (*SI*). The *RI* concept is based on existing remote sensing Geophysics techniques to quantify the effect of the terrain on the UGV. As a result this thesis crosses the bridge between two different disciplines. The proposed *RI* is a function of the terrain profile and the vehicle's dynamic and geometric characteristics. A closed form expression of the maximum allowable vehicle speed as function of *RI* is developed. The proposed *SI*, on the other hand, is used to represent the vehicle's stability. In addition of the terrain profile and the vehicle's characteristics, e.g., centre of gravity and suspension, the *SI* is also a function of the vehicle state, i.e., speed and radius of turn.

The proposed approach used to determine the UGV's speed is generic enough that it can be employed in and type of ground vehicle. Two selected navigation examples, among the numerous examined, are presented to illustrate the implementation of the proposed terrain assessment technique. The first example illustrates how the proposed terrain assessment can be used to plan the speed of the vehicle while following a given path on an unknown terrain. The second example illustrates the proposed technique used by a UGV to find the optimum path to traverse on a pre-known terrain. Due to its relative simplicity the developed technique can be used in real time to navigate UGVs from point A to point B at the highest (yet safe) vehicle speed while maintaining the integrity of the vehicle. Although the proposed technique is novel and shows great consistency, this thesis concludes with many unanswered questions.

Acknowledgements

I would like to thank those who provided advice, support, or assistance throughout my degree. Of special note, I would like to thank my supervisor Dr. Alejandro Ramirez-Serrano for everything he has done to make this thesis possible. I would also like to thank my family, especially my wife May Taha, my mother Amany El-Khouly, and the memory of my father Samir El-Kabbany for their motivation, support, and patience and without whom I would have never have had completed this work.

Table of Contents

List of Tables

List of Figures and Illustrations

List of Symbols, Abbreviations and Nomenclature

Symbols	Definition
α	Terrain pitch
β	Terrain roll
Δ_i	Dimensionless displacement of the base excitation at the i^{th} wheel
$\dot{\Delta}_i$	Dimensionless velocity of the base excitation at the i^{th} wheel
δ_i	Displacement of the base excitation at the i^{th} wheel
$\dot{\delta}_i$	Velocity of the base excitation at the i^{th} wheel
ϵ_{eff}	Radial distance between the projection of CG and C_{eff}
ϵ_{st}	Radial distance between the projection of CG and the edge of the stability region
θ_{eff}	C_{eff} angular position measured from the positive X axis
θ_x	The vehicle roll
θ_y	The vehicle pitch
λ	Vehicle turn radius of curvature
ρ	Harmonic wave radius of curvature at a particular point
B	Vehicle's mass original elevation from the reference level (zero potential energy)
C_{eff}	Centre of effect of the vertical terrain reaction (R_z) on the vehicle
CG	Centre of Gravity
c_i	damping coefficient of the i^{th} resilient element
D	Vehicle dissipated energy
E	Vehicle kinetic energy

f_c	A 4x1 vector representing the vehicle centrifugal force (body force) in turns
f_s	Harmonic wave frequency in the displacement domain (s)
f_w	A 4x1 vector representing the vehicle weight (body force)
G	Gravitational acceleration
H	Vehicle CG height from the ground
H	Vehicle ground clearance
L	Vehicle wheel bas length
J_x	Vehicle mass moment of inertia about x axis
J_y	Vehicle mass moment of inertia about y axis
K	Stiffness matrix
k_i	Stiffness of the i^{th} resilient element
M	Mass matrix
M	Vehicle mass
R_x	Resultant terrain force reaction on the vehicle in the X direction
R_y	Resultant terrain force reaction on the vehicle in the Y direction
R_z	Resultant terrain force reaction on the vehicle in the Z direction
Res	The terrain sampling resolution
RI	Roughness Index
R	Wheel radius
S_x	Offset of C_{eff} from the projection of CG in the X direction
S_y	Offset of C_{eff} from the projection of CG in the Y direction
SI	Stability Index
T_1	Homogenous transformation matrix for vertical displacement

T_2	Homogenous transformation matrix for rotation about y axis
T_3	Homogenous transformation matrix for rotation about x axis
T_x	Resultant terrain moment reaction on the vehicle in the X direction
T_y	Resultant terrain moment reaction on the vehicle in the Y direction
Tz	Resultant terrain moment reaction on the vehicle in the Z direction
U	Vehicle potential energy
U	The vehicle vertical displacement
V	Vehicle speed
W	Vehicle wheel base width
$\dot{z}_i'$	The vertical velocity of the ith suspension point
z_i'	The vertical displacement of the ith suspension point
$[\acute{x}_i \quad \acute{y}_i \quad \acute{z}_i]^T$	A vector represents the final position of the ith suspension point w.r.t. the vehicle frame of reference

Acronyms

JPL	Jet Propulsion Laboratory
NASA	National Aeronautics and Space Administration
UGV	Unmanned Ground Vehicle

Chapter One: Introduction

Mobile ground robots, also referred to as autonomous or Unmanned Ground Vehicles (UGVs), are increasingly being applied in natural, i.e., unconstructed, environments for which no or very little information is a priori known about the terrain. Few examples of such applications include: search and rescue operations within disaster zones, such as earthquakes, boarder patrolling within unpaved surfaces for security purposes, and planetary exploration [1-7]. Due to numerous UGVs' advances and advantages, traditional vehicles, e.g., passenger cars, are been enhanced with UGV technologies such as automated parallel parking [1]; and highway driving [2].

Despite of their popularity, cars are severely under developed in terms of automation. While other means of transportation such as aeroplanes are almost fully automated by using advanced fly-by-wire as well as Autopilot systems, cars are still mostly human-operated equipment. Recently, technologies such as Automatic Parallel Parking have started to be incorporated in passenger cars [1]. Automating cars to travel autonomously is not just convenient, but have the potential to enable cars to be safer, avoiding human error, and more economical, e.g., more efficient fuel consumption. These same thoughts have been taken by others such as Google's CEO Eric Schmidt who in October 2010 said "your car should drive itself; It just makes sense.", [2] lamenting that cars were invented before computers. As a result, since early 2010, Google has been developing a driverless car, Figure 1.1 which is now under final evaluation for production [3]. The project's leader, Dr. Sebastian Thrun, a well-recognized name in the field of autonomous robots and a protagonist of autonomous vehicles, has elaborated on their merits that they "know speed limits, traffic patterns and road maps," and also "use video cameras, radar sensors and lasers to detect other cars, [2]. Thus, cars automation according to him makes sense.

Google's project is not the first effort on this front. It is built on many years of work in other, yet related fields, including computer vision, sensing positioning, path planning, obstacle avoidance, and more relevant to mobile robotics work.

Figure 1.1 Google driverless car, [4]**.**

When compared to traditional transportation vehicles, UGVs have reached higher levels of automation while having the possibility to be used in complex aggressive terrains, where traditional vehicles would not be used. NASA/JPL rovers landed on Mars in two separate landings, 1997 and 2004. Due to the terrain complexities, among other issues, the 1997 rover traversed short distances, a few meters, on flat, rocky terrain under close human supervision. The 2004 rover traversed longer distances through sloped, loose terrain, with some autonomous operation, but still under human control. Future rover space missions are expected to explore water-shaped geographical features and related terrain complexities where the corresponding features and effects on robots and vehicles are unknown. Although significant progress has been made, a number of problems still need to be resolved before UGV's are able to perform such and other missions at

high speeds, especially in outdoor/unknown environments. Future Mars rovers, for example, will require to traverse rough, sloped terrains with dense rock distribution and loose drift material, which current UGV's cannot traverse autonomously [10, 11]. These characteristics are also required in other applications such as search & rescue.

1.1 Challenges

UGV's ability to, autonomously, navigate an outdoor un-prepared, non-engineered, environment is greatly influenced by the terrain's geometry and physical properties [12, 13]. The general geometric terrain properties taken into account by the vehicle, or operator in a manned vehicle, include: elevation, slope, roughness, and obstacles, e.g., depressions or elevations, among others. On the other hand, some of the terrain's physical properties that determine how well a UGV moves and manoeuvres include: hardness, density and terra-mechanics, the interaction between the wheels/tracks and the ground/terrain, – traction. As a result, in order to perform effective navigation and vehicle movement, the terrain needs to be sensed prior to traversing it. In order to perceive the terrain geometric properties and be able to navigate, UGVs rely on a number of on-board sensing systems, such as cameras, sonar, range finders, and stereo imaging. However, any data collected via any sensing system contains diverse levels of uncertainty. These uncertainties come from a variety of sources such as terrain complexity and the sensors' own characteristics, including noise, sensitivity, and sensing accuracy. As a result, the obtained data must be analysed through limited on-board computational resources before path planning or any motion within the environment can be performed. After a motion decision/plan is made, the UGV's actuators, e.g., speed and steering angle, can be controlled to negotiate the environment and execute the planned mission. However, to be effective such decision must consider the physical limitations of the vehicle such as ground clearance, power, maximum speed, and suspension characteristics. Based

on these and other aspects, the UGVs' three main challenges that this thesis works with, relating to enabling UGVs to deal with outdoor terrain navigation, are:

1. Sensing system uncertainty,
2. Limited on-board computational resources, and
3. Vehicle physical properties, e.g., motors, structure, suspension, etc.

The goal of this thesis is not to attempt providing a specific solution to such challenges but rather to develop effective, real-time, tools to tackle them in order to facilitate the high speed navigation of UGVs in complex unknown rough terrains.

1.2 Thesis Objective

The goal of this thesis is to enable UGVs to navigate a given unknown terrain at high speeds while maintaining the integrity of the UGV at all times. To achieve high speed navigation, UGVs should interpret their environment fast and accurately. However, this is constrained by the available limited on-board computational resources and the information obtained from their sensors to plan their manoeuvres, based on speed and turning radius. This thesis addresses the problem of terrain assessment, not terrain classification, for high speed navigation. The goal is to use simple yet effective mechanisms to prevent extensive unnecessary computation efforts that would limit the navigation speed to classify terrains. Furthermore, this thesis proposes a novel method to quantitatively evaluate the quality of the terrain region ahead of the vehicle based on two terrain geometric characteristics: i) slope and ii) roughness. While other terrain properties (such as traction and hardness) are still important for UGV navigation, in order to ease the complexity of the problem, they are out of the scope of this work, while still having effective (fast) mechanisms that can be implemented and used successfully. The technique proposed in this thesis has the aim to be modular and flexible (capable of using a number of available mathematical tools and hardware

systems). Thus incorporating (adding/changing) other sophisticated terrain and/or vehicle characteristics in the future should not be a problem. The proposed technique (described in Section 3.3) is developed to be part of a typical UGV navigation system (i.e., not a standalone system). As a result, the approach should be able to fit within any existing and future UGV architecture. Thus, complementary navigation modules (e.g., path planning and low level speed control) will be able to use the output of the proposed terrain assessment module to achieve autonomous high speed navigation in unknown complex terrains.

The proposed technique correlates the terrain geometric properties and the vehicle's physical and locomotion characteristics to determine the vehicle's allowable maximum speed and sharpest allowable radius of turn that can be used to safely and effectively navigate the given terrain. Such approach will also enhance current path planning algorithms by using the terrain and the vehicle's characteristics to move from point "A" to point "B" in the shortest time.

In this thesis, high speed navigation refers to the UGV's speed at which the limitation is the vehicle capability, such as power or integrity, not the computational capability of the navigation system. In other words, the speed at which a vehicle can effectively navigate depends on a number of factors such as the terrain quality, the aggressiveness of the manoeuvre, the interaction effects between the vehicle and the terrain, and the vehicle's own mechanical structure and power characteristics. The interaction between these and other factors will limit the speed and motion of the UGV in a number of ways. The proposed technique takes this into consideration and reduces the needed calculation load to achieve a highly effective real-time solution. It is known that diverse terrain types and terrain configurations can have similar effects on a given vehicle. For example, grass and compacted soil can potentially have very similar effects in terms of vehicle traversability. Thus, classifying the terrain into one or another class as proposed by others [5]–[7], grass or

compacted soil, is not necessary in the proposed approach. This makes the developed methodology more effective when compared to other terrain navigation tools. The core philosophy of the proposed technique is to use as minimal as possible computations when interpreting terrain of how to navigate it, and by doing so imitate how humans operate vehicles navigating in an unstructured terrain with no prior knowledge about them. As an illustration, consider a biker navigating a cross-country trail at high speed, Figure 1.2. It is important for the biker to determine the edge of the trail, the effect of the terrain's roughness on his performance and on the bike itself, predict the upcoming turn and evaluate its curvature. Accordingly, the biker determines the appropriate bike's speed and steering angle not to mention its own body posture on the bike as it manoeuvres the terrain. On the other hand, determining the size and locations of the rocks and trees might be computationally expensive and potentially irrelevant of the path being navigated.

Figure 1.2 Typical biking trail.

1.3 Novelties

Numerous research projects have addressed the problem of terrain assessment for autonomous navigation, as will be shown in Chapter 2. In this thesis terrain is not classified as numerous approaches do. As a result, this thesis work is unique in two aspects:

1. This thesis proposes two new indices: i) a Roughness Index (*RI*), and ii) a Stability Index (*SI*), used to describe the terrain roughness and slopes, respectively. Both indices are used to determine the UGV's speed and turning radius in real time while achieving speeds and navigation schemes not achieved before.

2. This thesis proposes a novel UGV terrain assessment approach via the RI & SI indices that relays on a comprehensive understanding of the vehicle's dynamics and its correlation with the terrain geometry and vehicle state.

1.4 Thesis outline

In the next chapter, a comprehensive literature review is presented on a number of areas that are considered in this research. Such literature review is then used to highlight and justify the novelty of the proposed work. Chapter 3 presents the problem statement addressed in this work followed by its hypothesis, the definitions, assumptions, and constraints used within this work, and a brief description of the proposed approach. Chapter 3 also describes how the proposed technique considers the terrain geometry to be perceived as a 3D cloud of points which enables us to use diverse perception system, e.g., laser scanning or stereo imaging, available in the market. Based on the problem statement and proposed solution described in Chapter 3, the following chapter defines the hardware characteristics, i.e., UGV and the perception system, considered. Section 4.1 describes the general requirements of the needed perception system, e.g., resolution and scan rate. Section 4.2 presents a generic dynamic model of the UGVs that can be used to control a wide range of vehicles such as UGVs and tracked UGVs with or without an active suspension. Subsequently, Chapter 5 describes the proposed *RI* and presents corresponding experimental data. Chapter 6 provides applications and usage of the developed terrain's *RI*. Following the same architecture of Chapters 5 and 6, Chapter 7 focuses on the development and usage of the proposed *SI*. Chapter 8 integrates the proposed *RI* and *SI* into a common UGV high speed navigation architecture. This chapter illustrates the operation of the proposed approach, discusses its advantages and highlights the corresponding limitations. The application of the *RI* and the *SI* together are illustrated in real life problem. For this Chapter 8 presents two application examples: i) speed planning, and ii) path

planning where the novelty of the proposed developments are tested and highlighted. Finally, Chapter 9 summarizes the achieved contributions, provides a set of conclusions, and identifies future work in this area.

Chapter Two: Literature Review

In recent years an increasing effort and investments have been directed to the development of driving assistant systems in traditional passenger cars. Such developments include automated parallel parking [1], object identification and avoidance, and automatic distance control between cruising cars [8]. These developments have been motivated by a number of different aspects ranging from economical to having more user friendly and safer vehicles. These developments, triggered from R&D in mobile robotics, are facilitating the development of completely autonomous UGVs and using them with confidence in complex structured or unstructured environments. In addition to being a potential future personal mean of transportation, the applications of UGVs includes traversing unknown natural, unconstructed, environments/terrains for diverse missions/tasks. Examples of such applications include planetary exploration, search and rescue, patrolling borders, exploring disaster sites, e.g., floods and earthquakes, among many other possibilities. Such applications require UGVs to have a performance superior to human operated vehicles, yet autonomous. This thesis aims to provide new developments in the area of high speed UGV navigation in a priori unknown terrain based on real time unknown terrain assessment.

This chapter summarizes recent literature related to the work proposed in this thesis. It navigates and synthesizes the variety of ways researchers address the problem of terrain assessment for UGV navigation. The literature review is divided into three main sections, each covers one of the traditional ways of handling the terrain assessment problem by UGVs: i) *terrain classification*, ii) *terrain assessment*, and iii) *vehicle modeling*.

2.1 Terrain classification

The simplest terrain assessment approach has been to classify terrains into two main groups: drivable and undrivable [9]. Such classification obviously is highly dependable on the vehicle's characteristics. While a terrain can be drivable by one vehicle type it might be undrivable by another. This has not been considered to a large extent in the unmanned vehicle literature. In the literature, undrivable regions (e.g., occupied by obstacles) are terrain features such as steep slopes, ditches, diverse snow/mud densities or tall objects over which the vehicle cannot drive safely [10]. Obstacles (e.g., trees, humans, holes, and water bodies) should be detected and avoided/negotiated during navigation. Due to the complexities associated with the terrain assessment problem numerous researchers have used the simplistic drivable vs. undrivable terrain identification to traverse unknown terrains, e.g., [11]–[14]. Visual images perceived via cameras provide a considerable amount of information about the UGVs' environment (surroundings) and terrain. However, visual images are 2D mapping of a 3D environment. To detect the third dimension in visual images (i.e., depth), needed for effective terrain assessment, depth from focus technique has been used [15]. As computers advance and their computing power increases, computationally intensive terrain sensing techniques have been used. Stereo images have been used to detect obstacles [16], [17] and create high definition 3D maps of the terrain. Recently, 3D range finders have gained popularity in obstacle detection for autonomous ground vehicle navigation [18]. Due to the complexity of identifying objects and their properties, some studies have focused on detecting specific obstacles and use such information to guide robots through the environment. For example: identifying water hazards (e.g., ponds or streams) [19], and slip hazards (e.g., sandy slopes) [20] have been the main focus of many papers. Once obstacles are detected, diverse

techniques have been used to avoid/negotiate them. Some of the common approaches include potential fields [21], [22], and reactive navigation [23], [24].

Drivable terrain detection has been used to stay on a given trail, autonomously, for several hundreds of kilometres [25], [26]. However, such techniques cannot be used to autonomously determine the appropriate vehicle speed when driving across different terrains which may change constantly. As a result the vehicle speed has been traditionally pre-defined/set-by-the-user for each drivable course, route, along a pre-planned path. Such speed can be, and had been, modified when unexpected conditions arise, e.g., unforeseen obstacle detection or a priori terrain misclassification, at the expense of the interrupting the execution of the given mission. In such cases, when the vehicle is allowed to make the corresponding decision, an UGV will either act with unnecessary caution, e.g., significantly reducing its speed, or with excessive risk, e.g., providing little speed change. In either case there has not been a truly vehicle speed management system that can be used in real-time and in an effective way.

To overcome this limitation and provide effective speed management, drivable terrains have been further classified in different classes based on their nature, such as grass, sand, pavement, and gravel. A terrain type has been usually determined via image analysis and computer vision which then identifies a terrain type by a region within a segmented image or space. The set of terrain regions is further divided into disjoint subsets. From the classification point of view each subset which includes some common features, e.g., color, texture, depth, traction, is called a class [27]. Accordingly, a list of pre-defined terrain classes is used to classify a terrain region [5]–[7]. Such terrain classes provide necessary information for proper UGV navigation and pre-defined speed control. However, if the terrain at hand contains a class not included in the pre-defined list of terrain classes, the UGV fails to navigate with proper speed.

A good comparison between different terrain classification techniques is presented by M. Hebert et al. [28]. Terrain classification approaches can differ in the used sensory system, e.g., vision or multispectral LIDAR. Terrains have been typically classified/labelled as per their appearance, e.g., color and texture, via visual images [29], [30]. For night, dark, or poor visibility conditions, stereo Thermal Infra-Red (TIR) cameras have been used to perceive the terrain located in front of the vehicle [31]. When using remote sensing tools, e.g., cameras, terrain classification can fail when the required conditions for the sensor used are not met, e.g., when fog is encountered. To cope with such problems, internal vehicle sensors, e.g., vibration and traction, have been used to perceive and classify the immediate terrain traversed by the vehicle [32], [33]. More specific studies have focused on classifying a given terrain in terms of its quality, such as slippery. Such approaches are based on the vehicle's reaction to the terrain [34]. While other studies have aimed to reduce the required computational effort for terrain classifications, [35] other studies have targeted enhancing the terrain classification performance by combining terrain classification with obstacle avoidance mechanisms [36].

Despite numerous developments, current terrain classification methodologies have two main limitations: i) they require pre-knowledge of the working environment to determine a list of expected classes and the appropriate speed at which vehicles can safely traverse the corresponding class, and ii) current terrain classification approaches are computationally expensive, making them unsuitable to be used in high speed UGV navigation. This is especially true in cases of encountering new terrain classes, not included in the priori terrain class list.

2.2 Terrain assessment

To cope with the limitations of the terrain classification methodologies, a given terrain has been associated with an index representing its quality in terms of traversability. A traversability index

was introduced in 1999 by H. Seraji as a new and simple measure to identify the degree of difficulty by which mobile robots can traverse planetary surfaces [37]. This index was developed using fuzzy logic, and expressed by linguistic fuzzy sets that quantify the suitability of the terrain for traversability based on its physical properties, such as slope and roughness. In this approach, poor/excellent terrain, e.g. rocky/pavement, is associated with a low/high index value which is used to define how the given terrain should be traversed (low/high speed). Such methodology however does not consider the properties of the vehicle and thus the determined speed might only be suitable for a specific UGV. For more than a decade, many studies attempted to employ the traversability index concept in autonomous ground vehicle navigation [38]–[42]. Some studies have employed the traversability index approach on two levels: global path planning, determining the path that optimizes a combination of terrain roughness and path curvature, and local path planning, using sensory information to get around the newly discovered obstacle [43]. Although this, and other similar techniques, provide advances, two main limitations have been identified. First, assessing the terrain traversability from the vehicle's sensory data, e.g., stereo images or range finders, is very computationally expensive. As a result such approaches limit the speed at which UGVs can traverse a given terrain. The second limitation is the poor relation of the terrain traversability to the vehicle's dynamics. Some researchers have addressed this limitation by estimating the terrain parameters, e.g., roughness, hardness, and traction, based on the perceived vehicle dynamic behaviour as it traverses the given terrain [44]. Although effective, however, this gives very little room for the autonomous navigation system to plan ahead how to negotiate challenging terrains ahead of the vehicle. This is due to the fact that the vehicle has to first experience the effects of the terrain and then react accordingly. Thus, these types of approaches are reactive rather than deliberative. This drawback can be resolved by using: i) remote terrain

perception (perceive distant terrain) to have enough time assessing the terrain before traversing it, and by ii) providing, using, a reliable vehicle dynamic model. Such tool can be used to effectively determine how the vehicle will react to a given terrain.

2.3 Vehicle modeling

Modeling of UGVs has been addressed from various viewpoints and goals. Kinematics and dynamics of mobile ground robots on flat terrain have been investigated for decades, e.g., [45]–[48]. Kinematic analysis of UGVs in rough terrains has been addressed more recently from different aspects. Stability of a mobile robot moving on a rough terrain while following a pre-planned path was considered in [49]. On an actively articulated wheeled robot, displacement analysis has been presented to insure effective uneven terrain traversal [50], [51]. Kinematic analysis has also been used on sophisticated vehicles such as the one presented in [52] which manoeuvres terrain using four wheel modules, each having three degrees of freedom. Force analysis, e.g., terrain induced forces on the UGV, has also been incorporated in mobile robotics research to determine how vehicles react to a given terrain. Legged locomotion systems have also been analysed to find the appropriate force distribution to traverse uneven terrains [53], [54]. Diverse configurations of wheeled vehicles, e.g., cars, six-wheel and three-wheel, have been kinetically studied as well [55], [56].

To the best of our knowledge, very few works in the literature have considered the effect of the terrain properties on the vehicle's dynamic behaviour. On the other hand, the dynamic effect of various natural obstacles on the vehicle has been studied, e.g., [57] [58]. In such developments a combination of visual, tactile and vibration perception systems have been used to classify terrain regions [59] and predict the corresponding terrain properties [60]. Recently, classifying terrain regions, based on vibrations induced on the vehicle's structure via terramechanics principles, e.g.,

wheel-terrain interaction during driving, has gained attention [61]–[63]. Yet, in these contributions, the vehicle has not been dynamically modeled. In these contributions instead, different system identification tools have been employed, e.g., neural networks, to correlate the terrain and vehicle interaction characteristics. Furthermore, these contributions have not provided enough understanding of the relationship between the terrain properties, e.g., slope and roughness, the vehicle's properties, e.g., mass, suspension and dimensions, and the navigation state, e.g., speed, acceleration, and turning radius. This kind of knowledge is not only important and needed for navigation, but also for potentially designing and tuning a given UGV for a specific application.

2.4 Summary

This literature review covers what this thesis considers the most relevant recent efforts in terrain assessment for the purpose of UGV high speed navigation in a priori unknown rough terrains. Significant developments have been achieved in improving the UGVs' perception systems, data processing, and terrain interpretation. Research in automotive development has reached advanced levels of vehicle understanding and used in controlling the vehicle dynamics [64], [65]. However, the area of terrain assessment for UGV navigation, based on the analytical understanding of the dynamic effect of the terrain properties on the vehicle dynamics, has been practically uncovered. This thesis attempts to develop a novel approach for terrain assessment based on the dynamic interaction between the UGV and the terrain. A generic analytical model of wheeled vehicles is developed and employed in this work. The proposed terrain assessment technique utilizes less computational effort when compared to existing methodologies. , This takes into consideration the limited computational capabilities available onboard a traditional UGV. This will enable UGVs to achieve higher navigation speeds when compared to current methodologies.

Chapter Three: Problem statement

The literature review identified the following three general needs which are required to be solved before UGV' can efficiently be deployed at high speeds without human intervention:

- *Accurate high speed terrain sensing:* better and faster sensors are needed.
- *Precise terrain-robot interaction:* detailed robot behavior based on the perceived terrain is needed. Hence, better models are needed that can plan ahead instead of reacting to the current terrain.
- *Better and faster terrain assessment:* an effective terrain assessment capable of dealing with diverse complex terrains with no prior knowledge about the terrain.

From the identified general needs, this thesis addresses the problem of unknown terrain assessment for high speed UGV navigation. Thus the problem statement addressed in this thesis is described as follow:

> *"Develop terrain assessment tools that can be used in real time to enable effective and safe high speed navigation of unmanned ground vehicles in a priori unknown unstructured outdoor rough terrains through/by forecasting the UGV-terrain interaction and its effect on the vehicle dynamic behaviour".*

Based on the above problem statement the following goal is envisioned within the context of this thesis: *enable UGVs to autonomously travel at the maximum speed allowed by the terrain and the vehicle's power & physical limitations while maintaining the integrity of the vehicle at all times during the navigation process*. In other words, the time required for assessment, interpretation and

planning should not be a factor that limits the vehicle speed. For this it is assumed that no prior knowledge about the terrain or environment is available.

Development of autonomous ground vehicles has been tackled by many researchers since the early 80's [66]. Due to the fact that unmanned vehicle systems (*UGV*) is a nascent area of research, and due to the numerous complexities associated to the area, current UGVs and their associated control algorithms are not well suited to be used within unknown rough terrain environments. Due to the fact that current *UGV* are swimming in sensors and drowning in data, most of the research encountered in the literature has approached the problem from a data processing point of view. Very little work has considered the physical interaction between the vehicle and the terrain from a dynamic point of view. Vehicle/terrain dynamics have been extensively covered in other fields of research, e.g., automotive dynamics, but not applied to autonomous UGVs. This thesis proposes a novel terrain assessment technique that is based on an analytical analysis of the vehicle-terrain dynamic interaction. Due to the complexities associated with the problem at hand, and in order to ease the problem, only geometric characteristics of the terrain are addressed in this thesis. Assessing other terrain characteristic such as hardness and traction are left out of the scope of this thesis for a number of reasons including unavailable sensors capable of remotely characterizing such terrain properties precisely.

3.1 Definitions

This section defines critical terms that are used throughout this thesis. Thus, the proposed assessment technique is to be considered within the context of the following definitions.

Drivable terrain; is a terrain region that the vehicle at hand can traverse, even with very limited mobility e.g., low speed or restricted turning. Terrain drivability is a function of the characteristics

of the terrain and the vehicle. Though it is obvious, it is important to indicate that a terrain could be drivable for one particular vehicle but not for another.

Undrivable terrain; is a terrain region that cannot be traversed by a particular UGV. Undrivable terrains are considered obstacles and shall be avoided. In this thesis, only terrain geometry is considered. Accordingly, examples of undrivable terrains can be a rock or a hole on that are higher or deeper than the vehicle ground clearance.

Ground clearance; is the distance from the terrain surface under the vehicle to the bottom of the vehicle's chassis (unless otherwise indicated in the context of the thesis). Terrain points higher (from the terrain mean surface) than the ground clearance are considered obstacles and shall be avoided. By this definition in this thesis we do not consider vehicles such as tanks that can overcome obstacles greater than their ground clearance.

High speed; refers to the UGV's speed at which the limitation is not the speed of terrain interpretation. The UGV's speed should be only limited by the vehicle capabilities, e.g., power, and integrity, to negotiate the terrain. The UGV's speed is considered high in this thesis when it is physically impossible to go faster, even if a faster computer, better sensors, or even a human operator is available.

Distant terrain; is a terrain region within the perceptual range of the vehicle; though it is far enough that the vehicle needs more time to reach it (at full speed) than to assess it and plane the navigation configuration. A distant terrain for a mobile platform of a 30 Km/hour maximum speed may be not distant for a passenger car with 180 Km/hour maximum speeds.

Vehicle configuration; is the geometric and mechanical characteristics of the vehicle. This includes the number of wheels, distribution of the wheels, weight of the vehicle, centre of gravity of the vehicle, etc.

Navigation state; is the characteristics of the vehicle mobility at a particular moment. For example, the vehicle speed, steering angle, roll, pitch.

3.2 Scope

The scope of this thesis is restricted to the assessment of two terrain geometric characteristics: i) Roughness, and ii) Slope. The following restrictions apply to the scope of this thesis.

1. Only vehicles with wheeled locomotion system are considered. However, the proposed technique may be applicable to tracked vehicles by approximating tracks as a large, possibly infinite, number of small adjacent wheels. Other locomotion systems (e.g., legged) are not considered in this thesis.
2. Perception of the terrain geometry is restricted to a 3D cloud of points. Of the wide diversity of sensors that can be used to obtain this 3D point cloud, e.g., stereo cameras, LiDAR, a 3D infrared range camera was used in this thesis, as a generic sensor to obtain the required terrain data. The performance of the proposed system can be dramatically improved by incorporating more complex perception systems, such as a combination of range finder and visual cameras. Though, the used 3D infrared camera is sufficient to prove the concept and applicability of the proposed approach.

3.3 Assumptions and constraints

Due to the numerous complexities associated with the problem at hand, a set of assumptions are used. The purpose of these assumptions is to ease the problem while allowing us to develop a suitable solution. Terrain assessment for UGV navigation can be complex. The following assumptions are used to simplify the problem.

1. The terrain is infinitely hard (non-deformable). No terrain deformation is considered due to the forces transmitted from the vehicle to the terrain. Thus, wheel-terrain interaction (Terramechanics) is out of the scope of this thesis. In some scenarios this assumption can be conservative as in the case of grass terrain. The grass is perceived as a rough terrain while in reality the grass will bend, the soil might deform as the *UGV* passes on top, and potentially be perceived as a smooth terrain. On the other hand, a muddy terrain is perceived as a smooth terrain, while it may be not drivable due to its softness.
2. The traction between the terrain and the vehicle wheels is assumed to be perfect. Rolling without slipping of the wheel on the terrain is considered. While this assumption does not reflect reality, it simplifies the modeling of the vehicle dynamics and the wheel-terrain interaction.
3. Each of the vehicle's wheels assumed to be always at contact with the terrain in one and only one point. Wheel-terrain separation (wheel take off) due to the inertia of the wheel and/or resilient element (stiffness and damping) is not considered. Also, wheel-terrain contact in more than one point due to large wheel size compared the terrain features is not considered, Figure 3.1. As a result, the vehicle wheels are considered to exactly follow the terrain profile at all times. Terrains with features that are too fine for the wheel to copy (follow) are out of the scope of this thesis. This simplifies the modeling of the vehicle dynamics.
4. The vehicle can't traverse terrain regions with features higher or deeper than the vehicle ground clearance. Terrain features exceeding this limitation are considered obstacles. Obstacle avoidance is out of the scope of this thesis.

5. Vehicle dynamics are assumed linear. Nonlinearities due to large displacements and/or rotations of the vehicle body (mass) are not considered. In reality, large displacements and/or rotations are associated to large forces and moments that are to be avoided in this thesis. Accordingly, dealing with the math of nonlinear dynamic equations is not justified.
6. The terrain sensor is assumed to be perfect. That is, sensor critical aspects such as certainty and accuracy are not addressed in this context. This assumption allows us to focus on the problem at hand without having to deal with inherent sensor errors.

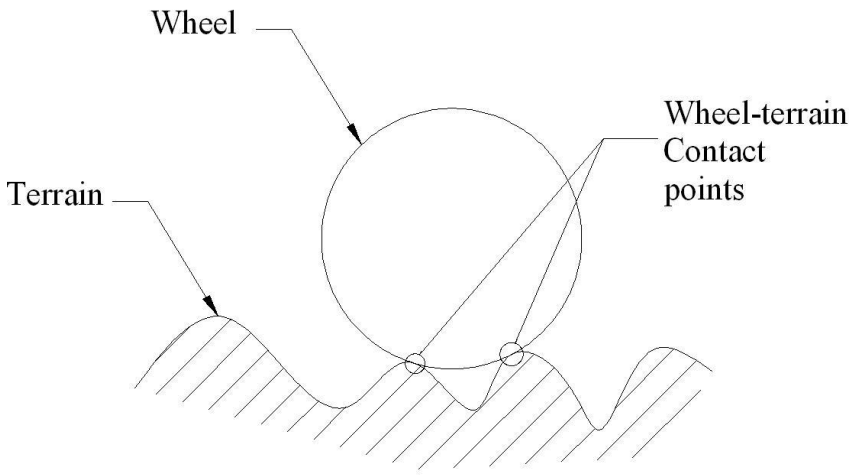

Figure 3.1 Wheel/terrain contact in more than one point

3.4 Proposed approach

Based on the problem statement and considering the studied constraints and assumptions, the proposed approach to solve the problem at hand within this thesis can be summarized in the following 3 steps.

1. Perceive the terrain as a 3D point cloud via the perception system. In this thesis, a 3D range camera is used.

2. Process the perceived data to determine the traversability of the terrain quantitatively into two indices: i) Roughness Index (*RI*) and ii) Stability Index (*SI*).
3. Based on the *RI* and *SI*, a maximum allowable vehicle speed is calculated. This value is transmitted to the navigation system to take action, i.e., determines the navigation states, toward accomplishing the mission.

A simplified block diagram of the proposed UGV onboard computational system (brain) shows the navigation system at the centre of the UGV's computational solution to be embedded in the system, Figure 3.2. The navigation system, Figure 3.2, is considered to be the decision making module. It renders the received information (that is received from the sensing system and the terrain assessment module) into a plan that is executed by the UGV controls (e.g., motors, engine, steering, active suspension, etc). The operator provides the navigation system with the destination and a set of navigation requirements (constraints) to be satisfied such as: maintaining maximum speed, rendering the shortest path, or optimizing power consumption, Figure 3.2. The terrain assessment module feeds the navigation system with information about the terrain characteristics that is vital to perform a reliable navigation processes, e.g., path planning, speed profile planning, obstacle avoidance, etc. This module represents the core work performed in this research work.

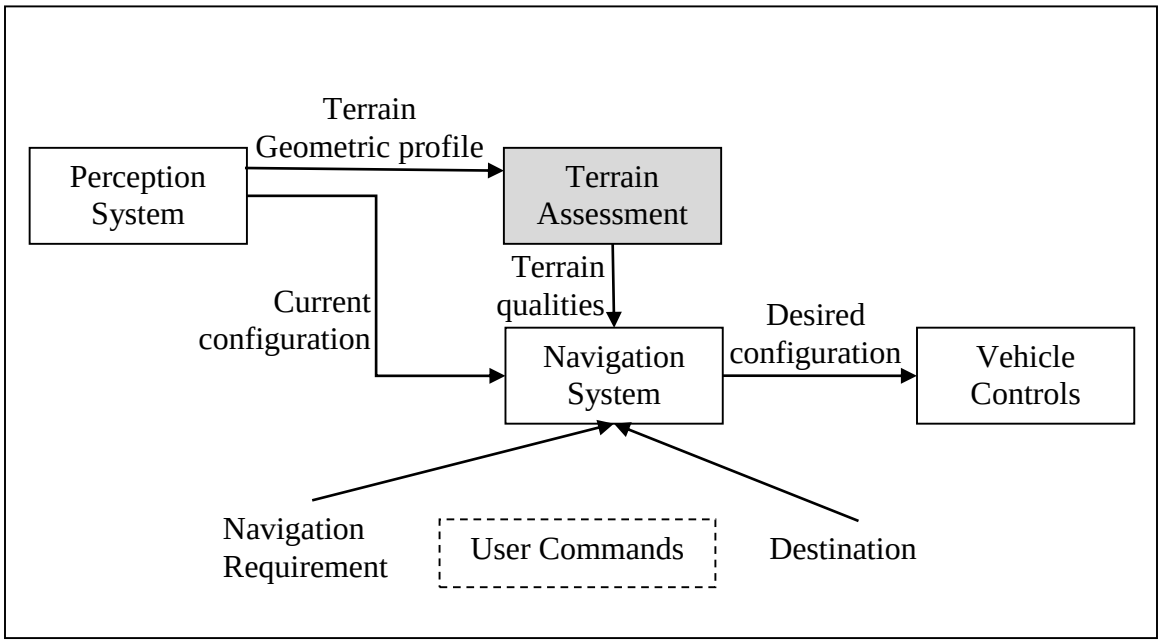

Figure 3.2 Proposed UGV's data processing architecture

The terrain assessment module, receives raw data representing the terrain geometric profile from the available perception system. The task of this module is to interpret the terrain data and provide usable information about the terrain qualities, to the navigation system which is turn will compute the UGV control decisions, Figure 3.2. For example, the terrain assessment module that adopt classification algorithms assesses the terrain traversability and pass this information to the navigation system. The navigation system decides if this terrain is traversable and also which is the appropriate navigation state to traverse the terrain. The proposed terrain assessment technique in this thesis adopts and extends the traversability index method proposed in [37]. A schematic illustration of the proposed terrain assessment is shown in Figure 3.3.

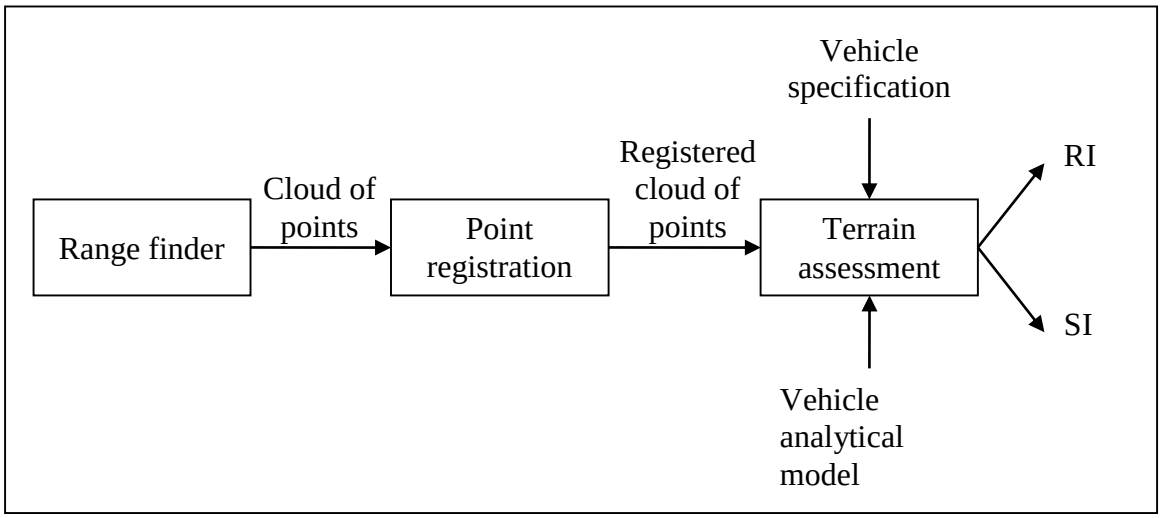

Figure 3.3 Proposed terrain assessment module

The proposed technique implements a range finder that is capable of providing a 3D cloud of points that represents the terrain geometric profile, Figure 3.3. The first step to interpret this data is to register the cloud of points into the vehicle frame of reference, i.e., to transform the point coordinate to the vehicle's frame of reference. The proposed terrain assessment uses this cloud of point along with the information available about the vehicle, e.g., vehicle specification, and vehicle dynamic model, to produce two indices: i) Roughness index *(RI*) and ii) Stability Index (*SI*), Figure 3.3. *RI* is used to represent the geometric unevenness of the terrain while *SI* is used to identify the possibility of the vehicle to flip over due to the terrain slopes in the vehicle's roll and pitch directions. The proposed *RI* and *SI* have the following three characteristics.

1. Each index is described via a number between 0 and 1, where 0 indicates a very poor terrain and 1 indicates an ideal drivability terrain, in terms of the corresponding index, i.e., Roughness or Stability.
2. The values of *RI* and *SI* are independent of each other and dependent only on the specific/corresponding terrain characteristics. In other words, one index can be 1 and the

other can be 0. For example, consider a perfectly smooth terrain (resembling a sheet of glass) which is inclined at 90 degrees. This terrain will be given a *RI* of 1 and a *SI* of 0, i.e., impossible to traverse. A terrain having a *RI* and a *SI* equal to 1 will be used to represent a flat and horizontal terrain, i.e., highly traversable; while a terrain having *RI* and a *SI* equal to 0 will be used to represent an extremely rough terrain having steep slopes (i.e., impossible to traverse).

3. Both indices are not a characteristic of the terrain region only. In contrast, each index correlates terrain and vehicle characteristics. For example, a terrain region that is considered rough for a low ground clearance sport vehicle could be consider smooth for an SUV.

Chapter Four: Unmanned ground vehicle

UGV is a vehicle that operates autonomously, i.e., with no human interaction, while in contact with the ground. Unlike other mobile robots, e.g., aerial, surface, and underwater, terrain assessment is a key challenge for navigation to UGV's. There are two classes of UGV's: i) teleoperated, and ii) autonomous. This thesis addresses the problem of terrain assessment which is applicable to both classes of UGVs. Just like any feedback loop control system, the UGV system consists of three main components, Figure 4.1.

1. Control system, plant.
2. Controller.
3. Perception system, i.e., sensor.

For a typical UGV, the vehicle is the control plant which consists of the following five components, Figure 4.1:

1. Mechanical structure, e.g., frame and suspension.
2. Power train, e.g., motors, engine, and gear box.
3. Power source, e.g., batteries, fuel tank, solar cells, etc.
4. Actuators, e.g., accelerator pedal, speed controller, steering controller, etc.
5. Perception system, e.g., sensors, cameras, range finders, IMU, accelerometers, GPS, etc.

The perception system, i.e., sensory system, collects data from the environment. The measured data is transmitted to the controller which acts as the brain of the UGV. The UGVs' controllers widely vary depending on the complexity of the vehicle, the considered environment, and the task to be performed by the UGV. Typical UGVs' controller consists of diverse modules each of which does a specific function such as:

1. terrain assessment,

2. navigation,
3. positioning,
4. obstacle avoidance, and
5. power management.

The controller transmits commands, e.g., change speed, steering angle, etc, to the vehicle, i.e., system, to execute them. As the vehicle progresses in the environment, this cycle runs as a closed loop control system.

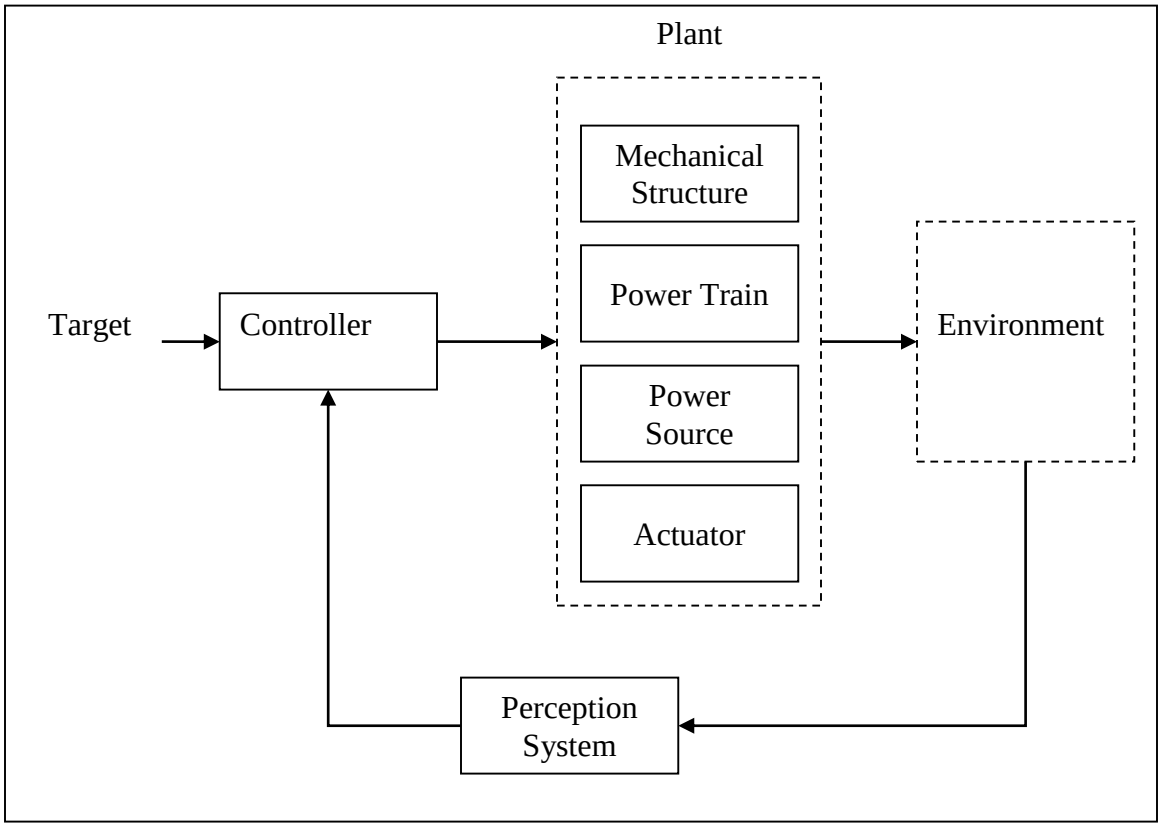

Figure 4.1 UGV's system components

Before describing the proposed solution to the problem at hand the following section, Section 4.1, addresses the required specifications of the UGVs' perception system by the proposed terrain assessment approach. Subsequently, Section 4.2, presents a generic dynamic model of the vehicle

platform. This model will be used in the next chapters to correlate the terrain roughness and the vehicle speed.

4.1 Perception System

This thesis considers UGVs as a one rigid mass connected to a moving base, i.e. wheels, via a number of resilient elements each represented as a spring-damper system. As the vehicle moves, each wheel might move vertically with respect to the UGV's frame of reference, coping with the corresponding terrain profile. The motion of each wheel, generated due to the terrain profile, is considered as an independent, from other wheels, random base excitation transmitted to the vehicle's mass, as illustrated in Figure 4.2. The wheels' random motion, copied from the terrain profile, is a function of the vehicle's horizontal travel, in the x direction, Figure 4.2.

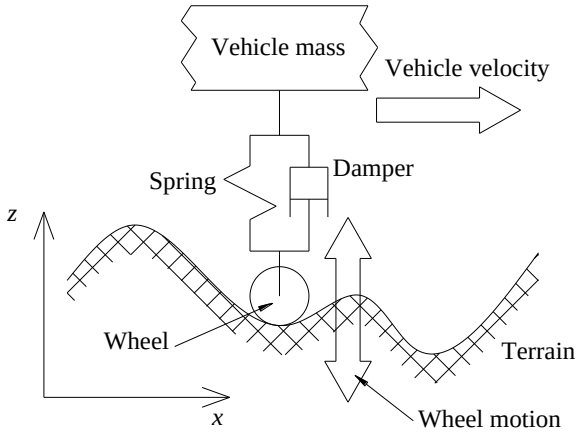

Figure 4.2 Vehicle's wheel subjected to a base excitation

To simplify the modeling, the random terrain profile is considered to consist of equal amplitude harmonic components over an infinite frequency span, white noise. This is in agreement with the described assumptions in Section 3.3. Due to wheel-terrain geometry, the wheel can't follow sharp features, high frequency terrain components, where the wheel cannot fit, thus, high frequency components of the terrain can be neglected due to the wheel-terrain geometry. Figure 4.3 illustrates

a vehicle wheel traversing a harmonic terrain profile. This schematic shows a critical point, described as the valley of the sinusoidal wave, at which the wheel can potentially contact the terrain at more than one point.

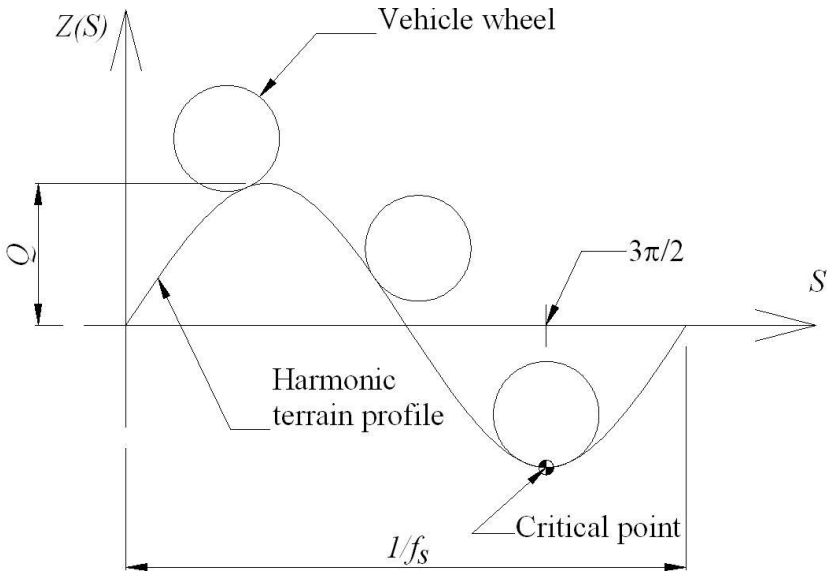

Figure 4.3 Wheel terrain interaction

In agreement with Assumptions No. 3, Section 3.3, the radius of curvature of the terrain profile at the critical point ($\frac{3\pi}{2}$), according to Figure 4.3, must be greater than or equal to the wheel radius (r). Herein, the terrain's critical point is defined as the point of the harmonic terrain profile at which the function is minimal. If this assumption is not satisfied, the wheel will contact the terrain in 2 or more points of its wheel perimeter. Mathematically, the radius of curvature (ρ) of a harmonic terrain profile at the critical point is given by Equation (4.1),

$$\rho = \frac{1}{4\pi^2 f_s^2 Q} \tag{4.1}$$

where f_s is the harmonic terrain frequency in the wheel displacement domain (s).

Accordingly, the maximum considered wheel frequency is given by Equation (4.2),

$$f_s = \sqrt{\frac{1}{4\pi^2 Qr}} \quad (4.2).$$

Frequencies higher than f_s do not satisfy Assumptions 3. In real life, the UGV's wheel motion will not exactly copy the terrain geometry. To visualize this, Figure 4.4 shows how a hypothetical wheel responds to the high frequency terrain's harmonic components. In this example the motion of the wheel will almost indicate driving on flat terrain. In other words, the UGV's wheel will act as a low pass filter, filtering out high frequency terrain components. As a result, in this thesis the effects of terrain's high frequency components, higher than f_s, on the vehicle are neglected. According to Assumption No. 4, Section 3.3, points greater than the vehicle's ground clearance (h) are not considered in this analysis as well. As a result, the maximum terrain amplitude (Q), Figure 4.3, is considered to be equal to h. To simplify the math, the wheel radius (r) is taken to be equal to h. In a typical off road vehicle the ground clearance (h) is typically greater than the wheel radius (r). However, the wheel assembly mounts the wheel from the centre. Accordingly, any terrain point higher than the r can hit the wheel assembly and shall be considered an obstacle. Based on the above considerations the maximum terrain frequency is obtained by Equation (4.3),

$$f_s = \frac{1}{2\pi h} \quad (4.3).$$

Accordingly, the terrain profile is considered as a band limited random variable where the maximum required terrain sampling resolution is $2f_s$, in one dimension, to avoid aliasing. The terrain sampling resolution in two dimensions (*Res*) can then be obtained by Equation (4.4),

$$Res = 4f_s^2 = \left(\frac{1}{\pi h}\right)^2 points/unit\ area \quad (4.4).$$

According to Equation (4.4) a vehicle with a wheel diameter of 20cm, the same as the vehicle ground clearance, requires a terrain sampling resolution of 11 points/m^2 in order to assess the

terrain effectively. This is an important derivation obtained in this thesis, which will influence how fast a vehicle can navigate while effectively perceiving the terrain. A higher resolution, for this particular vehicle, would be redundant and would unnecessarily increase the computational load. On the other hand, a lower resolution will prevent obtaining enough information about the terrain to be effective in computing the forces transmitted to the vehicle.

The effect of the vehicle speed on the acquired terrain points is ignored. The terrain region to be assessed is assumed to be scanned instantaneously, as in stop-and-scan. According to the sensing system, considering the effect of the vehicle speed may be vital for the terrain 3D image quality.

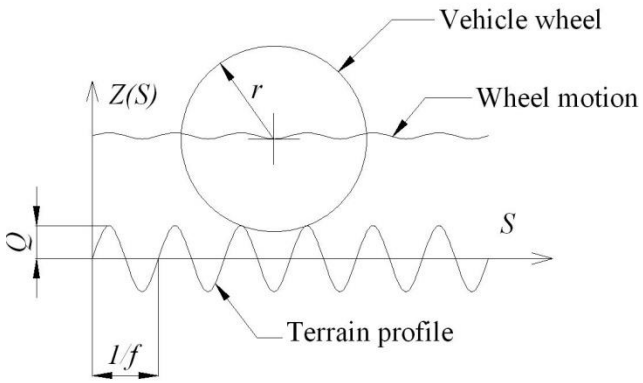

Figure 4.4 Vehicle's wheel does not copy terrain's high frequency harmonic components

4.2 Vehicle Modeling and Transmitted Forces

A corner stone in this thesis is correlating the terrain features to the dynamic behavior of the vehicle analytically. Modeling a wheeled vehicle with independent resilient elements is a classic dynamic system modeling problem [67]. While it is not a novel contribution, this thesis presents a derivation of a simplified wheeled vehicle model. The purpose of this simple model is to allow us to focus on proving the concept of the proposed terrain assessment technique. More sophisticated models can be employed from the literature in real world applications.

This thesis considers UGVs as a three-degrees-of-freedom dynamic system: i) vertical translation, ii) roll, and iii) pitch. The vehicle's frame, i.e., chasis, is considered perfectly rigid and supported by an arbitrary suspension system at N points, wheels. Each suspension point, originally located at $[x_i \quad y_i \quad z_i]^T$ for $i = 1$ to N w.r.t. the vehicle's frame of reference, consists of a resilient element, i.e., spring and damper, and a wheel, Figure 4.5. The vehicle's mass is also considered to have three degrees of freedom (up/down, roll and pitch) and considered to have no yaw movement, Figure 4.6. The reason for this is that the location of the UGV's centre of gravity (CG) coincides with the vehicle frame of reference. As a generalization, the locations of the suspension points are arbitrary. Thus, the developed equations are generic and can be employed on any wheeled vehicle, e.g., unicycles, ATVs, etc.

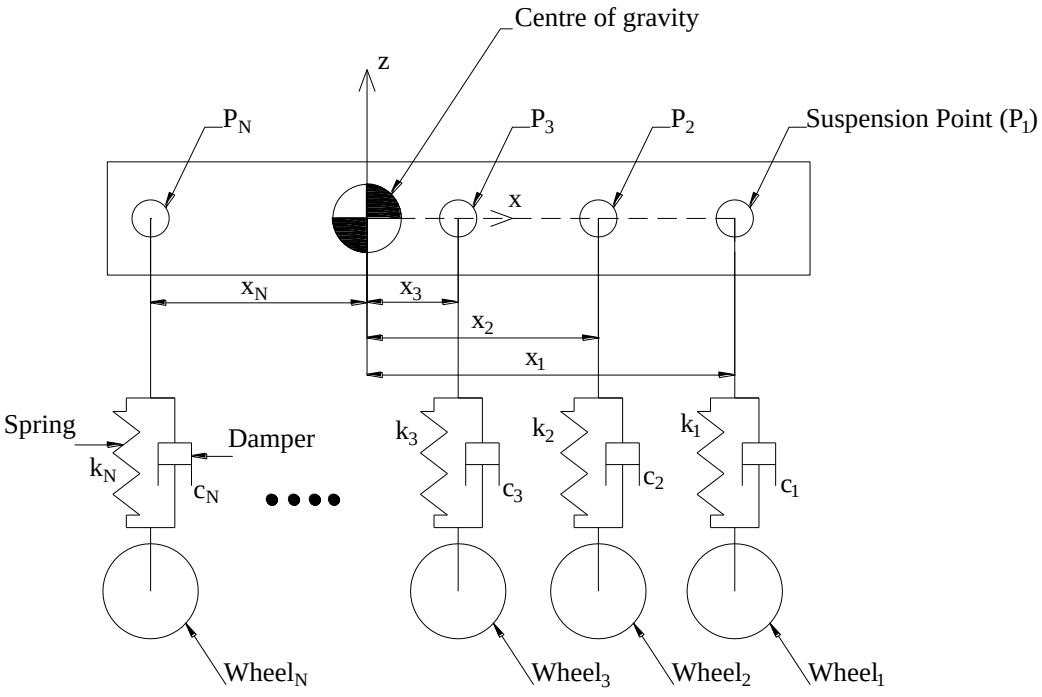

Figure 4.5 Vehicle's mass supported by multi-wheels

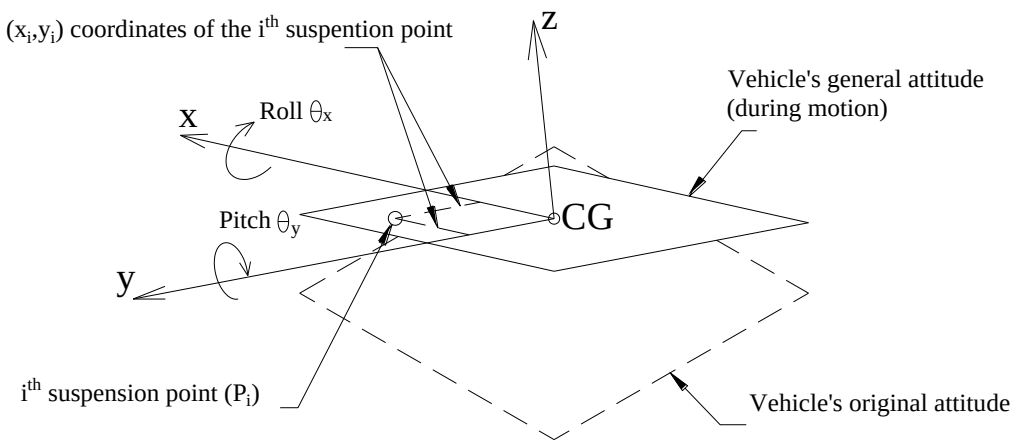

Figure 4.6 Vehicle's frame of reference at general orientation

In this thesis, a Cartesian vehicle's frame of reference is used. The frame of reference is originated at the vehicle centre of gravity (CG), where *z* is vertical, *x* is to the front and *y* is perpendicular to booth, Figure 4.5. In order to reach any attitude in the 3D space, i.e., position & orientation, the vehicle is considered to undergo the following series of successive movements w.r.t. its frame of reference: i) vertical translation in the *z* direction (u), ii) rotation about the *y* axis (θ_y: pitch), and iii) rotation about the *x* axis (θ_x: roll). Figure 4.6 shows a schematic diagram of the vehicle's frame in the original and final attitudes, after undergoing u, θ_y and θ_x movements. Herein, homogenous transformation matrices are used to determine the final position of the i^{th} suspension point (p_i)

$[x_i' \quad y_i' \quad z_i']^T$, which is needed to obtain the potential and the dissipated energy at the resilient elements. Equation (4.5),

$$T_1 = \begin{bmatrix} 1 & 0 & 0 & 0 \\ 0 & 1 & 0 & 0 \\ 0 & 0 & 1 & u \\ 0 & 0 & 0 & 1 \end{bmatrix}, T_2 = \begin{bmatrix} \cos\theta_y & 0 & sin\theta_y & 0 \\ 0 & 1 & 0 & 0 \\ -sin\theta_y & 0 & cos\theta_y & 0 \\ 0 & 0 & 0 & 1 \end{bmatrix}, and\ T_3 = \begin{bmatrix} 1 & 0 & 0 & 0 \\ 0 & cos\theta_x & -sin\theta_x & 0 \\ 0 & sin\theta_x & cos\theta_x & 0 \\ 0 & 0 & 0 & 1 \end{bmatrix} \quad (4.5),$$

shows the transformation matrices of the successive movements, T_1 (vertical displacement), T_2 (pitch), and T_3 (roll), respectively. To obtain the final transformation matrix T, the individual transformation matrices are multiplied as shown in Equation (4.6),

$$T = T_3T_2T_1 = \begin{bmatrix} cos\theta_y & 0 & sin\theta_y & usin\theta_y \\ sin\theta_x sin\theta_y & cos\theta_x & -sin\theta_x cos\theta_y & -usin\theta_x cos\theta_y \\ -cos\theta_x sin\theta_y & sin\theta_x & cos\theta_x cos\theta_y & ucos\theta_x cos\theta_y \\ 0 & 0 & 0 & 1 \end{bmatrix} \quad (4.6).$$

As a result, the final position of p_i is obtained by Equation (4.7),

$$[x_i' \quad y_i' \quad z_i' \quad 1]^T = T[x_i \quad y_i \quad z_i \quad 1]^T \quad (4.7).$$

The vertical displacement and velocity of p_i are z_i' and $\dot{z}_i'$ are obtained by Equations (4.8),

$$z_i' = -x_i cos\theta_x sin\theta_y + y_i sin\theta_x + ucos\theta_x cos\theta_y \quad (4.8),$$

and (4.9),

$$\dot{z}_i' = x_i\dot{\theta}_x sin\theta_x sin\theta_y - x_i\dot{\theta}_y cos\theta_x cos\theta_y + y_i\dot{\theta}_x cos\theta_x + \dot{u}cos\theta_x cos\theta_y - u\dot{\theta}_x sin\theta_x cos\theta_y - u\dot{\theta}_y cos\theta_x sin\theta_y \quad (4.9).$$

Once the position and velocity of every suspension point is obtained, Lagrange's equation of motion is used to develop the equations of motion of the generic UGV [68], as shown in the rest

of this section. Using the traditional symbols in what follows, the Kinetic (*E*), Potential (*U*), and Dissipating (*D*) energies are shown in Equations (4.10), (4.11), and (4.12), respectively;

$$E = \frac{1}{2}m\dot{u}^2 + \frac{1}{2}J_x\dot{\theta}_x^2 + \frac{1}{2}J_y\dot{\theta}_y^2 \tag{4.10}$$

where: m, J_x, and J_y are the vehicle's mass and the mass moment of inertias about both the x and y axis, respectively.

$$U = mg(b+u) + \frac{1}{2}\sum_{i=1}^{N} k_i(z_i' - \delta_i - \delta_{si})^2 \tag{4.11}$$

where b is the vehicle's mass original (CG) elevation from the reference level (at static equilibrium position), k_i is the stiffness of the i^{th} resilient element, δ_i is the base excitation displacement, due to terrain profile, at the i^{th} wheel, and δ_{si} is the static deflection of the i^{th} resilient element,

$$D = \frac{1}{2}\sum_{i=1}^{N} c_i\left(\dot{z}_i' - \dot{\delta}_i\right)^2 \tag{4.12}$$

where c_i is the damping coefficient of the i^{th} resilient element, and $\dot{\delta}_i$ is the velocity of the base excitation at the i^{th} wheel.

The UGV system has three equations of motion; Equations (4.13), (4.14), and (4.15),

$$m\ddot{u} + \sum_{i=1}^{N} c_i(\dot{z}_i' - \dot{\delta}_i)cos\theta_x cos\theta_y + mg + \sum_{i=1}^{N} k_i(z_i' - \delta_i - \delta_{si})cos\theta_x cos\theta_y = 0 \tag{4.13},$$

$$J_x\ddot{\theta}_x + \sum_{i=1}^{N} c_i\left(\dot{z}_i' - \dot{\delta}_i\right)(x_i sin\theta_x sin\theta_y + y_i cos\theta_x - u\, sin\theta_x cos\theta_y)$$

$$+ \sum_{i=1}^{N} k_i(z_i' - \delta_i - \delta_{si})\left(x_i sin\theta_x sin\theta_y + y_i cos\theta_x\right. \quad (4.14), \text{ and}$$

$$\left. - u\, sin\theta_x cos\theta_y\right) = 0$$

$$J_y\ddot{\theta}_y + \sum_{i=1}^{N} c_i\left(\dot{z}_i' - \dot{\delta}_i\right)(-x_i cos\theta_x cos\theta_y - u\, cos\theta_x sin\theta_y)$$

$$+ \sum_{i=1}^{N} k_i(z_i' - \delta_i - \delta_{si})\left(-x_i cos\theta_x cos\theta_y - u\, cos\theta_x sin\theta_y\right) \quad (4.15)$$

$$= 0$$

respectively.

As observed, the resulting UGV's equations of motion are nonlinear. For the sake of simplicity, this work considers small roll and pitch angles ($sin\theta_j = \theta_j$, and $cos\theta_j = cos\theta_j = 1$ where j = x and y) allowing us to linearize the equations while neglecting nonlinear terms. Considering Assumption 5 in Section 3.3, some terms cancel. The resulting linearized dynamic model is shown in Equation (4.16) in matrix form,

$$\begin{bmatrix} m & 0 & 0 \\ 0 & J_x & 0 \\ 0 & 0 & J_y \end{bmatrix}\begin{bmatrix} \ddot{u} \\ \ddot{\theta}_x \\ \ddot{\theta}_y \end{bmatrix} + \begin{bmatrix} \Sigma c_i & \Sigma c_i y_i & -\Sigma c_i x_i \\ \Sigma c_i y_i & \Sigma c_i y_i^2 & -\Sigma c_i x_i y_i \\ -\Sigma c_i x_i & -\Sigma c_i x_i y_i & \Sigma c_i x_i^2 \end{bmatrix}\begin{bmatrix} \dot{u} \\ \dot{\theta}_x \\ \dot{\theta}_y \end{bmatrix}$$

$$+ \begin{bmatrix} \Sigma k_i & \Sigma k_i y_i & -\Sigma k_i x_i \\ \Sigma k_i y_i & \Sigma k_i y_i^2 & -\Sigma k_i x_i y_i \\ -\Sigma k_i x_i & -\Sigma k_i x_i y_i & \Sigma k_i x_i^2 \end{bmatrix}\begin{bmatrix} u \\ \theta_x \\ \theta_y \end{bmatrix}$$

$$= \begin{bmatrix} c_1 & c_2 & \cdots & c_N \\ c_1 y_1 & c_2 y_2 & \cdots & c_N y_N \\ -c_1 x_1 & -c_2 x_2 & \cdots & -c_N x_N \end{bmatrix}\begin{bmatrix} \dot{\delta}_1 \\ \dot{\delta}_2 \\ \vdots \\ \dot{\delta}_N \end{bmatrix} \qquad (4.16).$$

$$+ \begin{bmatrix} k_1 & k_2 & \cdots & k_N \\ k_1 y_1 & k_2 y_2 & \cdots & k_N y_N \\ -k_1 x_1 & -k_2 x_2 & \cdots & -k_N x_N \end{bmatrix}\begin{bmatrix} \delta_1 \\ \delta_2 \\ \vdots \\ \delta_N \end{bmatrix}$$

Equation (4.16) is an equation of motion of a multi degrees of freedom system at which the system's inertia, stiffness, and damping are represented in matrices. The following chapters deal with the base excitation applied to the system, i.e., right hand side of Equation (4.16), which is shown in Equation (4.17),

$$\hat{f}_{3\times 1} = [c_e]_{3\times N}\hat{\dot{\delta}}_{N\times 1} + [k_e]_{3\times N}\hat{\delta}_{N\times 1} \qquad (4.17),$$

where $[c_e] = \begin{bmatrix} c_1 & c_2 & \cdots & c_N \\ c_1 y_1 & c_2 y_2 & \cdots & c_N y_N \\ -c_1 x_1 & -c_2 x_2 & \cdots & -c_N x_N \end{bmatrix}$, $[k_e] = \begin{bmatrix} k_1 & k_2 & \cdots & k_N \\ k_1 y_1 & k_2 y_2 & \cdots & k_N y_N \\ -k_1 x_1 & -k_2 x_2 & \cdots & -k_N x_N \end{bmatrix}$, $\hat{\dot{\delta}} = \begin{bmatrix} \dot{\delta}_1 \\ \dot{\delta}_2 \\ \vdots \\ \dot{\delta}_N \end{bmatrix}$, and $\hat{\delta} = \begin{bmatrix} \delta_1 \\ \delta_2 \\ \vdots \\ \delta_N \end{bmatrix}$.

The dynamic model, Equation (4.16), provides other important information about the vehicle: Eigen values, i.e., natural frequencies, and Eigen vectors, i.e., mode shapes. An Eigen value problem is not directly employed in the work associated to this thesis. However, it is an essential piece of knowledge when dealing with any dynamic system to understand its behaviour. From Equation (4.16), the mass and stiffness matrices (*M* and *K* respectively) are obtained. The Eigen value problem is shown in the following equations,

$$M = \begin{bmatrix} m & 0 & 0 \\ 0 & J_x & 0 \\ 0 & 0 & J_y \end{bmatrix} and\ K = \begin{bmatrix} \Sigma k_i & \Sigma k_i y_i & -\Sigma k_i x_i \\ \Sigma k_i y_i & \Sigma k_i y_i^2 & -\Sigma k_i x_i y_i \\ -\Sigma k_i x_i & -\Sigma k_i x_i y_i & \Sigma k_i x_i^2 \end{bmatrix} \quad (4.18) \text{ and}$$

$$\det(A_{3\times3} - \lambda_{3\times3} I_{3\times3}) = 0 \quad (4.19),$$

where $A = M^{-1}K$, I is an identity matrix, and λ is a diagonal matrix with the Eigen values on the diagonal.

In what follows, the Argo vehicle, a 6-wheeled all terrain amphibious vehicle, is considered, Figure 4.7, as a numerical example to illustrate the Eigen value problem calculation. The vehicle specifications are shown in Table 4.1. Some Argo specifications were obtained from the manufacturer, i.e., dimensions, ground clearance, and mass, while the rest of the specifications are measured in the lab, i.e., stiffness and damping, due to the difficulty obtaining them. It has also been assumed that the Argo's CG is at the geometric centre of the vehicle and that the wheel are distributed symmetrically about the x and y axis. Accordingly, the Argo has three natural frequencies: 2.1, 29.3, and 44 rad/second, respectively. The associated mode shapes (Eigen vectors) are: pure vertical, pure pitch, and pure roll oscillations, respectively.

Table 4.1 Argo vehicle specifications

Vehicle Dimensions (L X W X H)	1455 mm X 1473 mm X 1016 mm
Mass (*m*)	700 Kg
Ground clearance (*h*)	240 mm
Suspension stiffness	250 N/m
Suspension damping coefficient	300 N.s/m

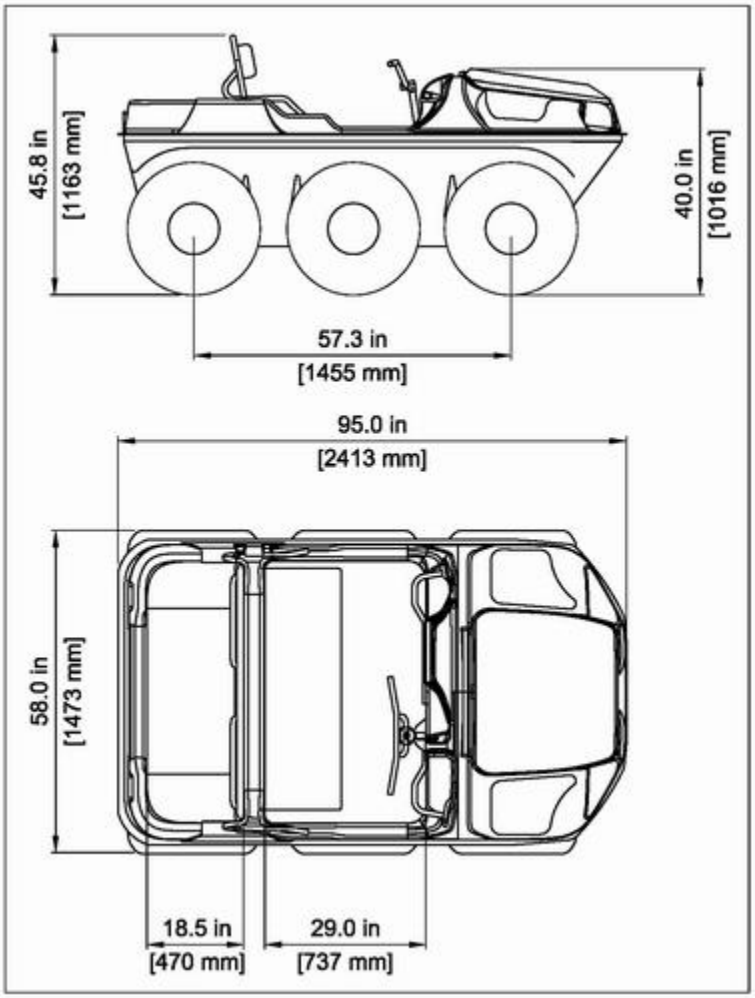

Figure 4.7 Argo vehicle is considered as a numerical example

4.3 Summary

In this chapter two basic topics have been addressed: the perception system and the vehicle's dynamic model. Specifying the perception system minimum requirements for collecting the required information about the terrain geometry is a key issue. It is desirable to reduce the amount of data to be processed in order to reduce the online computations. In the first section of this chapter a minimum terrain sampling resolution has been driven. A higher resolution is redundant and unnecessarily increases the computational load. On the other hand, a lower resolution is insufficient for an effective navigation.

In the second section of this chapter, a simplified generic dynamic model of the vehicle has been presented. From the system's equation of motion, the amount of transmitted forces to the vehicle's structure has been obtained, right hand side of Equation (4.15). In the next chapters, these forces are correlated to the terrain roughness and the vehicle speed. The vehicle dynamic model was used to calculate the vehicle's Eigen values (natural frequency) and Eigen vectors (mode shapes). While this information is not used in the rest of the thesis, it helps in understanding the dynamic behaviour of the vehicle system.

Chapter Five: Roughness index (*RI*)

Inspired by geophysics techniques, [69], this thesis proposes a novel index to represent the terrain roughness, the Roughness Index (*RI*). The proposed *RI* is a function of: i) the terrain geometry, and ii) the vehicle characteristics. The used UGV characteristic is the vehicle ground clearance h. The next chapter illustrate how to incorporate and use the vehicle dynamic properties; e.g., stiffness, damping, and the RI; in order to calculate the vehicle maximum allowable speed. For example, a certain terrain could be too rough for a small vehicle, with small ground clearance, while fairly smooth for another vehicle, large SUV. The *RI* is a number in the range of [0,1], where *RI=0* corresponds to the roughest perceived terrain, e.g., rocky terrain which is impossible to be traversed by a particular vehicle, and *RI=1* corresponds to the smoothest perceived surface, e.g., like a sheet of glass. While this definition of the *RI* may not seem obviously intuitive, it facilitates the derivation of equation as shown in the rest of the thesis. For the determination of *RI*, two main assumptions are highlighted:

1. The terrain under consideration has zero mean slope and height, and
2. The vehicle can't traverse areas of elevation (i.e., deviation from terrain mean surface) greater than the vehicle's ground clearance (Assumptions 4 in Section 3.3).

5.1 Derivation of *RI*

In this thesis the terrain is perceived as a set of three dimensional points in space where each point is a 3D vector $[x \quad y \quad e]^T$, representing the point position in a 3D Cartesian space, w.r.t. the vehicle's frame of reference. The proposed technique to obtain the terrain roughness utilizes only the elevation component (e) which minimizes the required memory and associated computation needed to assess the terrain. All elevation components obtained for a given terrain region (i.e., area) are gathered in one vector $\hat{e}$. In order to generalize the analysis in a dimension-less format,

the vector $\hat{e}$ is normalized w.r.t. h. For this, the standard deviation, σ, of the resulting vector is used and calculated using Equation (5.1),

$$\sigma = STD(\frac{\hat{e}}{h}) \quad (5.1).$$

Based on assumptions No. 4 in Section 3.3, the elevation component of vector $\hat{e}$ elements is limited to $\pm 0.5h$,. Thus, σ ranges from zero, a perfectly smooth terrain, to 0.5. The upper limit of σ, i.e., 0.5, corresponds to the roughest possible terrain for a particular vehicle, having ground clearance h. For the sake of demonstration, we consider a linear relationship between *RI* and σ. Accordingly, the normalized value for *RI* can be obtained using Equation (5.2),

$$RI = 1 - 2\sigma \quad (5.2)$$

As a result the *RI* values in Equation (5.2) range between 0, corresponding to $\sigma=0.5$, and 1, corresponding to $\sigma=0$. It is worth noting that more complex definitions of *RI*, correlation between *RI* and σ, could be used, e.g. polynomial, exponential, for different terrain roughness representations, if needed. As the real terrain elevation component might not be limited to the vehicle's ground clearance, σ can exceed 0.5. In such cases, the value of *RI* will be negative. Negative value of *RI*, below "0" (zero) represents the threshold to run an obstacle avoidance algorithm, which is out of the scope of this thesis. In this thesis, $RI=0$ corresponds to a terrain regions that can't be traversed. Accordingly, when negative *RI* occurs, it is saturated at 0.

5.2 RI Calculation Example

To illustrate the application of the proposed *RI*, 3D scans of several terrain types, using a 3D camera were acquired. The used camera is SR4000 3D camera from MESA Imaging, Figure 5.1a. The camera works based on the "time of fly" concept. It determines the distance to an object by measuring the time taken by an infrared pulse to travel from the camera to the object andback to

the camera. The camera has a detection range of 0.1-5.0 meters and an absolute accuracy of +/- 10mm. As a result, the terrain is perceived as a cloud of points in a spherical coordinate system having its origin at the camera's current focal point, which moves as the vehicle moves. In the proposed approach the terrain points are then transformed to the vehicle's Cartesian frame of reference, which is labelled with the subscript *v* in Figure 5.1b. The homogenous transformation matrix used for this purpose is shown in Equation (5.3),

$$T = \begin{bmatrix} 0 & -1 & 0 & 0 \\ cos(\Theta + 90) & 0 & -sin(\Theta + 90) & -Hsin(\Theta + 90) \\ sin(\Theta + 90) & 0 & cos(\Theta + 90) & Hcos(\Theta + 90) \\ 0 & 0 & 0 & 1 \end{bmatrix} \quad (5.3),$$

where Θ is the camera tilt angle and H is the height of the camera from the vehicle's frame of reference origin as illustrated in Figure 5.1b.

Herein the vehicle centre of gravity (*CG*) is considered its frame of reference origin. The transformation from the camera to the vehicle frame of reference is done as per Equation (5.4),

$$P_t = TP_c \quad (5.4),$$

where *Pt* is the 3D point representation in the terrain frame of reference, and *Pc* is the point representation in the camera frame of reference.

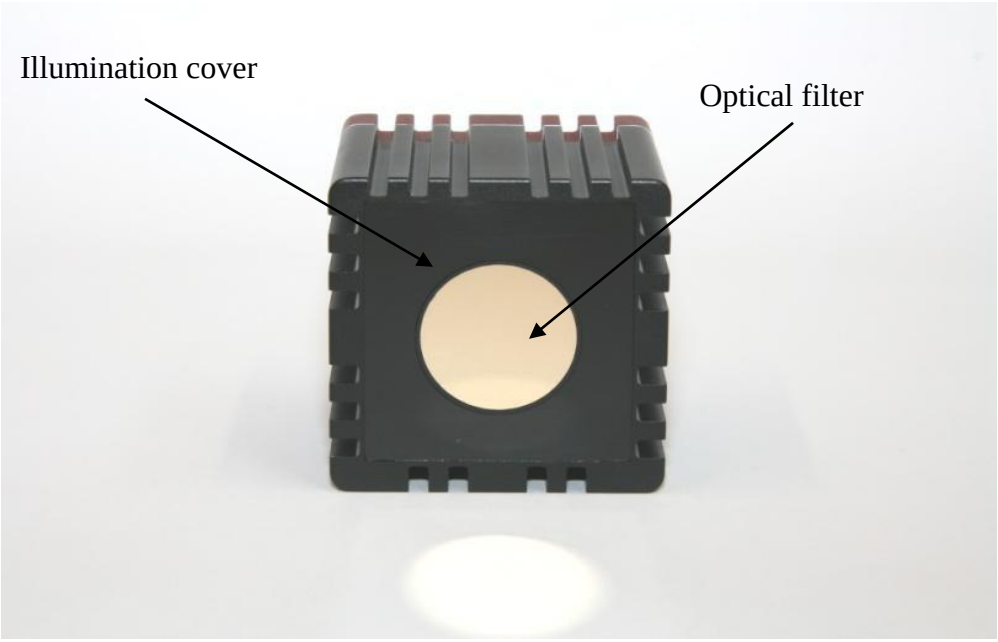

(a) SR4000 3D camera from MESA Imaging

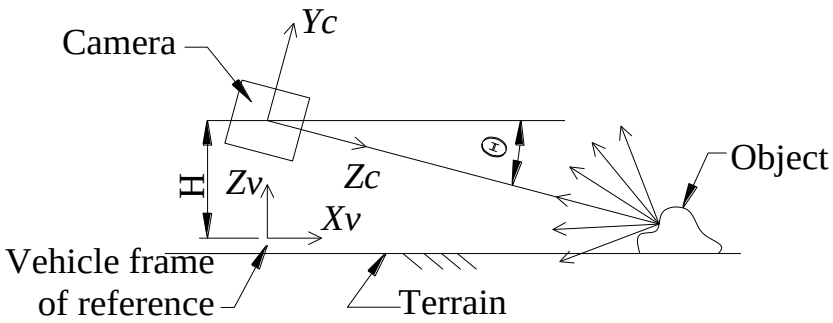

(b) Time of fly concept and coordinate system transformation

Figure 5.1 *3D Camera.*

In order to apply Equation (5.2) there is a need to consider/select a particular vehicle from where the needed parameters can be obtained. Figure 5.2 shows the four wheel vehicle used in this example. The vehicle is the GAIA platform from AAI Canada. The vehicle's mass, width, length, and ground clearance dimensions are: *m=40KG, w=470mm, l=280mm,* and *h=r=110mm* respectively. The scans of three types of terrain are illustrated in Figure 5.3: a) asphalt, b) grass,

and c) rocky. Applying Equation (5.2), the *RI* of the asphalt, grass, and rocky terrains, captured from real outdoor surfaces within the vicinity of the University of Calgary, are 0.82, 0.71, and 0.26, respectively. Herein, and only for illustration, Delaunay triangulation is used to mesh the terrain points into a surface. Note that terrain points triangulation is computationally expensive. Fortunately, it is not needed for the terrain assessment calculations.

(a) Experimental Vehicle (b) Vehicle's dimensions

Figure 5.2: ***Example of 4-wheels vehicle.***

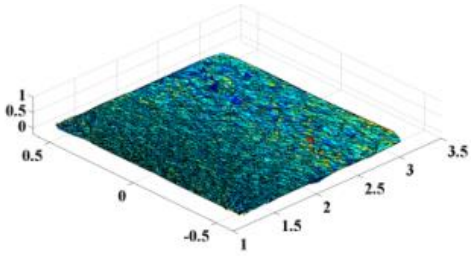

(a)

Asphalt

RI = 0.82

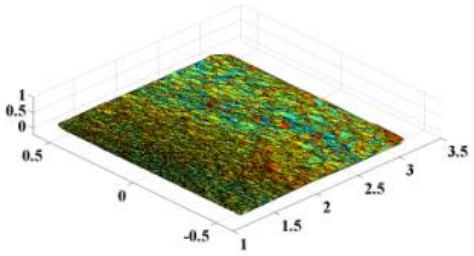

(b)

Grass

RI = 0.71

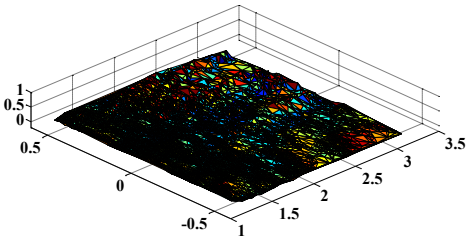

(c)

Rocky

RI = 0.26

Figure 5.3: Examples of different terrain types.

5.3 Summary

In this chapter, the concept of *RI* has been presented. The *RI* concept is based on existing Geophysics techniques [69]. In this work, the terrain is perceived as a cloud of points in a 3D w.r.t. the vehicle frame of reference. The proposed technique uses only the elevation components of the points' positions. An *RI* expression has been developed based on:

1. the standard deviation of the points' elevation components of the points from the mean terrain level, and
2. the vehicle characteristics.

In the second section, Experimental terrain scans have been presented, considering a small 4 wheels mobile platform. The terrain has been perceived using a 3D infrared camera that works based on the time of fly concept. The *RI* has been calculated for each scanned terrain. The results showed consistency, where *RI* for smooth terrain was high and for rough terrain was low. In the rest of the thesis, *RI* will be employed to assess terrain regions and determine the vehicle speed and/or path.

Chapter Six: *RI* Examination & UGV Max Speed Determination

6.1 Maximum Allowable UGV's Speed Expression

For safe and efficient navigation, autonomous vehicles should be able to change their speed according to the terrain condition. That is, effective manoeuvring of UGVs would allow/enable vehicles to react and manage their behaviours based on changes (transitions) of the terrain surface, sensed or predicted conditions. The governing criteria in the proposed approach is to keep the base excitation loads, due to the UGV-terrain interaction, $\hat{f}$, forces and moments below a permissible limit. This section presents a closed form expression of the maximum allowable vehicle speed. The proposed expression is a function of five parameters/characteristics: i) the vehicle dimensions, i.e., length l, width w, and ground clearance h, ii) the vehicle dynamic properties, e.g., stiffness, and damping, iii) the terrain roughness, iv) the permissible range of transmitted excitation loads to the UGV, and v) the required certainty of not exceeding the permissible loads. Due to the randomness of the base excitation (i.e., terrain), a stochastic approach is employed.

Equation (4.17) is a system of 3 simultaneous algebraic equations representing the base excitation forces and moments due to the vehicle terrain interaction. The units of the first equation (i.e., 1st row in Equation (4.17) are units of force (Newton); while the units of the second and third rows are moment (Newton • meter). For simplification of handling such equations, dimensionless format is used. To unify the units of these equations we first divide the 1st row in Equation (4.17) by hk_{max}. Then the 2nd row is divided by $\frac{wh}{2}k_{max}$, and the 3rd row by $\frac{lh}{2}k_{max}$, where k_{max} is the stiffness coefficient of the stiffest suspension point, w is the vehicle's width, and l is the vehicle's length. The resulting dimensionless system of equations is given in Equation (6.1), where upper case letters indicate normalized quantities. For example, $\widehat{\dot{\Delta}} = \frac{\hat{\dot{\delta}}}{h}$, and $\widehat{\Delta} = \frac{\hat{\delta}}{h}$,

$$\hat{F} = C_e\hat{\dot{\Delta}} + K_e\hat{\Delta} \tag{6.1},$$

Where $\hat{F}$ is the dimensionless forces and moments vector, $\hat{\Delta}$ and $\hat{\dot{\Delta}}$ are the dimensionless deflection of the resilient element and the rate of deflection of the resilient elements vectors respectively, and K_e and C_e are the normalized stiffness matrix and damping matrix respectively.

Normalized stiffness and damping matrices are,

$$C_e = \frac{1}{K_{max}}\begin{bmatrix} c_1 & c_2 & \cdots & c_N \\ \frac{c_1 y_1}{\frac{w}{2}} & \frac{c_2 y_2}{\frac{w}{2}} & \cdots & \frac{c_N y_N}{\frac{w}{2}} \\ \frac{-c_1 x_1}{\frac{l}{2}} & \frac{-c_2 x_2}{\frac{l}{2}} & \cdots & \frac{-c_N x_N}{\frac{l}{2}} \end{bmatrix} \tag{6.2 and}$$

$$K_e = \frac{1}{K_{max}}\begin{bmatrix} k_1 & k_2 & \cdots & k_N \\ \frac{k_1 y_1}{\frac{w}{2}} & \frac{k_2 y_2}{\frac{w}{2}} & \cdots & \frac{k_N y_N}{\frac{w}{2}} \\ \frac{-k_1 x_1}{\frac{l}{2}} & \frac{-k_2 x_2}{\frac{l}{2}} & \cdots & \frac{-k_N x_N}{\frac{l}{2}} \end{bmatrix} \tag{6.3}.$$

Note that $\hat{\delta}$ is a subset of the early defined terrain elevation points elevation vector $\hat{e}$, Section 5.1. While $\hat{e}$ is the elevations of all the scanned points of a particular terrain region; $\hat{\delta}$ is the elevation of only those points that are traversed by the vehicle's wheels. Due to the randomness of the terrain's cloud of points, we can consider that the variance of the dimensionless elevation subset, $\hat{\Delta} = \frac{\hat{\delta}}{h}$, and the superset, $\frac{\hat{e}}{h}$, are equal, i.e., $Var[\hat{\Delta}] = Var[\frac{\hat{e}}{h}]$. Recalling the definition of RI in Equations (5.1) and (5.2), the variances of the base excitation displacement can be obtained via Equation (6.4),

$$Var[\hat{\Delta}] = \frac{1}{4}(1 - RI)^2 \quad (6.4).$$

Referring to Section 4.1, Δ is a random variable which consists of equal amplitude harmonic components over a finite frequency span as illustrated (shown) in Equation (6.5).

$$\hat{\Delta} = \sum_{i=1}^{N} A_i \, sin(2\pi f_{si} vt + \phi_i) \quad (6.5).$$

In Equation (6.5), A_i, f_{si} and ϕ_i are the i^{th} harmonic component amplitude, frequency and phase shift respectively, and v is the vehicle speed. A_i, f_{si} and ϕ_i are dimensionless. The time derivative of Δ, $\dot{\Delta}$ is shown in Equation (6.6),

$$\hat{\dot{\Delta}} = \sum_{i=1}^{N} 2\pi A_i f_{si} v \, cos(2\pi f_{si} vt + \phi_i) \quad (6.6).$$

Given that,

1. $A_i = A$ for any harmonic component,
2. ($Var[cos(\theta)] = Var[sin(\theta)] = 0.5$) for any continues variable θ, and
3. using variance algebra,

$Var[\dot{\Delta}]$ is shown in Equation (6.7),

$$Var\left[\hat{\dot{\Delta}}\right] = 2\pi^2 v^2 A^2 \sum_{i=1}^{N} f_{si}^2 \quad (6.7).$$

Since the values of f_{si} are multiples of f_s, then Equation (6.7) can be simplified to Equation (6.8),

$$Var\left[\hat{\dot{\Delta}}\right] = 2\pi^2 v^2 A^2 f_s^2 \sum_{i=1}^{N} i^2 \quad (6.8).$$

$Var[\dot{\Delta}]$ can be represented as in Equation (6.9),

$$Var\left[\hat{\dot{\Delta}}\right] = \frac{1}{12}V^2(1-RI)^2 \tag{6.9}$$

taking the following into consideration:

1. The maximum terrain frequency to be considered is ($\frac{1}{2\pi h} = Nf_s$).
2. Variance of the base excitation displacement given in Equation (6.4).
3. $Var[sin(\theta)] = 0.5$
4. For large N, $\frac{1}{N^3}\sum_{i=1}^{N} i^2 \cong \frac{1}{3}$.

In Equation (6.9), $V = \frac{v}{h}$ is the normalized vehicle speed.

In order to calculate the variance of the excitation loads, Equation (6.1), the following assumptions are considered:

1. Base excitation at the i^{th} wheel (Δ_i and $\dot{\Delta}_i$) is independent from other wheels. Some types of wheeled vehicle suspensions are excluded due to this assumption, e.g., wheels on common axel, and wheels connected using a stabilizer bar.
2. Due to terrain randomness, $\hat{\dot{\Delta}}$ can be considered to be independent from $\hat{\Delta}$.
3. All wheels are subjected to the same terrain at the same speed (i.e., homogeneous terrain under the vehicle's wheels). Sometimes this assumption is not true, e.g., when the vehicle traverses the edge of the road where one side of the vehicle on a paved road and the other side on a rocky terrain.

The variance of the first row of Equation (6.1) is

$$Var[F(1,1)] = \sum_{i=1}^{N}\left(Var\left[\frac{c_i}{k_{max}}\dot{\Delta}_\iota + \frac{k_i}{k_{max}}\Delta_i\right]\right) \tag{6.10}$$

Due to Δ and $\dot{\Delta}$ independence from each other, Equation (6.10) can be written as

$$Var[F(1,1)] = \sum_{i=1}^{N} \left(Var\left[\frac{c_i}{k_{max}} \dot{\Delta}_i\right] + Var\left[\frac{k_i}{k_{max}} \Delta_i\right] \right) \tag{6.11}$$

Using variance algebra, Equation (6.11) can be written as

$$Var[F(1,1)] = \sum_{i=1}^{N} \left(\left(\frac{c_i}{k_{max}}\right)^2 Var\left[\dot{\Delta}_i\right] + \left(\frac{k_i}{k_{max}}\right)^2 Var[\Delta_i] \right) \tag{6.12}$$

Because $Var\left[\dot{\Delta}_i\right] = Var\left[\dot{\Delta}_j\right]$ for all $i \neq j \in [1, N]$ and $Var[\Delta_i] = Var\left[\Delta_j\right]$ for all $i \neq j \in [1, N]$, Equation (6.12) can be manipulated to

$$Var[F(1,1)] = Var\left[\hat{\dot{\Delta}}\right] \sum_{i=1}^{N} \left(\frac{c_i}{k_{max}}\right)^2 + Var\left[\hat{\Delta}\right] \sum_{i=1}^{N} \left(\frac{k_i}{k_{max}}\right)^2 \tag{6.13}$$

Using the same approach, the variance of the second and third rows of Equation (6.1) can be manipulated to be

$$Var[F(2,1)] = Var\left[\hat{\dot{\Delta}}\right] \sum_{i=1}^{N} \left(\frac{c_i y_i}{\frac{w}{2} k_{max}}\right)^2 + Var\left[\hat{\Delta}\right] \sum_{i=1}^{N} \left(\frac{k_i y_i}{\frac{w}{2} k_{max}}\right)^2 \tag{6.14}$$

$$Var[F(3,1)] = Var\left[\hat{\dot{\Delta}}\right] \sum_{i=1}^{N} \left(\frac{c_i x_i}{\frac{l}{2} k_{max}}\right)^2 + Var\left[\hat{\Delta}\right] \sum_{i=1}^{N} \left(\frac{k_i x_i}{\frac{l}{2} k_{max}}\right)^2 \tag{6.15}$$

Using Equations (6.13), (6.14), and (6.15) and substituting for $Var\left[\dot{\Delta}\right]$ and $Var[\Delta]$ from Equations (6.9) and (6.4) respectively, the variance of the base excitation forces and moments $\hat{F}$ can be represented by Equation (6.16),

$$Var[F] = \frac{V^2}{12}(1 - RI)^2 C_e^* + \frac{1}{4}(1 - RI)^2 K_e^* \tag{6.16},$$

where C_e^* and K_e^* are the summation of squares defined in Equation (6.17),

$$C_e^* = C_e^2 \begin{bmatrix} 1 \\ 1 \\ \vdots \\ 1 \end{bmatrix}_{N\times 1} \quad and\ K_e^* = K_e^2 \begin{bmatrix} 1 \\ 1 \\ \vdots \\ 1 \end{bmatrix}_{N\times 1} \tag{6.17}$$

The squared matrices in Equation (6.17), i.e., C_e^2 and K_e^2, refer to the Hadamard Product, element wise product, [32]. By manipulating Equation (6.16), an expression for the dimensionless maximum allowable vehicle speed (V) can be obtained, Equation (6.18).

$$V = \sqrt{\frac{12}{(1-RI)^2}\left[C_e^{*T} C_e^*\right]^{-1} C_e^{*T}\left(Var[F] - \frac{1}{4}(1-RI)^2 K_e^*\right)} \tag{6.18}$$

Up to this point, V is a function of a desired *Var[F]*, the vehicle properties and terrain Roughness. The aim of this thesis is to calculate the maximum vehicle speed at which the excitation loads do not exceed a certain allowed limit. Stochastically, it is impossible to guarantee that the base excitation loads remain below the allowable limit. A more practical approach, is to develop an expression of the maximum vehicle speed, at which the probability that the base excitation loads remain within the allowable limit, is within desirable level. Assuming F is normally distributed random variable, the cumulative probability function (Φ) is,

$$\Phi(F, \sigma^2) = \frac{1}{2}\left[1 + erf\left(\frac{F}{\sigma\sqrt{2}}\right)\right] \tag{6.19}$$

where, erf is the error function. The probability that F remains within the allowable limit is,

$$P[|F| \leq F_{all}] = Prb = \Phi(F_{all}, \sigma^2) - \Phi(-F_{all}, \sigma^2) \tag{6.20}$$

Substituting from Equation (6.19) and considering that $erf(-x) = -erf(x)$, Equation (6.20) can be written as,

$$Prb = erf\left[\frac{F_{all}}{\sigma\sqrt{2}}\right] \tag{6.21}$$

Isolating $Var[F] = \sigma^2$ from Equation (6.21),

$$Var[F] = \sigma^2 = \frac{F_{all}^2}{2(\text{erf}^{-1}(Prb))} \quad (6.22).$$

We substituted *Var[F]* from Equation (6.22) into Equation (6.18), the resulting expression for *V* is ,

$$V = \sqrt{\frac{12}{(1-RI)^2}\left[C_e^{*T}C_e^*\right]^{-1}C_e^{*T}\left(\frac{F_{all}^2}{2(erf^{-1}[Prb])^{\,2}} - \frac{(1-RI)^2}{4}K_e^*\right)} \quad (6.23).$$

Equation (6.23) is a closed form expression of the vehicle maximum allowable vehicle speed. This speed is function of i) the vehicle dynamic properties: damping coefficients, stiffness, and the configuration of the vehicle suspension, ii) the predetermined allowable base excitation loads, iii) the predetermined required certainty of not exceeding this allowable loads, and iv) the terrain roughness index. The user/operator of the vehicle should define/provide both F_{all} and *Prb* to suite the vehicle and its desired application before putting the UGV into use. For example, large heavy vehicles (e.g. military tanks) can deal with large F_{all} with low *Prb*. On the other hand, smaller vehicles or vehicles transporting sensitive materials should be set to very low F_{all} and very high *Prb*.

6.2 Initial assessment on the applicability of Equation (6.23)

To illustrate the application of Equation (6.23), the four wheels vehicle available in the laboratory, Figure 5.2, is considered. Suspension points data of this vehicle is provided in Table 6.1. The data provided in Table 6.1 is used to calculate C_e^* and K_e^*. In what follows, it will be assumed that the vehicle's frame can support a dimensionless external loads F_{all} up to $[40 \quad 40 \quad 40]^{\mathrm{T}}$ (dimensionless forces/moments, referring to Equation (6.1)). Due to the randomness of the terrain, a 100% certainty that the terrain transmitted force *F*, will not exceed F_{all} is not feasible. For this scenario, the maximum allowable vehicle speed (V) is calculated as per Equation (6.23). Hence, a

slightly lower certainty (99%) is used for practical calculations. Figure 6.1 shows the relation between the vehicle speed and the roughness index for the vehicle shown in Figure (5.2). As expected, Figure 6.1, shows that the maximum allowable vehicle speed increases for higher roughness indices, i.e., smoother terrain. However, the vehicle speed remains limited to the maximum vehicle speed. That is, in Figure 6.1, V actually saturates at V_{max} for RI values higher than 0.55.

Table 6.1 Laboratory vehicle suspension points data

Suspension point index (i)	x_i (m)	y_i (m)	k_i (N/m)	c_i (N/m)
1	0.140	0.235	250.000	300.000
2	0.140	-0.235	250.000	300.000
3	-0.140	0.235	250.000	300.000
4	-0.140	-0.235	250.000	300.000

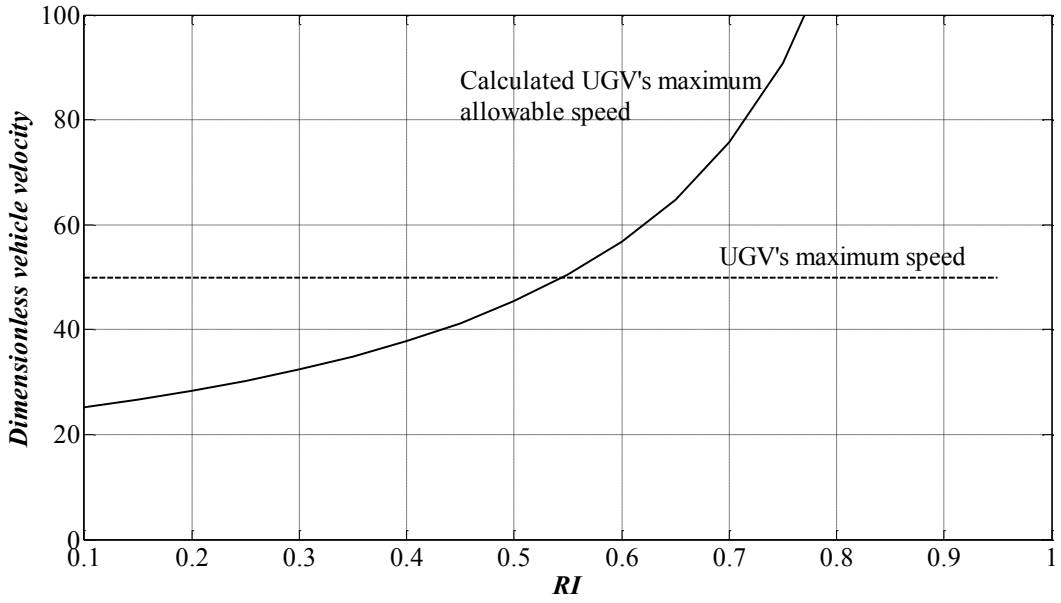

Figure 6.1 Vehicle velocity (Experimental vehicle shown in Figure 5.2) vs. RI.

Considering the terrain roughness as a random base excitation, the dynamic forces transmitted to the frame have been approached from a dynamic modeling point of view. An extensive analytical work, employing stochastic methods, has led to a closed form expression of the transmitted forces variance, as function of the vehicle properties, terrain roughness, and vehicle speed, Equation (6.16). Given the required probability that the transmitted forces will not exceed F_{all}, an expression for the maximum allowable vehicle speed has been presented, Equation (6.23). For the purpose of illustration, Figure 6.1 shows how the allowable maximum vehicle speed changes w.r.t. to the change of RI. The remaining two sections of this chapter present examples of applications of the proposed vehicle maximum allowable speed based on RI.

6.3 UGV Navigation on a Heterogeneous Rough Terrains

To investigate how the vehicle speed changes as the terrain *RI* changes, a series of tests were performed. In this section, a simulation of the vehicle described in Section 5.2 (Figure 5.2) traversing an experimentally perceived terrain is presented. The given terrain compromises three different terrain types, asphalt, rocks, and grass, Figure 6.2, which were earlier scanned offline using a 3D infrared range camera before the simulation study was conducted, Figure 5.1. As a result, once the terrain data is collected, a virtual terrain course is created, Figure 6.2. The vehicle was then simulated to traverse this virtual terrain course rendering straight line path perpendicular to the *RI* change edges. As the UGV progresses through the virtual terrain course, the proposed navigation process conducts the following set of tasks:

1. Scan a 1mX1m terrain region in front of the vehicle and register the points using Equation (5.4).
2. Calculate the associated *RI*, Equation (5.2).

3. Calculate the maximum allowable vehicle speed, Equation (6.23).
4. Go back to step #1 until the UGV reaches its destination.

Using Equation (4.4), the minimum resolution required of terrain is 10 points per square meter. In this particular simulation, the vehicle perceives a terrain area of one square meter each step. The collected terrain data, for this simulation, allows more than 7000 terrain point each step, which is tremendously redundant for the vehicle considered in this simulation. The maximum allowed vehicle speed, labeled "Vehicle Speed" in Figure 6.3, is calculated for row terrain data, and for down-sampled data. Only 10 randomly picked terrain points are considered to calculate vehicle speed for down-sampled data. In practice, full resolution data should be filtered before down-sampling, or sensor band width should be adjusted to the required resolution.

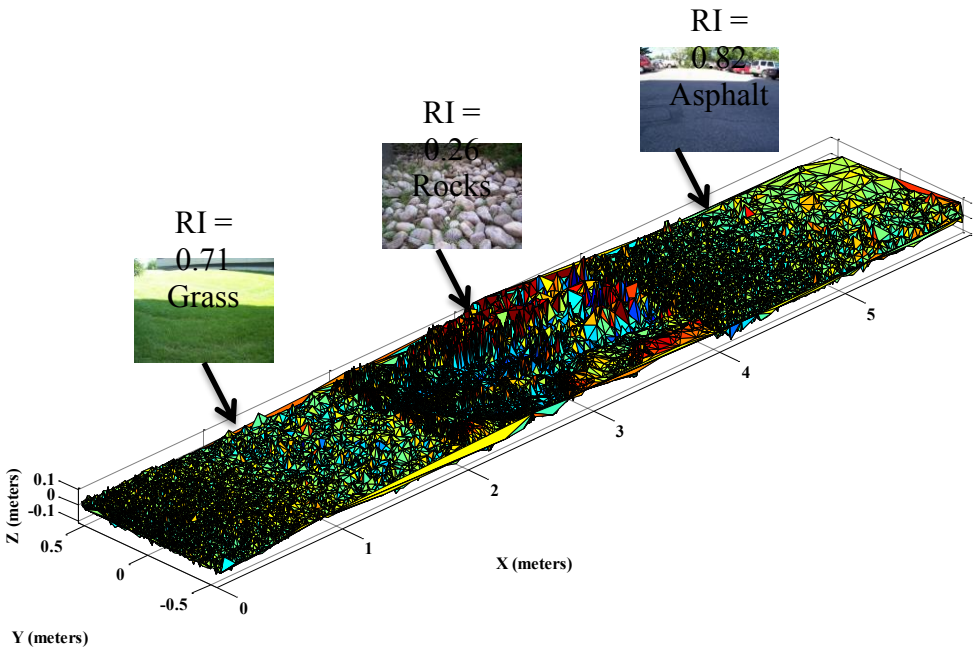

Figure 6.2 Terrain course.

The target of the proposed technique is to limit the base excitation loads, with a desired certainty, below the allowable levels. To validate the proposed technique, the variance of the base excitation

loads is calculated from Equation (6.17), based on the actual *RI* not the perceived one. Assuming the base excitation loads are normally distributed random variable, the probability of not exceeding the allowable limits is calculated. Figure 6.4 illustrates a comparison between the probabilities that base excitation loads are not exceeding the allowable limits for down-sampled vs row terrain data. This simulation has been repeated several times. The computation time for down-sampled data is consistently 50% less than for the row data.

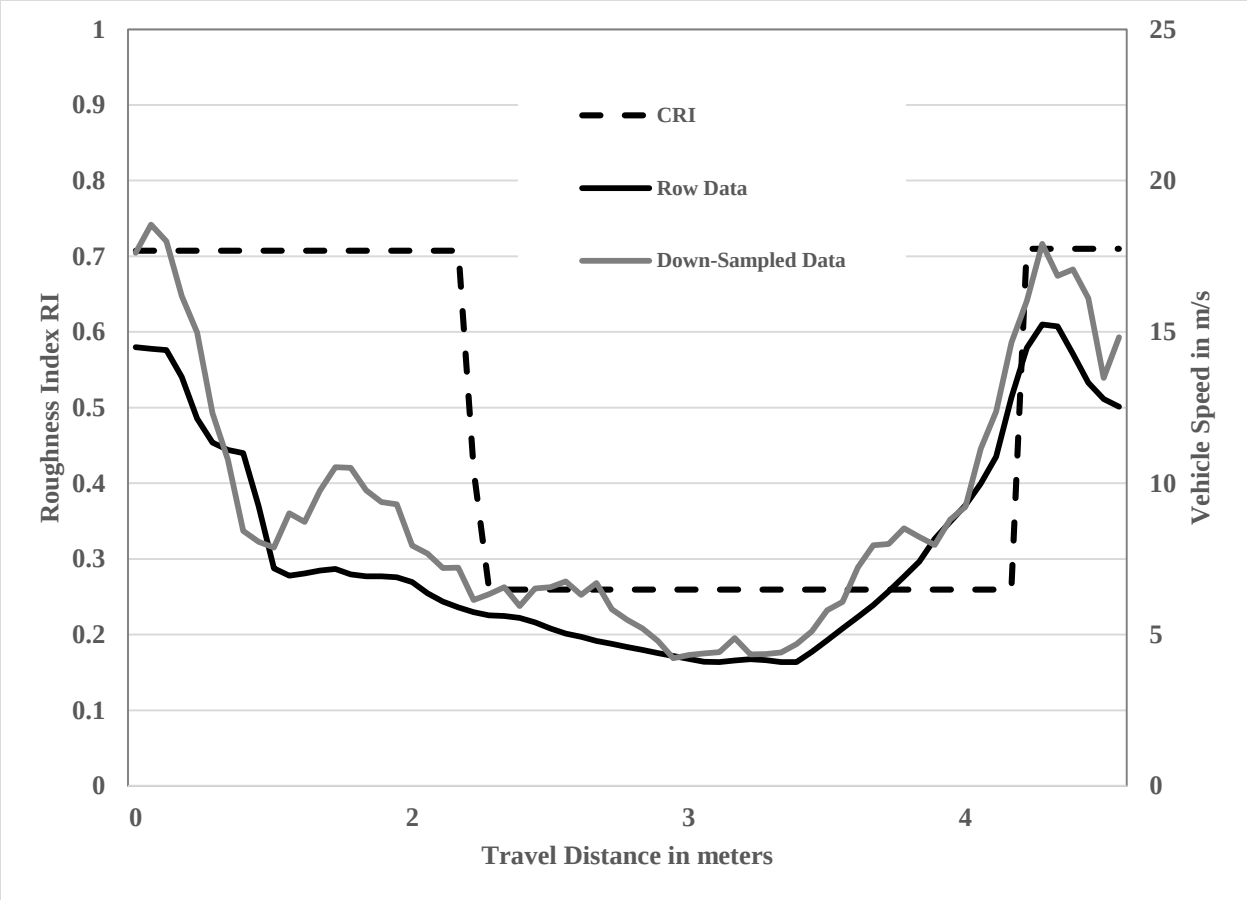

Figure 6.3 Obtained results, variable vehicle maximum allowable speed as it traverse sharp terrain transitions with different RI values.

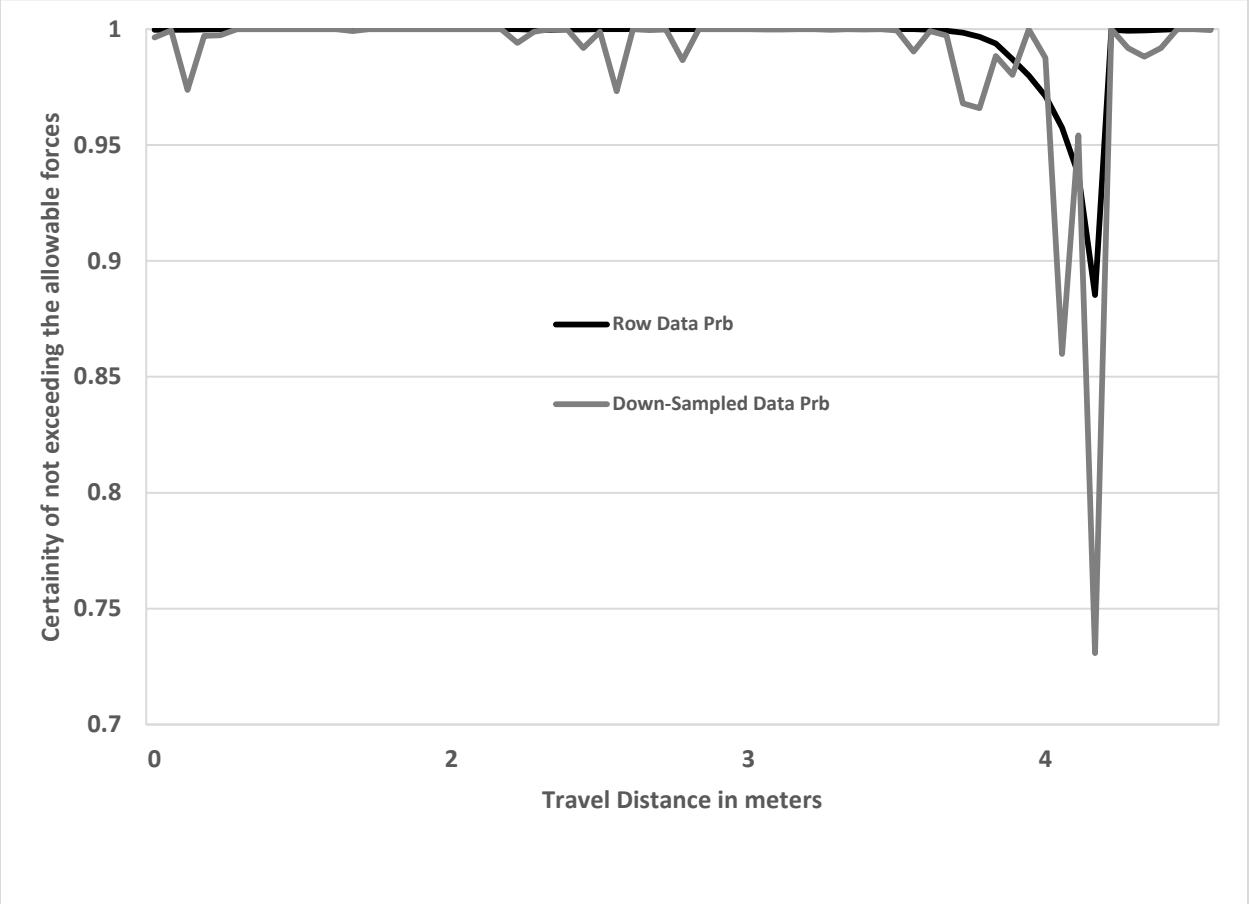

Figure 6.4 Certainty of not exceeding the allowable base excitation loads as the vehicle traverses sharp terrain transitions.

By studying Figure 6.3 and Figure 6.4, the following can be concluded.

1. The proposed terrain assessment technique enables the vehicle to predict the traversability of the remote terrain down the path and adapt its speed accordingly.
2. Although the vehicle adapted to the less traversable terrain as desired by slowing down, the vehicle speeds up early when perceiving more traversable terrain. This behaviour significantly compromises the certainty of not exceeding the allowable loads, as can be noted in Figure 6.4 near the end of the simulation. This observation indicates a limitation

of the proposed technique when moving from less traversable terrain to more traversable one. Studying and fixing this limitation will be left for future work.

3. The reduced resolution of the terrain sensing reduces the computational load be 50%. This reduction is not associated with significant compromise of the vehicle performance. The marginal effect of a reduced resolution can be counted for by selecting a slightly higher desired certainty.

6.4 Effect of the Number of Wheels

The proposed *RI* and the vehicle maximum speed calculation, Equation (6.23), were used to assess the terrain in the previous section. The same proposed development can be used to assess the vehicle capability to traverse rough terrain and to compare different designs of vehicles to negotiate a particular terrain. In this section, *RI* and Equation (6.23) are used as a vehicle design tool.

This section provides a quantitative example of the effect of increasing the number of wheels to improve the ability of a heavy vehicle to traverse rough terrains. The proposed expression of the vehicle's maximum allowable speed, Equation (6.23), is used to illustrate that increasing the number of wheels in a particular vehicle increases the vehicle's ability to traverse rough terrains at higher speeds (as it was expected). To demonstrate this, a vehicle with infinite number of wheels, i.e.,, tracked vehicle, such as the German made military tank LEOPARD 1, was chosen for this study as its characteristics were available, Figure 6.5. The specifications of the LEOPARD 1 are shown in Table 6.2. The mass moment of inertia is calculated based on the obtained dimensions of the tank while considering the mass uniformly distributed. The tank has 14 suspension points (wheels), 7 on each side, which are gathered up by tracks. Suspension of each point consists of a torsion par suspension (spring) and hydraulic shock absorber (damper). Four suspension points (in the middle of the vehicle) have no damping. For simplification, all resilience elements are assumed

to be identical (have the same damping coefficient). To illustrate the effect of the number of wheels, the effect of the tracks is neglected.

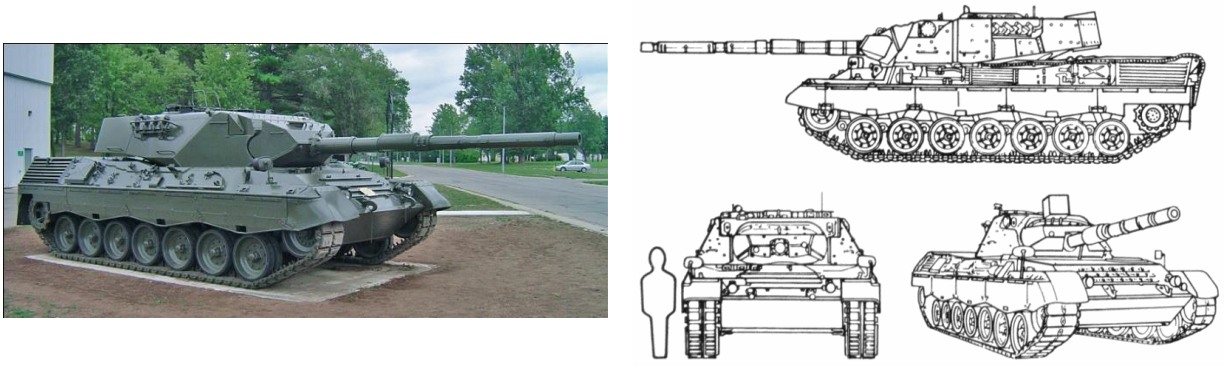

Figure 6.5: ***Military tank LEOPARD 1.***

Table 6.2: ***LEOPARD 1 specifications.***

Length	4.2 *m*	J_x	57673 $kg.m^2$
Width	2.7 *m*	J_y	190530 $kg.m^2$
h	0.44 *m*	Total stiffness	1.67×10^6 *N/m*
m	42400 *kg*	Total damping	0.8×10^6 *Ns/m*
V_{max}	65 km/hour	Suspension points	14

Once all required parameters are obtained, Equation (6.23) is used to calculate the change of the dimensionless vehicle velocity *V*, corresponding to changing in the number of wheels. For this test, the following parameter values are considered: $Prb = 0.99$ and $F_{all} = [34.7862 \quad 34.7862 \quad 34.7862]^T$. This takes place while changing the number of wheels, stiffness and damping at each wheel change, accordingly, to maintain a constant total stiffness and

damping coefficient for the vehicle. The *V*, the vehicle's calculated potential maximum speed Equation (6.23), vs. *RI* relationship is shown for different number of wheels, 4, 6, 8, 10, 12, and 14 wheels, on the given vehicle, Figure 6.6. Two obvious notes can be concluded from Figure 6.6:

1. For the same vehicle, *V* is proportional to *RI*, e.g., the vehicle can go faster on smoother terrains (high *RI*) vs. rougher terrains (lower *RI*).
2. For the same terrain, *V* is proportional (increases w.r.t.) to the number of wheels, reflecting an improved capability of traversing rough terrains with more wheels.

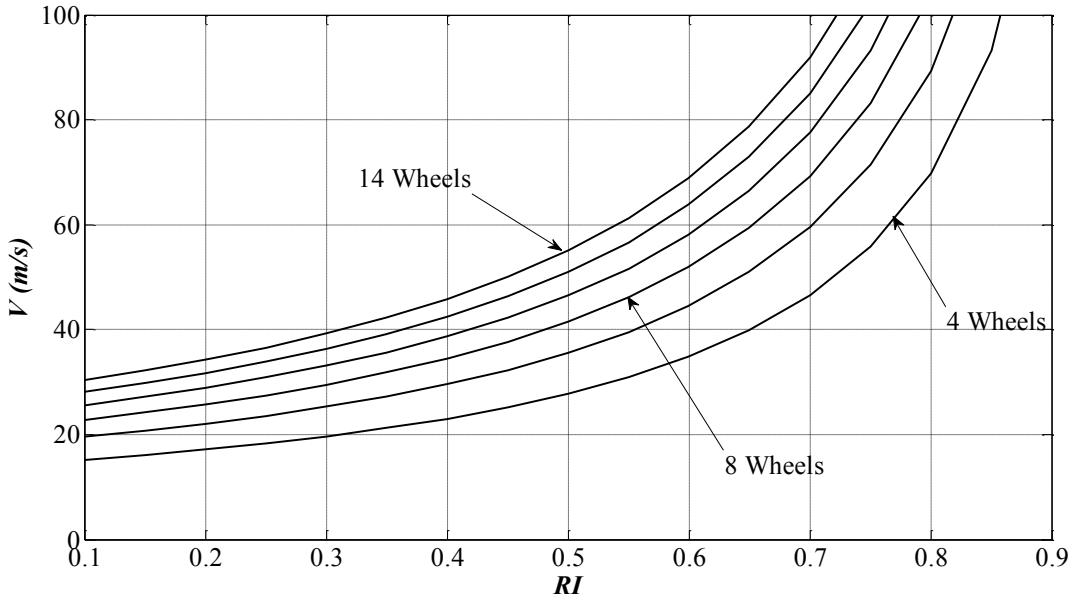

Figure 6.6: *V vs. RI* relationship for Leopard tank

The relationship between the maximum *V* that the vehicle can achieve and its number of wheels is shown in Figure 6.7 for a constant *RI* of value 0.5. *V* does not converge as the number of wheels increases. In contrast, Figure 6.7 shows a linear increase in *V* as the number of wheels increase. However, this conclusion is hypothetical as we can't infinitely increase the vehicle's number of wheels and simultaneously increase the velocity of which the vehicle traverses a given terrain

safely. Note that infinite number of wheels does not accurately imitate tracks; tracks could have a very different dynamics and behaviour characteristics. Limitations of this are listed below:

1. Increasing the number of wheels is geometrically constrained with the available space in the vehicle structure. Accordingly, to increase the number of wheels beyond a certain limit the wheels diameter needs to be reduced. This will correspondingly reduce the vehicle ground clearance and limits the vehicle capabilities of traversing rough terrain.
2. The vehicle has a maximum road speed, 65 km/hour for the example used in this section. This suggests that the vehicle does not have enough power to run faster even if the structure can sustain more transmitted loads. In this case, increasing the number of wheels does not provide any advantage to the vehicle's functionality.

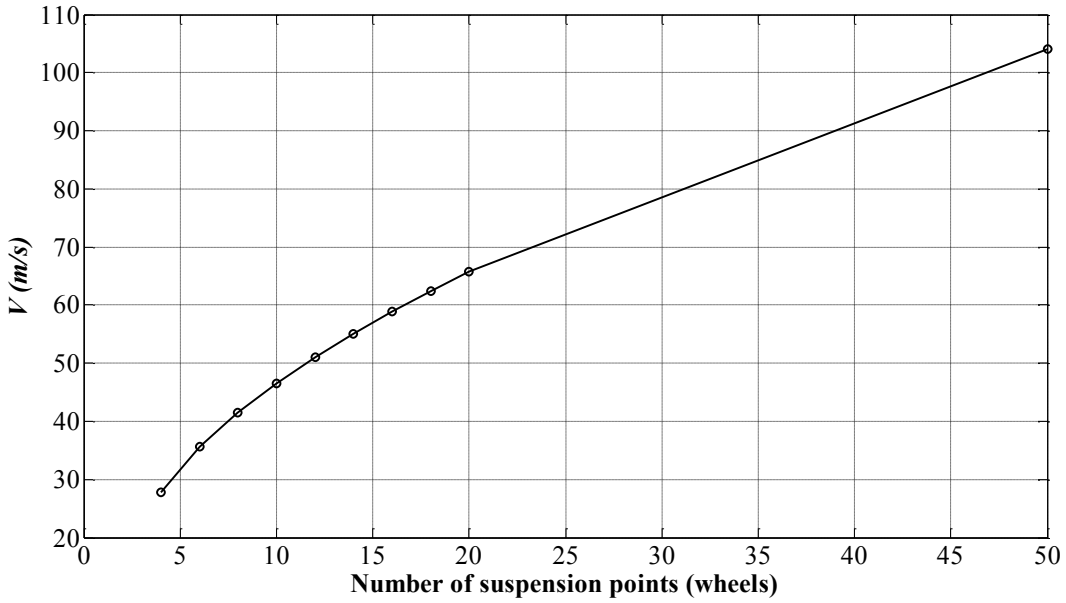

Figure 6.7: ***V vs. Number of wheels relationship.***

6.5 Summary

Considering the terrain roughness as a random base excitation, the dynamic forces and moments transmitted to the frame have been approached from a stochastic point of view. An extensive analytical work has lead to a closed form expression of the maximum allowable vehicle speed, as function of the vehicle properties, terrain roughness, permissible range of transmitted loads F_{all}, and required certainty of not exceeding this range *Prb*. The proposed technique studied:

1. the effect of a dramatic change of the terrain roughness (RI), and
2. the effect of changing the vehicle's number of wheels on the vehicle maximum allowable speed.

Results show that the proposed technique enable the vehicle to detect and traverse terrain roughness transitions smoothly. However, some limitations apply (e.g., vehicle speed could be either too slow or too fast at transitions. Limitations are left to be evaluated and adjusted for each application accordingly.

For a real vehicle (military tank LEOPARD 1), the results showed significant improvement in the vehicle`s capability to traverse rough terrain as the number of wheels increases. However, this improvement is limited by geometric constraints, such as limited space for wheels, and the vehicle maximum road speed. The example demonstrated the consistency of the proposed approach. Accordingly, it can be used in the design process of off-road vehicle to compromise/optimise the vehicle's number of wheels and dimensions.

Chapter Seven: Stability Index (SI)

Vehicle stability is a classical topic in the automotive research literature. The term "Rollover Index" appeared in the late 90's as a quantitative assessment of the vehicle tendency to rollover [70]. In the later years, the index was used to develop systems that control the vehicles' brakes, steering, and differential to prevent rollover, [71]–[74]. To the best of the author's knowledge, all the vehicle stability literature addressed the stability of the vehicle in the roll direction. The literature was concerned with predicting the vehicle rollover and preventing it. This chapter proposes a new vehicle stability assessment concept. The proposed Stability Index (SI), assesses the total stability of the vehicle in both roll and pitch directions. The SI is used in this thesis to avoid conditions that may destabilize the vehicle, not to correct an unstable vehicle.

Maintaining vehicle stability is a key issue in UGV navigation, especially when moving on unknown rough terrain. The vehicle is considered unstable when it is about to tip or roll over, i.e. turns upside down. If the vehicle can't recover, such a situation could lead to a mission failure. In less critical situations, the vehicle losing its stability could cause serious damage to the vehicle itself, its sensing system, e.g., on board cameras and sensors, or the vehicle's load, in case of material handling/transportation. Thus maintaining the stability of the vehicle traversing at high speeds in natural terrain is necessary. The vehicle's stability is a function of three factors: i) terrain geometry, ii) vehicle characteristics, e.g., mass and geometry, and iii) the vehicle's state, e.g., speed and radius of turn. In this chapter, a novel vehicle stability assessment methodology is proposed to enable fast and effective assessment of the vehicle's stability as a function of the terrain slopes, vehicle's characteristics, and vehicle status. Such stability assessment, denoted herein as Stability Index (*SI*), is then used to define the maximum velocity at which a UGV can navigate unknown terrain at high speed without compromising the stability of the vehicle.

7.1 Derivation

Similar to the *RI*, the Stability Index (*SI*) is defined as a real number in the range of [0,1], which represents the vehicle's tendency to tip over. Herein a value of *SI=1* is used to denote the most stable vehicle's state, e.g., a vehicle moving in a straight line at a constant safe speed on a perfectly horizontal surface; and *SI=0* in the other hand represents an unstable vehicle's state (e.g., a vehicle trying to sit on a vertical surface). Herein the *SI* neglects the terrain roughness, but combines the terrain geometry, i.e., slope, the vehicle physical properties, e.g., ground clearance, footprint and the UGV orientation w.r.t. the given terrain, and the vehicle's state, e.g., velocity and turning radius, in order to calculate the stability of the vehicle and its tendency to tip or roll over.

Two terrain geometric properties are involved in the *SI* calculation: terrain pitch (α) and roll (β), shown in Figure 7.1. These two parameters are defined w.r.t. the global frame of reference. To obtain them, the best 3D surface that fits the perceived terrain points is calculated. This is a typical linear regression process. However, due to the excessive number of terrain data points, a random set of points is picked for the linear regression calculation. The number of points picked is function of the required sensing resolution refers to Equation (4.4). It is quite strait forward to extract the slops of the resulting 3D surface in both the pitch (α), and roll (β) directions.

The vehicle properties considered in the calculation of *SI* are: the mass (m), wheel base width (w), wheel base length (l), the vehicle's center of gravity (CG) and height (H). Such properties are illustrated in Figure 7.1. The variables used to define the state of the vehicle are: the vehicle's current speed (v) and its radius of curvature (λ). The vehicle's radius of curvature is the distance between the centre of the turning radius and the vehicle's CG. For a straight line, λ equals zero. Figure 7.1 shows the vehicle's free body diagram where the CG is the origin of the vehicle's frame

of reference (X_v, Y_v, Z_v). This is the frame of reference according to which all sensory data is registered using homogeneous transformations.

When in motion, the vehicle is subjected to external forces/moments due to its interaction with the terrain (i.e., terrain reaction on the vehicle). The vehicle might also experience internal forces due to its motion (e.g., centrifugal force when the vehicle turns). The corresponding external forces and moments are represented as R_x, R_y, R_z. and T_x, T_y, and T_z, respectively, Figure 7.1. The moments are due to the offset between the terrain reaction at the individual wheels. The vehicle is also subjected to two body forces: vehicle weight (f_w) and, the centrifugal force (f_c) due to turning. To ease the determination of *SI* the vehicle is considered in a steady state having constant speed within the range of $0 < v < v_{max}$. Under this condition, the terrain rolling resistance, for the wheels/tracks, and the air resistance, drag, forces are balanced with the vehicle driving forces, i.e., $R_x=0$.

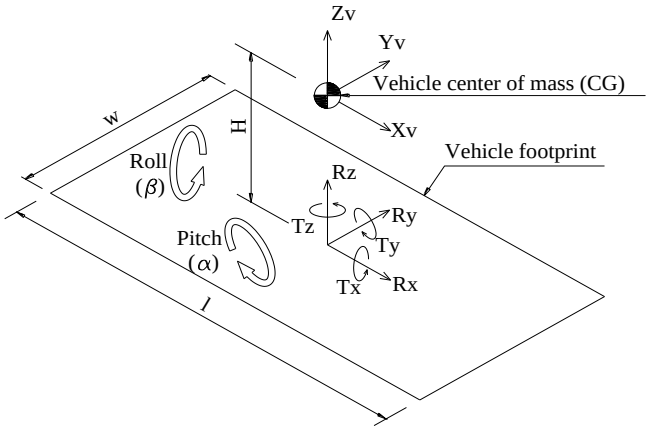

Figure 7.1. Vehicle's footprint on the terrain schematic diagram and the associated forces acting on the vehicle.

Considering the vehicle in an arbitrary given attitude (position and orientation), Figure 7.2, the body forces (f_w and f_c) in the global (world) frame of reference (named *G* in this thesis) are given in Equations (7.1) and (7.2),

$$f_w^G = \begin{bmatrix} 0 \\ 0 \\ -mg \\ 1 \end{bmatrix} \quad (7.1), \text{ and}$$

$$f_c^G = \begin{bmatrix} 0 \\ -m\frac{v^2}{\lambda} \\ 0 \\ 1 \end{bmatrix} \quad (7.2),$$

Respectively, where λ is the radius of turn in meters. The sign of λ is used to represent the direction of turn w.r.t. the vehicle's frame of reference (i.e., positive when of turning left and negative when turning right).

The superscript used in Equation (7.2) refers to the corresponding frame of reference, i.e., *G* for global and *V* for vehicle. The two subscripts employed in the equations are used to represent the type of force, i.e., *w* for weight and *c* for centrifugal.

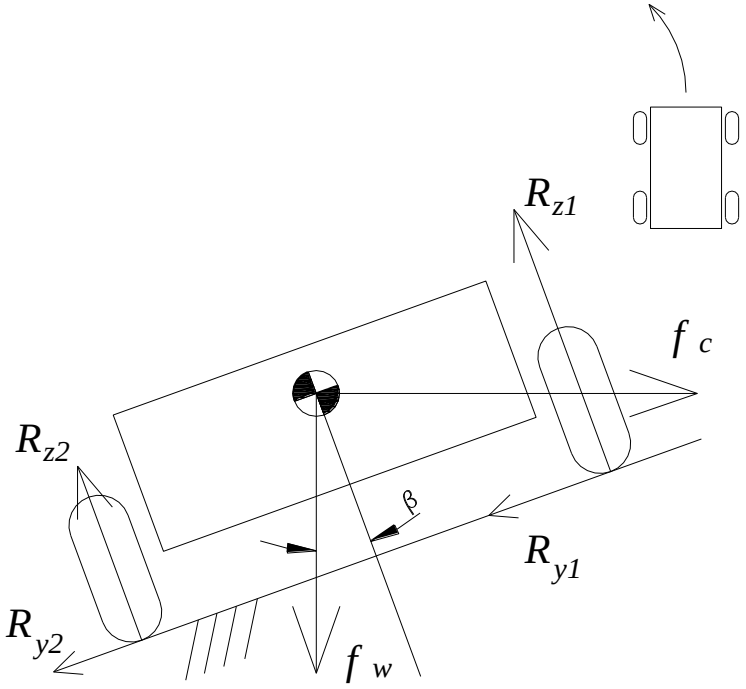

Figure 7.2 Vehicle body forces and terrain reactions on an inclined terrain while the vehicle turns left.

Once the vehicle body forces vectors are known, a homogeneous transformation (*T*) is used to transform the body forces vectors from the global frame of reference to the vehicle's frame of reference, Equation (7.3),

$$f_i^V = T f_i^G \tag{7.3}.$$

Two rotations: pitch, Equation (7.4),

$$T_{pitch} = \begin{bmatrix} \cos\alpha & 0 & -\sin\alpha & 0 \\ 0 & 1 & 0 & 0 \\ \sin\alpha & 0 & \cos\alpha & 0 \\ 0 & 0 & 0 & 1 \end{bmatrix} \tag{7.4},$$

followed by roll, Equation (7.5),

$$T_{roll} = \begin{bmatrix} 1 & 0 & 0 & 0 \\ 0 & \cos\beta & \sin\beta & 0 \\ 0 & -\sin\beta & \cos\beta & 0 \\ 0 & 0 & 0 & 1 \end{bmatrix} \quad (7.5),$$

are to take place when obtaining *T*. The final transformation matrix (*T*), Equation (7.6),

$$T = T_{roll}T_{pitch} = \begin{bmatrix} \cos\alpha & 0 & -\sin\alpha & 0 \\ \sin\alpha\sin\beta & \cos\beta & \cos\alpha\sin\beta & 0 \\ \sin\alpha\cos\beta & -\sin\beta & \cos\alpha\cos\beta & 0 \\ 0 & 0 & 0 & 1 \end{bmatrix} \quad (7.6),$$

assumes that the vehicle does not undergo any yaw motion. Although yaw is one of the vehicle's degrees of freedom, it does not affect the vehicle's stability as per the definition adopted in this thesis, tendency of the vehicle to tip or roll over. As a result of *T*, the body force vectors, gravitational and centrifugal, in the vehicle's frame of reference are given by Equations (7.7) and (7.8),

$$f_w^V = \begin{bmatrix} mg\sin\alpha \\ -mg\cos\alpha\sin\beta \\ -mgcos\alpha\cos\beta \\ 1 \end{bmatrix} \quad (7.7), \text{ and}$$

$$f_c^V = \begin{bmatrix} 0 \\ -m\frac{v^2}{\lambda}\cos\beta \\ m\frac{v^2}{\lambda}\sin\beta \\ 1 \end{bmatrix} \quad (7.8),$$

respectively.

Since the vehicle is considered at a steady state, static equilibrium applies. The vehicle body forces (weight and centrifugal forces) are balanced by vertical and lateral reactions, in the Z_V and Y_V directions respectively, at the wheels' contacts with the terrain. The vertical reactions at each of the *N* wheels comprising the UGV are compiled into one total normal reaction force (R_z), Equation (7.9),

$$R_z = mg\cos\alpha\cos\beta - m\frac{v^2}{\lambda}\sin\beta \tag{7.9}.$$

The point of effect of this total reaction is referred to herein as "center of effect" (C_{eff}), Figure 7.3. The roll and pitch moments, T_x, Equation (7.10), and T_y, Equation (7.11), respectively.

$$T_x = H\left(-mg\cos\alpha\sin\beta - m\frac{v^2}{\lambda}\cos\beta\right) \tag{7.10},$$

$$T_y = -Hmg\sin\alpha \tag{7.11},$$

respectively, are balanced by the moment generated by R_z and its offsets, S_x and S_y, from the vehicle's CG projection, Figure 7.3. The offsets from the vehicle's CG renders the reaction R_z into a moment of two components: i) a moment about X_V, and ii) a moment about Y_V, which balance T_x and T_y respectively.

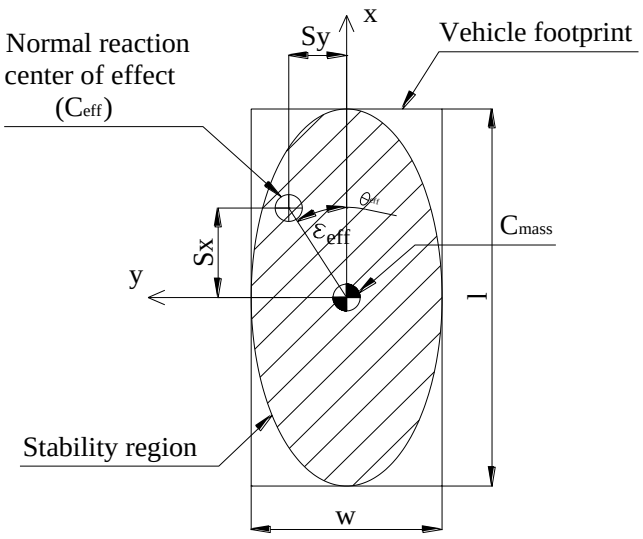

Figure 7.3. *Stability* region representation w.r.t. the vehicle's top view.

Figure 7.3 illustrates the vehicle's stability region. If the forces acting on the vehicle fall outside the stability region, the vehicle`s stability is considered lost. The vehicle`s stability is a function

of the offsets between C_{eff} and the vehicle`s position of its centre of gravity, S_x and S_y, shown in Equations (7.12) and (7.13),

$$S_x = \frac{T_y}{R_z} \quad (7.12), \text{ and}$$

$$S_y = \frac{T_x}{R_z} \quad (7.13),$$

respectively. The smaller the offsets, S_x and S_y, (C_{eff} is close to the *CG* projection) the more stable the vehicle is considered, and vice versa. In this thesis, the vehicle is considered stable as long as all wheels are in contact with the terrain. In such case, C_{eff} has to lie within a polygon that connects the *N* wheel points of contacts with the terrain. In the case where the C_{eff} is located on the edge or outside the polygon, the vertical reaction at one or more wheels will become zero or negative. A value of zero represents when the wheel is about to be detached from the ground. Simultaneously, negative values represent wheels that are in the air. In order to simplify the complexity of formulating a one closed form expression for the vehicle's stability, the stability region is herein considered as an ellipse touching the contact points polygon from inside, Figure 7.3. For the vehicle to be stable, C_{eff} has to lie inside such ellipsoidal curve. An example of four wheels vehicle is shown in Figure 7.3. In the case of a rectangular wheels configuration vehicle, the stability region major diameter is taken to be equal to the vehicle length (*l*) and the minor diameter will be equal to the vehicle width (*w*). Note that this considerations are conservative, as stable area, i.e., close to the corners, have been excluded from the stability region.

The equation of the stability region (ellipse) in the Cartesian coordinate is shown in Equation (7.14),

$$\frac{x^2}{l^2}+\frac{y^2}{w^2}=\frac{1}{4} \tag{7.14}.$$

Using the substitutions in Equation (7.15),

$$\begin{aligned} x &= \varepsilon\cos\theta \\ y &= \varepsilon\sin\theta \end{aligned} \tag{7.15},$$

Equation (7.14) can be written in the polar coordinate as shown in Equation (7.16),

$$\varepsilon=\frac{1}{2}\sqrt{\frac{l^2w^2}{w^2\cos^2\theta+l^2\sin^2\theta}} \tag{7.16},$$

where θ and ε are the angular position, measured from the positive *x* axis, and the radial distance, measured from *CG* projection, respectively. The angular position and radial distance of C_{eff}, θ_{eff}, and ε_{eff}, respectively, Figure 7.3. Equations (7.17) and (7.18),

$$\theta_{eff}=tan^{-1}\left(\frac{S_y}{S_x}\right)\rightarrow cos(\theta_{eff})=\frac{S_x}{\sqrt{S_x^2+S_y^2}}\ \&\ sin(\theta_{eff})=\frac{S_y}{\sqrt{S_x^2+S_y^2}} \tag{7.17}, \text{ and}$$

$$\varepsilon_{eff}=\sqrt{S_x^2+S_y^2} \tag{7.18}$$

respectively, show the expressions for θ_{eff} and ε_{eff}. By substituting for ($\theta=\theta_{eff}$) from Equation (7.17), the radial distance from *CG* to the edge of the stability region (ε_{st}), at θ_{eff}, is defined per Equation (7.19),

$$\varepsilon_{st}=\frac{1}{2}\sqrt{\frac{l^2w^2(S_x^2+S_y^2)}{w^2S_x^2+l^2S_y^2}} \tag{7.19}.$$

As a result, the Stability Index (*SI*) is defined as how much the C_{eff} is shifted from the projection of *CG*. Quantitatively, *SI* is the ratio between the distance between *CG* projection and both C_{eff} and the edge of the stability region respectively, Equation (7.20),

$$SI = 1 - \frac{\varepsilon_{eff}}{\varepsilon_{st}} \quad (7.20).$$

By substituting from Equations (6.9), (7.10), (7.11), (7.12), (7.13), (7.18) and (7.19) in Equation (7.20) and manipulating the expression, *SI* can be represented in a dimensionless form as in Equation (7.21),

$$SI = 1 - \frac{2H}{A}\sqrt{\frac{sin^2\alpha}{L^2} + B^2} \quad (7.21),$$

where:

$$A = \cos\alpha\, cos\beta - V\sin\beta$$

$$B = \cos\alpha\sin\beta + V\cos\beta$$

$$H = \frac{h}{w},\ L = \frac{l}{w},\ \text{and}\ V = \frac{v^2}{\rho g}.$$

Observing Equation (7.21), it can be seen that *SI* is a function of the following 3 aspects:

1. Terrain pitch α and roll β,
2. The two vehicle's aspect ratios (*H*) and (*L*), and
3. The vehicle's dimensionless speed (*V*).

For hypothetically 90° pitch or roll terrain, *SI* is infinity due to dividing by zero in Equation (7.21). To avoid computer numerical errors, values of perceived terrain pitch and roll shall be limited, i.e., saturated, to reasonable values before calculating *SI*.

The dimensionless format of *SI* (7.21) generalizes the expression and makes it applicable to the most popular vehicle configurations, e.g., 4 wheels and tracked vehicles. Thus, for a given terrain, the stability of the UGV is dependent not only on the terrain geometry, but also on how the robot traverses such environment. Thus the developed *SI* can make possible to achieve the objective of

the navigation system to traverse the perceived terrain as fast as possible while maintaining acceptable vehicle stability as illustrated in the following sections.

A perceived terrain region is assessed by evaluating *SI* and *RI* for a particular vehicle. Given the radius of turn, the vehicle has a maximum allowable speed at which it is just about to go unstable (critically stable). By putting *SI*=0 in Equation (7.21), a second degree polynomial of *V* can be driven, Equation (7.22). The standard closed form solution of the second degree polynomial, Equation (7.23), provides two solutions: one is physically applicable, while the other is not (e.g., negative or imaginary). The applicable solution is the maximum allowable vehicle speed.

$$OV_{max}^2 + PV_{max} + Q = 0$$

where:

$$O = 4H^2 \cos^2\beta - \sin^2\beta$$
$$P = 8H^2 \cos\alpha \sin\beta \cos\beta + 2\cos\alpha \cos\beta \sin\beta \tag{7.22}$$
$$Q = 4H^2\left(\frac{sin^2\alpha}{L^2} + \cos^2\alpha \sin^2\beta\right) - \cos^2\alpha \cos^2\beta$$

$$V_{max} = \frac{-P \pm \sqrt{P^2 - 4OQ}}{2O} \tag{7.23}$$

Note that this solution does not consider the roughness of the terrain (i.e., *RI*); or, in other words, considers a perfectly smooth terrain (i.e., *RI*=1). Given that for a very rough terrain (i.e., *RI*=0) the vehicle's maximum allowable speed is zero. A function can be assumed to map v_{max}, Equation (7.24), on the *RI* scale: 1 to 0. This research assumes a linear scale, according to Equation (7.25), where $v^*_{max}=v_{max}$ at *RI*=1 (i.e., a perfectly smooth terrain) and $v^*_{max}=0$ at *RI*=0. It is worth noting that different mapping functions can be assumed according to the application. For example, if the vehicle is used to transport shock, sensitive material (e.g., explosives) a different mapping function

could be used at which the terrain roughness has more influence on the vehicle's maximum allowable speed.

$$v_{max} = \sqrt{\rho g V_{max}} \tag{7.24}$$

$$v^*_{max} = v_{max} - (1 - RI) v_{vehicle\ maximum} \tag{7.25}$$

where v^*_{max} is the calculated vehicle's maximum speed, and $v_{vehicle\ maximum}$ is the vehicle maximum speed (a physical characteristic of the vehicle itself).

For the purpose of simulation, v^*_{max} in saturated between $v_{vehicle\ maximum}$ and 1% $v_{vehicle\ maximum}$.

7.2 *SI* Tests

Equation (7.21) can be used to simulate vehicles placed within diverse sloped environments. As an example of a typical set of results, consider a vehicle having a length equal to twice its width, and ground clearance of one quarter the robot's width, (*L=2* and *H=0.25*). Figure 7.4 shows the obtained vehicle's *SI* plotted vs. the terrain pitch and roll angles, where the velocity of the robot is considered to be zero. From this plot, it is quite clear that the vehicle is more stable in the direction of its largest dimension, i.e., *l*.

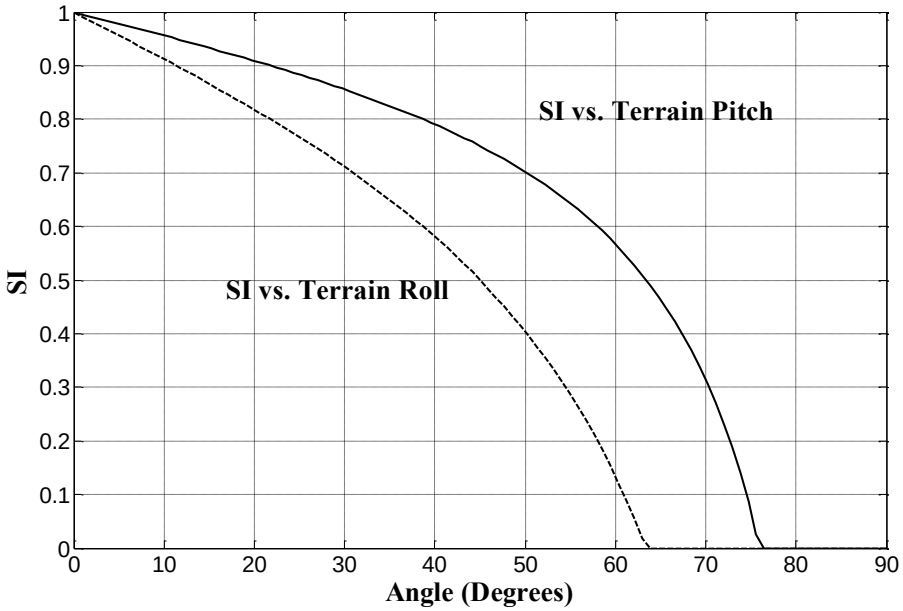

Figure 7.4. *SI* vs. Terrain Roll and Pitch.

tests were also performed when the vehicle velocity was changed while the vehicle traverse different curved trajectories. Figure 7.5 shows the obtained relationship between the vehicle`s *SI* and the vehicle`s speed for different radius of curvatures (ρ). For these tests, the terrain was considered perfectly horizontal, ($\alpha=\beta=0$). The obtained results show how the vehicle *SI* drops when the speed increases. From Figure 7.5, it can also be seen that the vehicle is less stable when moving in tight, smaller, radius of curvatures.

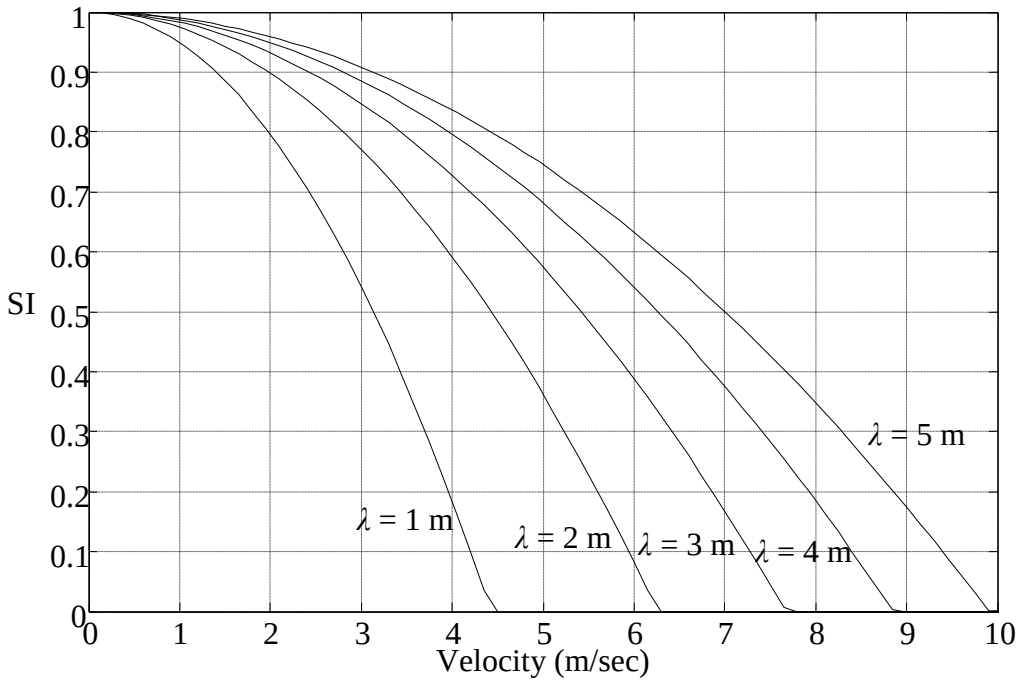

Figure 7.5. *SI* vs. UGV speed.

To demonstrate the combined effect of the terrain roll and the vehicle speed, a number of simulations were performed. Figure 7.6 shows a typical result. The results presented in Figure 7.6 were obtained while the vehicle traversed a turn to the left of 5 meters in radius on a terrain having a roll of -30^{o} (tilted down on the left side of the initial state of the robot).

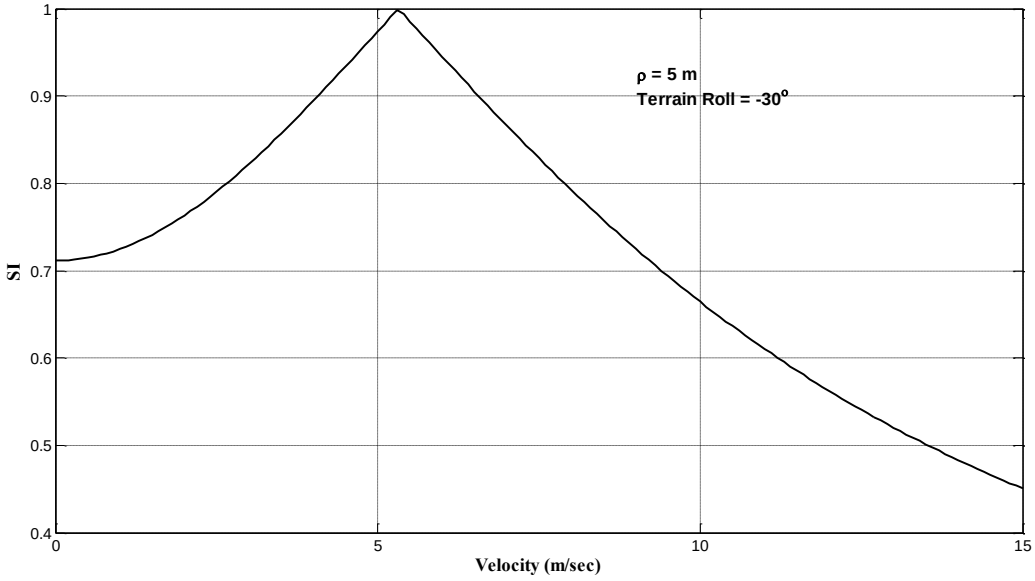

Figure 7.6. *SI* vs. Speed on a sloped terrain.

As speed increases, the centrifugal force counters the effect of the terrain roll (as expected). Accordingly, the *SI* increases up to a speed of 5.3 m/sec. At this speed, the effect of the centrifugal force equals the effect of the terrain roll. For higher speeds, the *SI* drops again because the centrifugal force effect becomes greater than the terrain's roll effect. Based on these results, it is concluded that *SI* captures the effect of the terrain on the robot as the robot navigates.

7.3 Summary

This chapter has proposed a novel methodology to assess vehicle stability as function of the following three characteristics:

1. the average terrain geometry α and β,
2. vehicle's characteristics (*m, w, l,* and *CG*), and
3. vehicle's state (e.g., speed *v* and radius of turn λ).

A new index has been proposed and developed, Stability Index (*SI*), to represent the vehicle's stability on a scale from zero (unstable vehicle) to one (perfectly static stable vehicle). An analytical derivation has been presented, leading to a closed for expression for *SI*. The *SI* expression has been derived in a dimensionless form to generalize its application to any wheeled or tracked vehicle.

In order to verify the consistency of new proposed *SI*, three simulations have been presented. First, the vehicle has been simulated while sitting on a sloped terrain up to 90 degrees. Different terrain slopes have been tried in both pitch (α) and roll (β) directions, Figure 7.4. This simulation showed that: i) the vehicle's stability deteriorates as the terrain slope increases, and ii) the vehicle is more stable in the direction of its longest footprint dimension. The second simulation showed the relationship between vehicle's stability vs. speed and radius of turn, Figure 7.5. The last simulation showed that the vehicle's stability changes while increasing the velocity for constant slope and radius of turn, Figure 7.6. Although the simulation results are quite obvious, they have showed that:

1. the application of the proposed *SI* to describe the vehicle stability, and
2. the consistency of the *SI* results in different situations.

Chapter Eight: Applications on Terrain Geometric Assessment

The previous chapters presented the RI and SI indices derivations, examples, and applications individually. This chapter provides computer simulations of two out of numerous examples using the RI and SI simultaneously to make a navigation decision. The two representative examples are: i) speed planning, and ii) path planning with high speeds. The examples are provided for demonstration only. Implementation of terrain assessment can significantly vary according to the application. As mentioned before, the proposed terrain assessment is meant to be flexible and adaptive to suit a wide range of applications.

8.1 Speed planning

The purpose of the speed planning is to demonstrate the capability of the proposed terrain assessment to change the vehicle speed according to the vehicle's determined terrain roughness and stability. For this case numerous examples are presented. In these examples the navigation system is given a path to follow. As the vehicle progresses through the path, the terrain assessment module perceives the immediate terrain region ahead of the vehicle. Subsequently, the associated RI and SI are calculated, and the maximum allowable vehicle speed that can be used to traverse the terrain is provided to the navigation system. While this application is not fully autonomous, i.e., the path is pre-planned and provided by the user, it addresses many real situations, e.g., patrolling, vehicle-vehicle tracking, and trail tracking.

This section presents two speed planning examples:

1. The first example considers a terrain course consisting of three different terrain regions having different roughness. The terrain course is leveled (i.e., no slopes)

2. The second example considers a terrain course consisting of two terrain regions of the same roughness. In this test the two terrain regions are of different elevations, while each of them is flat, i.e., no slope.

For these two examples, Equation (7.25) is implemented to calculate the vehicle maximum allowable speed as it navigates the given path.

A four wheels vehicle is considered in the tests, Figure 8.1, where the vehicle parameters are: l=0.7m, w=0.47m, h=r=0.1m, and b=0.4m. The other needed vehicle specifications are: m=100kg, longitudinal wheel span is w=0.28m, and the wheels are symmetrically distributed around the vehicle's frame of reference situated at the *CG* of the vehicle.

(a) Experimental Vehicle

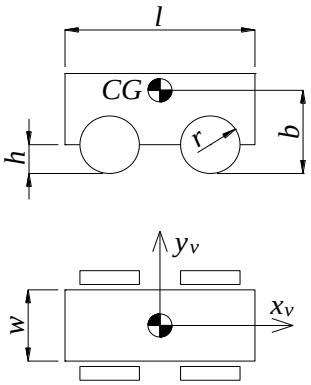

(b) Vehicle's dimensions

Figure 8.1: Example of 4-wheels vehicle.

8.1.1 Roughness transitions (no slope)

Figure 8.2 shows the selected leveled terrain of three different roughness regions. From the left to the right of Fig. 8.2, the *RI* of the regions are 0.7, 0.2 and 0.6, respectively. Two paths are studied between a start and an end point: i) path #1, a straight line connection the start and end points, and ii) path #2, a curved path connecting the same start and end points. Each path is described by a spline curve defined by 5 control points. Coordinates of 20 points equally separated along each

path are calculated at which the vehicle perceives the terrain region ahead of it and determines the maximum speed that should be used.

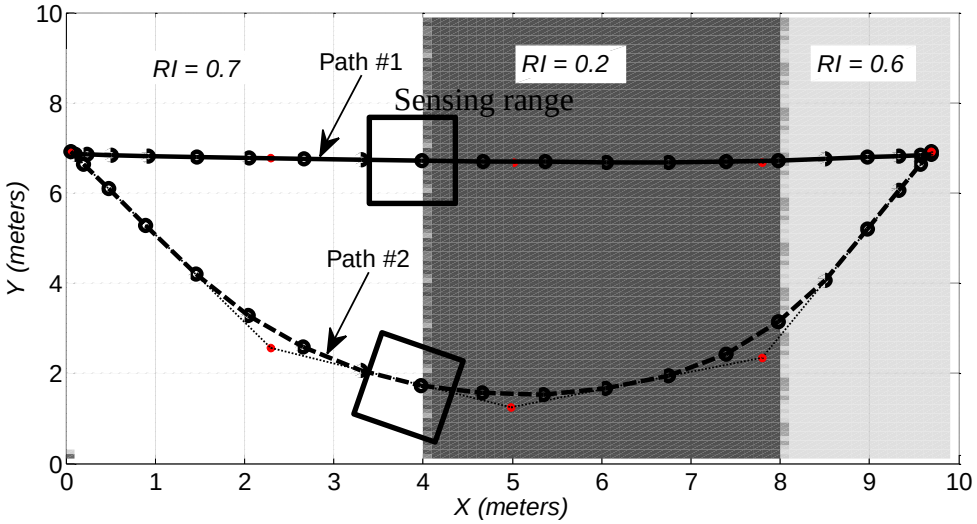

Figure 8.2 Leveled terrain course of different roughnesses.

Figure 8.3 shows the calculated maximum speed profile for each path. The maximum vehicle speed, of the experimental UGV, is 10m/s; the minimum vehicle speed is set to 0.1m/s to avoid having the vehicle stuck in a highly un-traversable terrain. The associated perceived RI and SI are shown in Figure 8.4 (a) and (b), respectively. For Path #1, the calculated speed drops prior and through the rough terrain region. The perceived SI along Path #1 remains high ($0.85 \leq SI \leq 1.0$) indicating a stable vehicle (moving strait on a leveled terrain). For Path #2 the calculated speed is generally lower than the speed along path #1. In Path #2 perceived RI is similar to Path #1's, Figure 8.4 (a), the perceived SI is lower, Figure 8.4 (b). The reduced SI indicates less stable vehicle due to the centrifugal force produced by the vehicle turn.

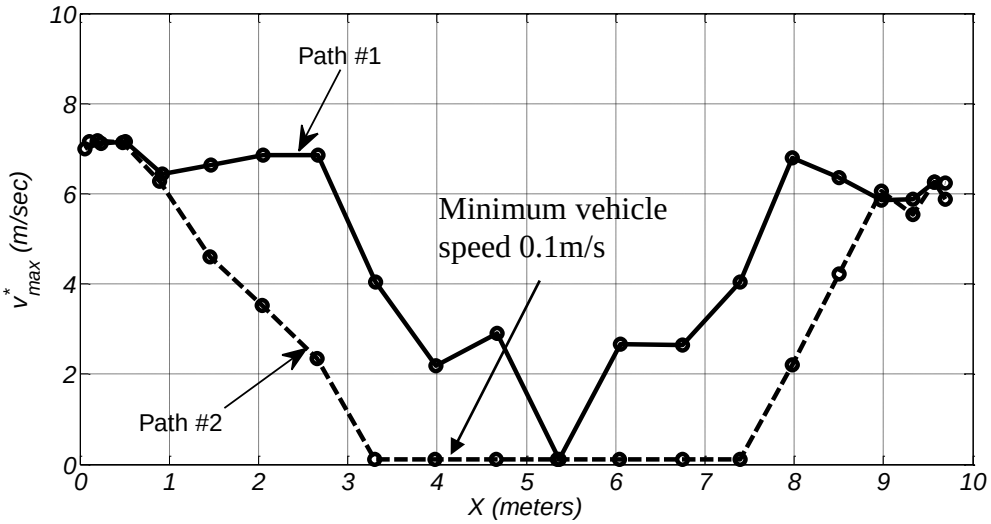

Figure 8.3 Calculated maximum allowable speed along a leveled terrain of different roughness's.

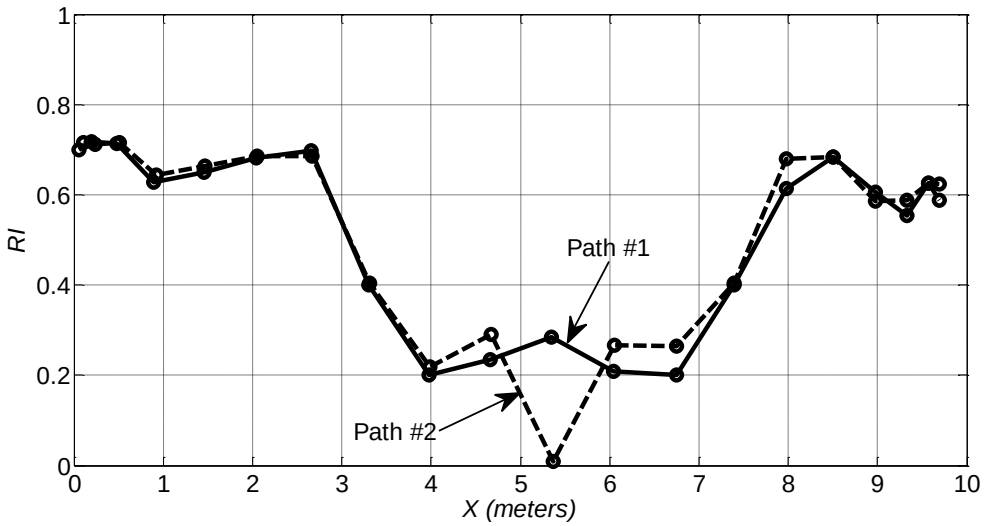

(a) Perceived RI

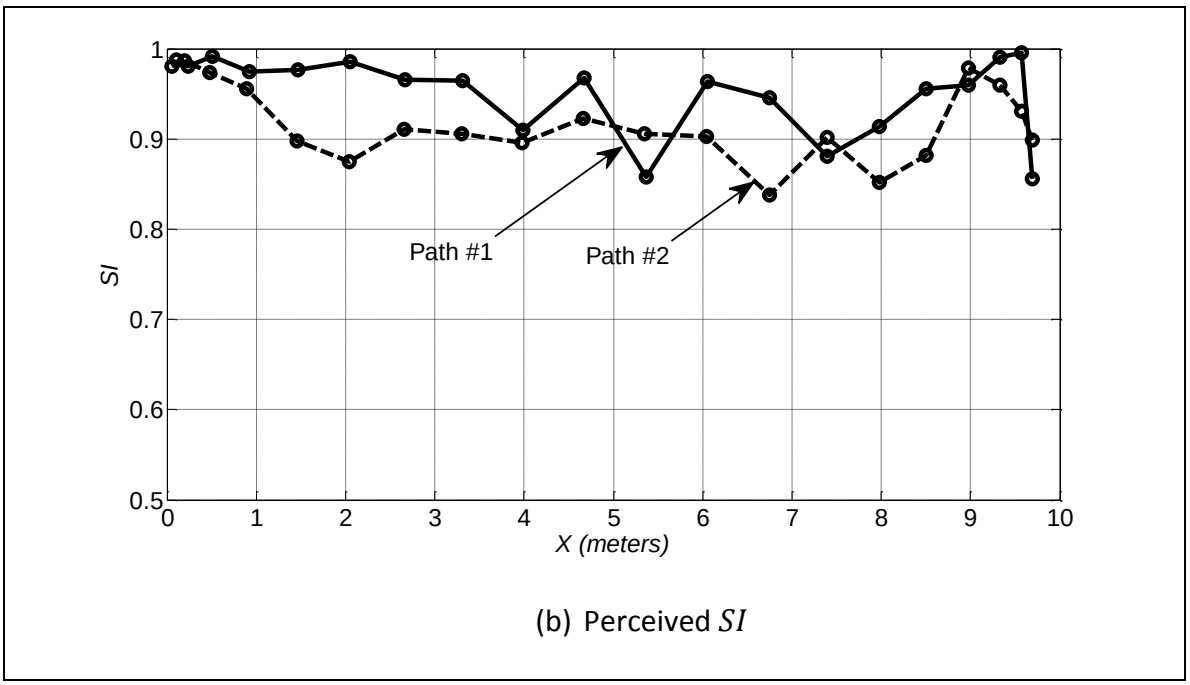

Figure 8.4 Perceived terrain characteristics along a leveled terrain of different roughness's.

8.1.2 Elevation transitions

One of the critical challenges facing an UGV is to detect and negotiate significant elevation transitions. In the 2nd illustrative example, the two smooth and leveled terrain regions having different elevations are considered. Each terrain can be traversed at high speed by the given UGV. However, the transition between the two regions needs to be traversed at a very low speed to avoid high impacts at each transition. In this section two terrain regions of 0.1 meters elevation difference are studied, Figure 8.5. This elevation difference is the maximum that the vehicle can negotiate as it is equal to the vehicle's ground clearance. Any larger elevation difference would be considered as an obstacle to be avoided not negotiated, Assumption 4 in Section 3.3. In this example, the UGV is commanded to traverse the terrain following a strain thine.

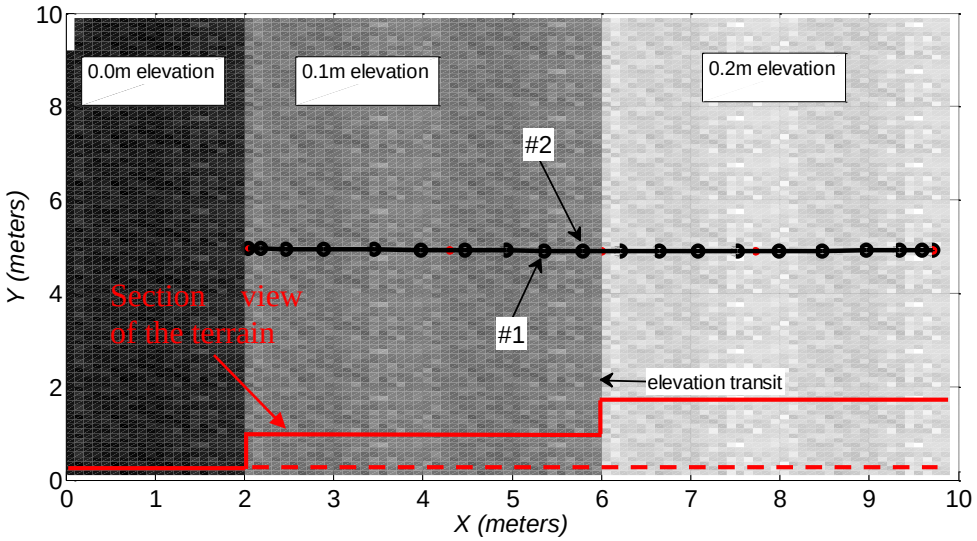

Figure 8.5 Leveled and smooth terrain regions at diffenete elevations.

Figure 8.6 shows the calculated speed profile for the straight path showed in Figure 8.5. The associated perceived *RI* and *SI* are shown in Figure 8.7 (a) and (b), respectively. The proposed terrain assessment module has indexes detected a reduced *RI* and *SI* at points #1 and #2, Figure 8.7. Accordingly, the calculated maximum allowable speed has dropped at points #1 and #2 Figure 8.6. at which points the detected terrain quality dropped, Figure 8.6. Although the terrain elevation transition has been detected and negotiated, the following issues are noted:

1. Human reaction in a similar scenario will be reducing the vehicle`s speed to the minimum in order to negotiate such a significant terrain elevation transition. The proposed terrain assessment technique does not interpret a terrain elevation transition. Instead, the system perceives the terrain points of different elevations, i.e. some points belong to a low terrain region and points belong to a high terrain region when the transition is sharp. The results (Fig. 8.6.) show that the demonstrated UGVs' performance could damage the vehicle or the cargo.

2. Simulation results show that the vehicle detected the transition at point #1 and #2 then started to accelerate before the vehicle actually reach the elevation transition. So, the vehicle traversed the actual elevation transition area at almost the full speed. This problem occurs because the proposed terrain assessment technique assesses the terrain region within the perception range in front of the vehicle. At points #1 and #2 the perceived terrain regions include the transition region. So, the interpreted terrain traversability (i.e., *RI* and *SI*) is reduced. Just before the vehicle hits the transition, the vehicle does not perceive the transition area and mainly perceives only the high terrain region. Accordingly, the perceived *RI* and *SI* are high and the calculated vehicle maximum allowable speed is high.

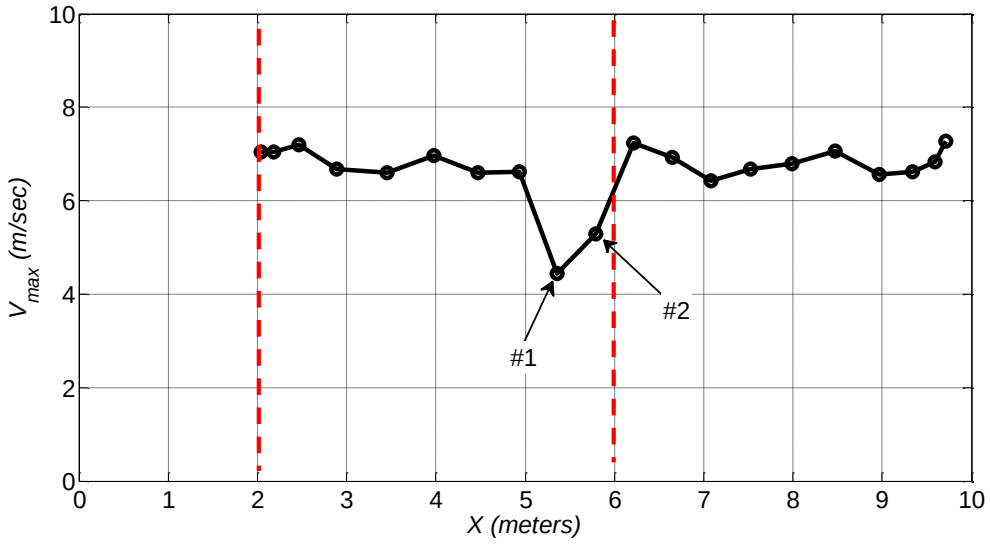

Figure 8.6 Calculated maximum allowable speed along leveled and smooth terrain regions of different elevations.

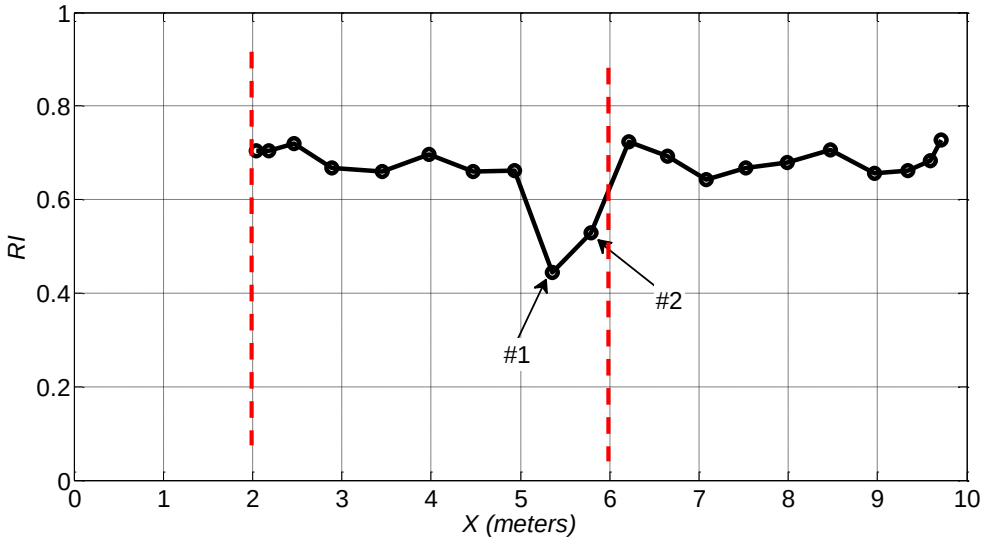

(a) Perceived RI

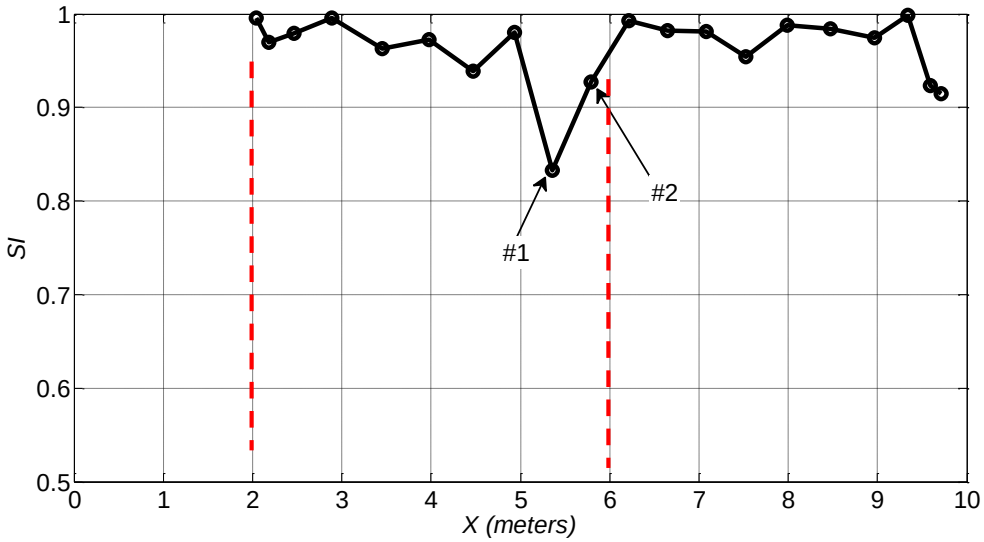

(b) Perceived SI

Figure 8.7 Perceived terrain characteristics along a leveled and smooth terrain of different elevations.

The limitations denoted in the proposed terrain assessment system can be dealt with as per application requirements. Dealing with these limitations is not addressed in this thesis. However, two general improvements are suggested:

1. A separate module for roughness, stability and elevation transition can be used based on the edge detection techniques in image processing.
2. A speed dependent delay can be used to calculate the maximum allowable speed corresponding to the terrain region being traversed, not the terrain region that the vehicle has not reached yet.

8.2 Path planning

The purpose of this section is to present examples that demonstrate the proposed terrain assessment system functioning as a module in a larger system. In this example, it is assumed that the terrain assessment module provides information to a path planning module to perform the task using the characteristics of the terrain. Accordingly, the path planning module finds the optimum path to the given destination. Path planning is a different application where a prior knowledge of the terrain is available but a path and speed profile needs to be calculated. In this example application, the proposed terrain assessment technique is implemented off-line to determine the best/optimum path between a start point and a destination point. A simple path planning module taken from the literature is used in this thesis to illustrate an application example of the proposed terrain assessment system. Given a 10mX10m terrain region, the path planning module finds path, that enables the UGV to reach its destination in the shortest amount of time, from a start point to a destination point. The provided path that the vehicle is commanded to is a 3^{rd} degree spline curve of four control points: start point, end point, and two control points along the path. A simple genetic algorithm is used to find the two middle control points, which determine the optimum path, [75].

Each control point consists of two coordinates, *x* and *y*. So, the chromosome`s length is four, two coordinates of each middle control point. The fitness function, which the genetic algorithm tries to minimize, is the time needed to complete the path from start point to destination, given the length of the path and the speed profile along it. Note that this simple genetic algorithm was only used in this paper for illustration purposes. In real applications, more sophisticated algorithms can be used. Details about the implementation of the Genetic Algorithm in Matlab are included in Appendix B: Matlab code for path planning and Genetic Algorithm.

The simplest case is to navigate a flat smooth horizontal terrain course. It is obvious that that the optimum path is a straight line from the start point to the destination point, Figure 8.8a. As the vehicle is moving straight on a flat smooth terrain (*SI*=1 and *RI*=1), the vehicle moves at full speed along the entire path, as seen in Figure 8.8b. The UGV user needs 1.33 seconds to reach the destination point. The vehicle is assumed to run at the maximum allowable speed of 10m/s. Acceleration and deceleration, at the beginning and end of the path, are considered to be instantaneous.

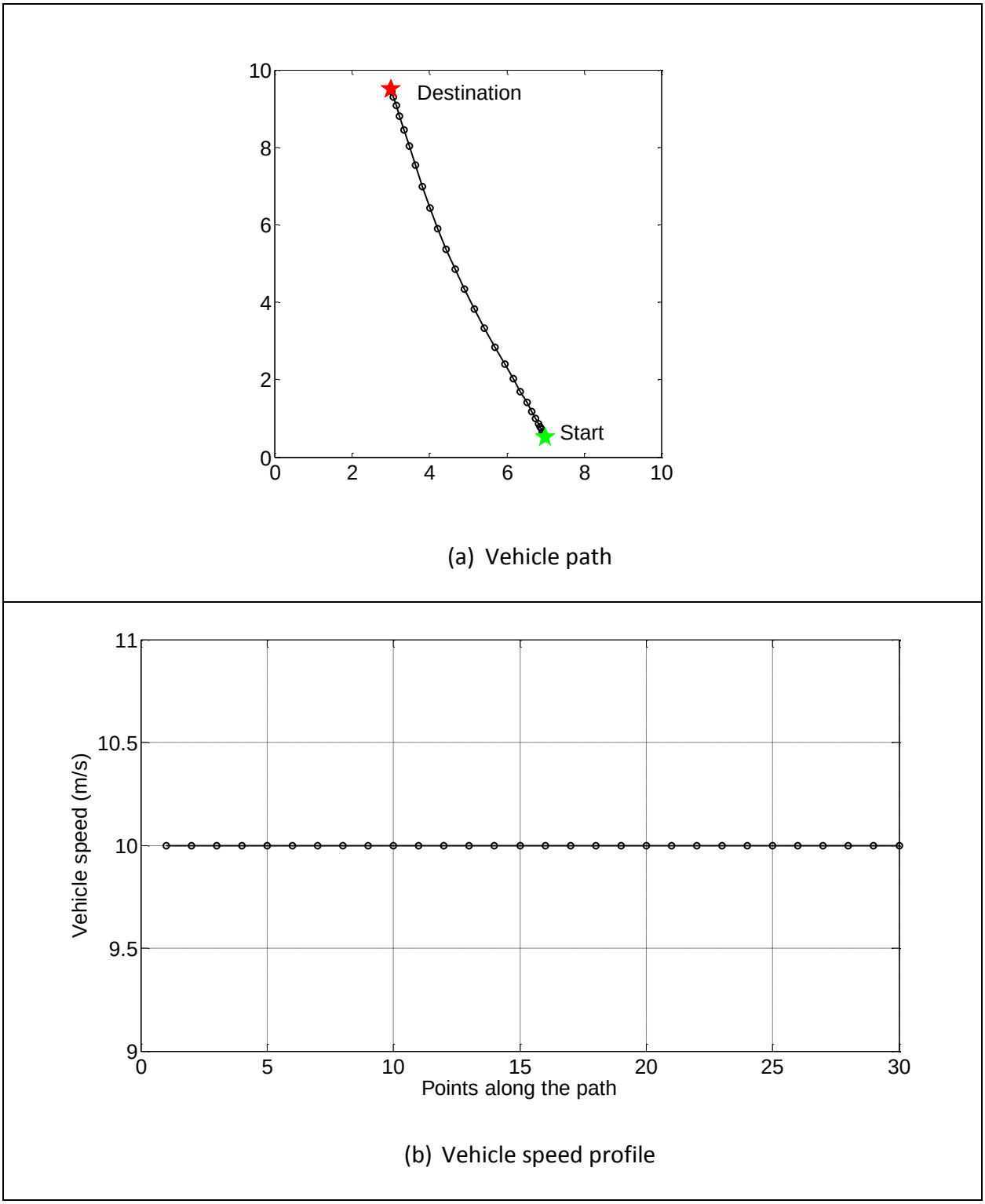

Figure 8.8: Path planning results for a perfect flat smooth terrain course. Ideal *RI* & *SI* values.

The vehicle is now subjected to a more challenging terrain course of identical dimensions but having two rough region areas, each one having *RI* at the value of *RI*=0. These two areas are indicated by the black areas in Figure 8.9 (a). Terrain roughness is represented in gray scale, where darker areas represent rougher terrain regions. Using the same simple path planning module used in the test described above (flat/smooth terrain), the optimum path is calculated. The calculated path avoids the first encountered rough region while maintaining the full vehicle speed. The vehicle slows down, to nearly zero m/s, while crossing the second rough terrain region, point "A" in Figure 8.9 (b). Under this new terrain, the UGV uses 17.76 seconds to reach the destination point.

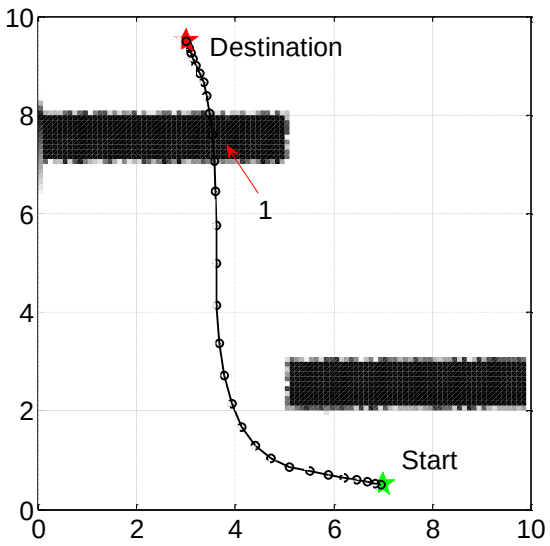

(a) Vehicle path

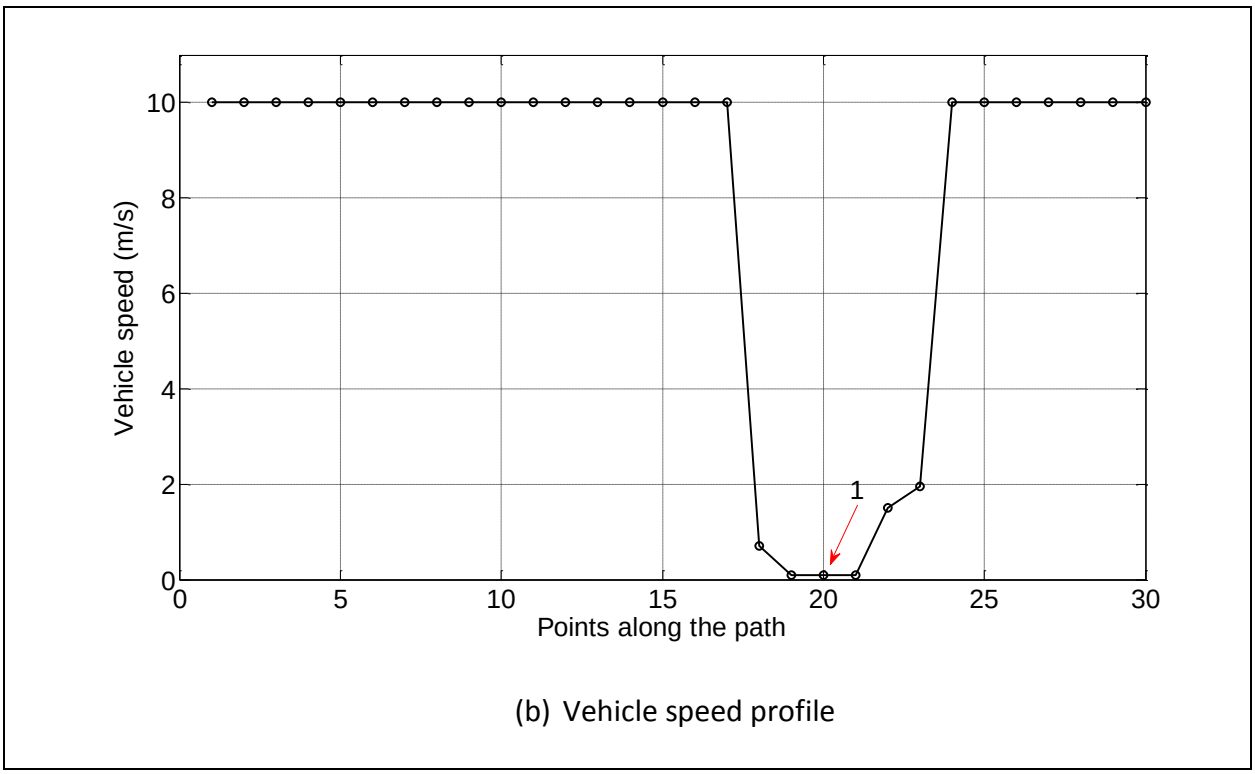

Figure 8.9: Path planning results for terrain course with super rough regions.

The third simulation run considers a terrain course which has rough and sloped regions simultaneously. The rough regions are exactly as in the previous simulation, Figure 8.9 (a). A general terrain slope geometry is superimposed on the roughness and represented by the contour plot in Figure 8.11(a), where blue contours represent low terrain regions and red contours represent high regions. The associated terrain profile, with no roughness, is illustrated in Figure 8.10. Simulation results for this run are illustrated in Figure 8.11. The corresponding points along the path are numbered on the path, Figure 8.11(a), and the speed profile, Figure 8.11(b). The generated optimum path goes straight avoiding the first encountered rough region. At Point (1) the speed has been reduced, to nearly zero m/s due to the steep slope going up the left side of the vehicle. The path continues straight while the UGV increases its speed until it reaches a flat horizontal region at Point (2) where the speed is reduced to anticipate the sharp right turn that the UGV will execute.

From that point, the path then heads straight to the target and speeds up. At Point (3) the speed decreases due to steep slope going down on the right side of the vehicle. Before the UGV reaches the second rough terrain, its the speed decreases again, to nearly zero m/s, then increases again before reaching the destination. From Figure 8.11(b) it can be observed that the path in this simulation is more likely to go straight due to the terrain slopes. The generated path needs 41.88 seconds to reach the destination point.

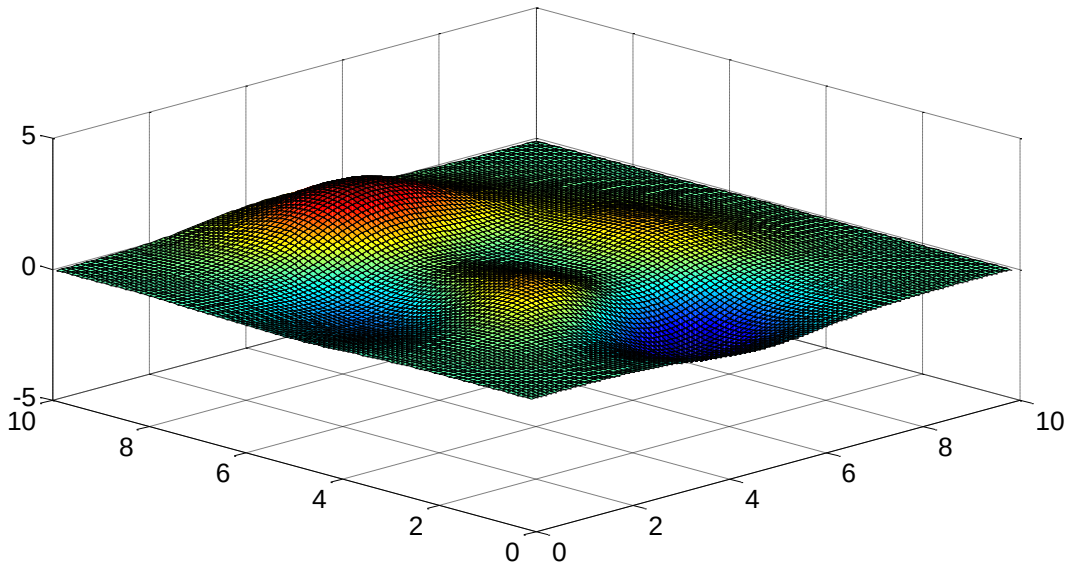

Figure 8.10: Path planning results for terrain course with super rough regions.

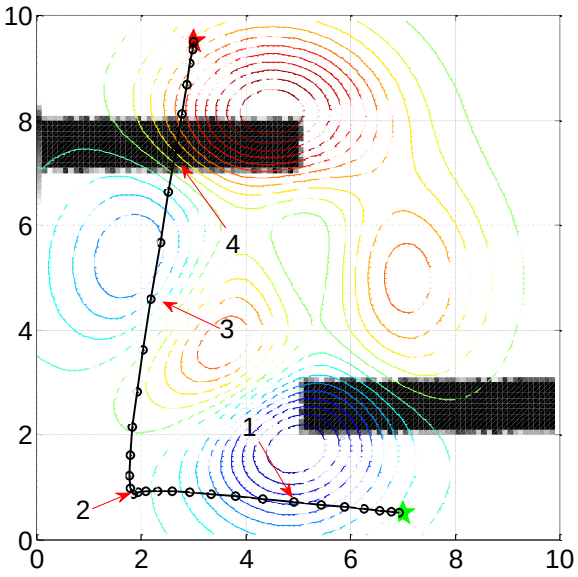

(a) Vehicle path

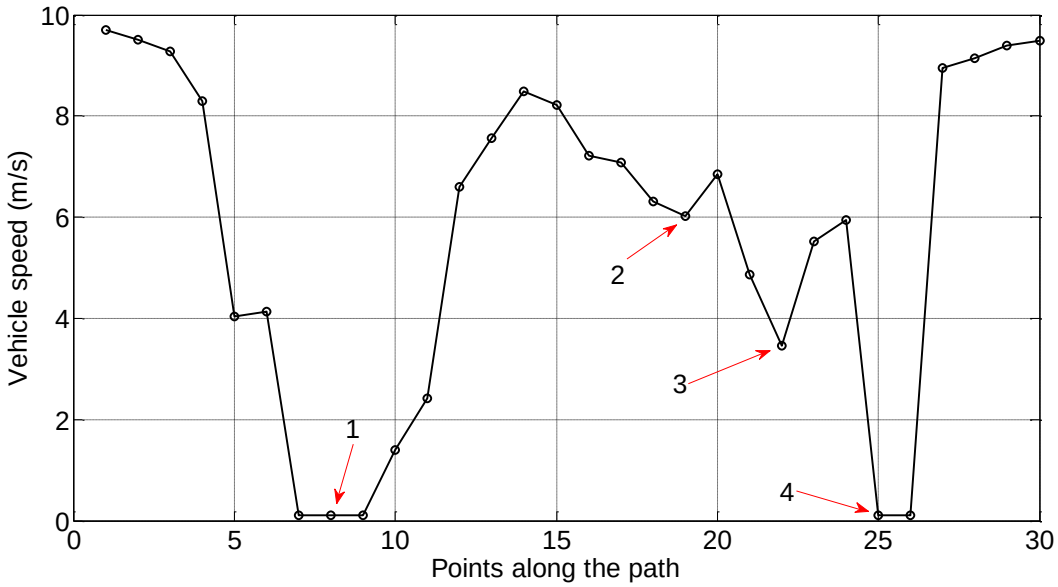

(b) Vehicle speed profile

Figure 8.11: Path planning results for terrain course with super rough regions.

8.3 Experimental test

The results presented in this thesis have been tested experimentally. G. Wilson and others, members of the Autonomous Reconfigurable Robotic Systems laboratory at the University of Calgary, implemented the proposed technique experimentally, [76]–[78]. The UGV used was a 4-wheeled UGV with independent suspension on each wheel, Figure 8.12.

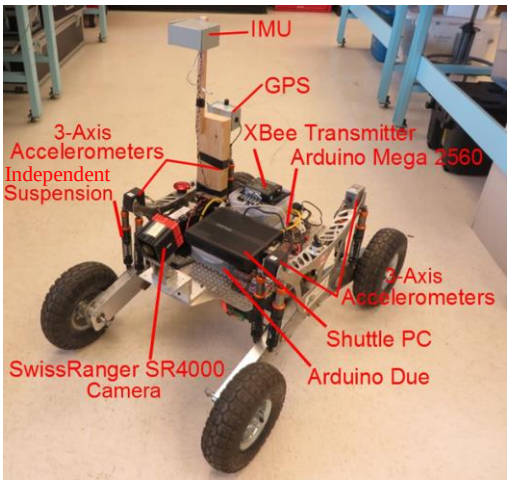

Figure 8.12 Experimental UGV [76]

The results of such work proved the applicability of the proposed technique. G. Wilson suggested three different methods of predicting the transmitted force: i) Instantaneous Elevation Change Model (IECM), ii) Sinusoidal Base Excitation Model – Excitation Force (SBEM.EF), and iii) Sinusoidal Base Excitation Model – Transmitted Force (SBEM.TF), all based on the concept first developed in this thesis. While this thesis assumes a random terrain profile, G. Wilson's proposed modified methods assume a terrain profile of sharp elevation change, IECM, and a terrain profile of sinusoidal shape, SBEM. Figure 8.13 shows a comparison between the predicted transmitted force using the technique proposed on this research work and the three alternative methods proposed by G. Wilson [76]. The tests also compared the measured transmitted force vs the predicted force. G. Wilson's simulations and experimental results show that the predicted

transmitted force proposed in this research document, and shown in Figure 8.13 using a black curve, is consistently higher than the measured force, black dots in Figure 8.13. The predicted transmitted force using two of G. Wilson's methods, IECM and SBEM.EF, are comparable to the force predicted using the technique proposed in this thesis. G. Wilson's SBEM.TF method yield an overly conservative prediction of the transmitted force. This indicates that the technique described in this thesis is consistently conservative and overall provides very good results. Results of G. Wilson's work shows that percentage of points where the measured force exceeds the predicted force using the proposed technique is less than 3%. The other three curves (red, green and blue) shown in Figure 8.13 show results generated with the modified approaches proposed by G. Wilson [76]. As can be inferred from Figure 8.13 the experimental results indicate that the mechanism can actually be used to drive UGVs and other vehicles (e.g., traditional manned automobiles) safely at high speeds over unknown rough terrains using diverse degrees of aggressiveness as demanded by the mission. The three top plots shown in Figure 8.13 represent the acceleration perceived by the accelerometer on the vehicle, the RI, and the speed at which the UGV maneuvered as it traversed the given rough terrain shown in Figure 8.14.

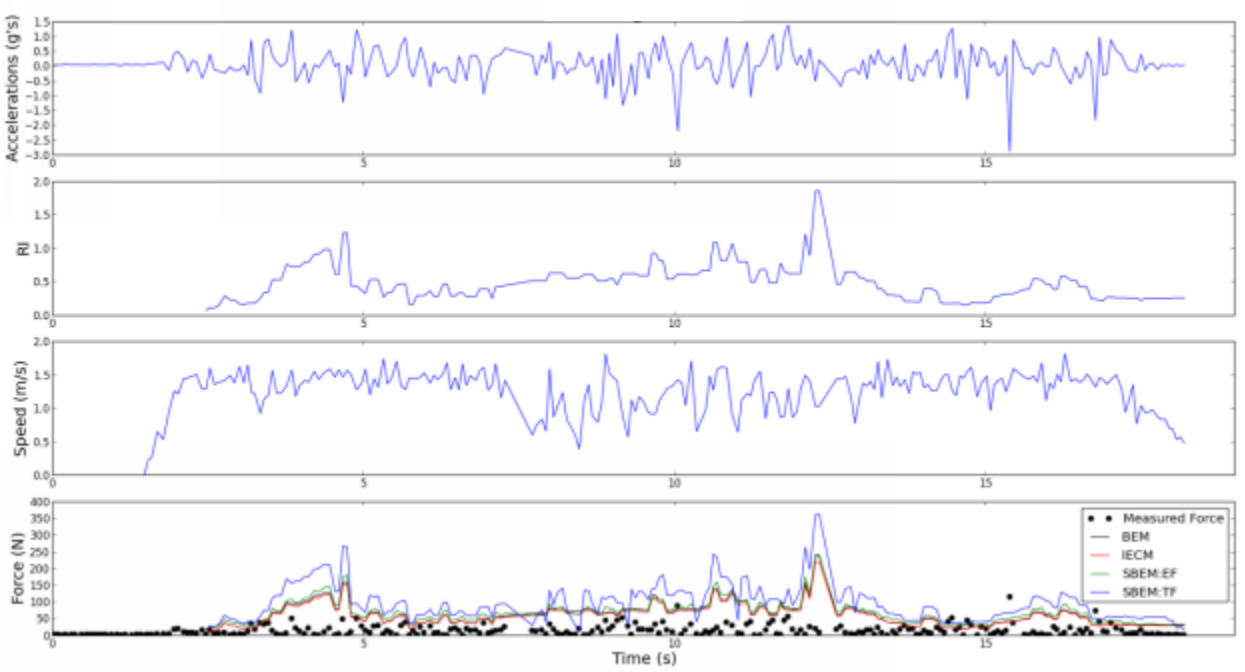

Figure 8.13 Comparison between measured and predicted forces transmitted to the frame of the UGV [76]

(a) Rough terrain with roots and trajectory of the UGV's center of mass (red curve).

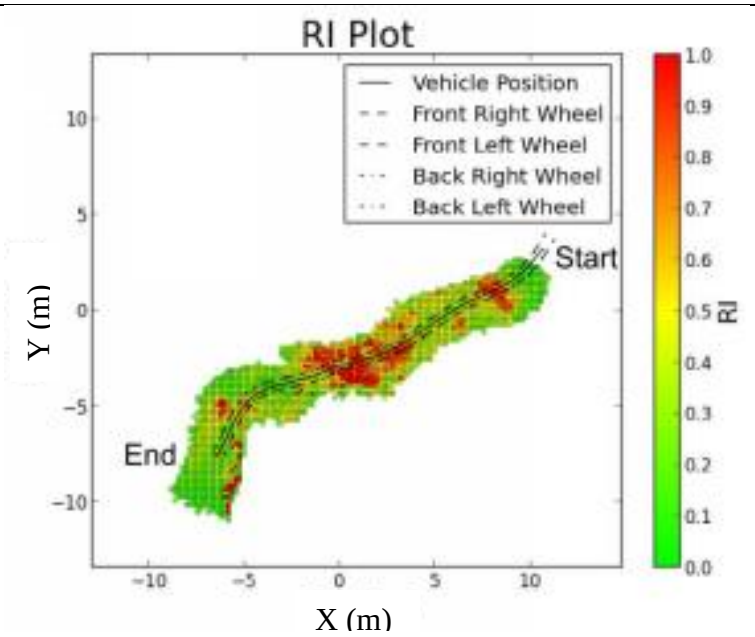

(b) RI determined by the UGV as it navigated the rough terrain.

Figure 8.14 Root traversal path example. By G. Wilson and others [76]

8.4 Summary

The proposed terrain assessment technique was developed to help the high speed UGV navigation system. It perceives the terrain, assess its traversability and provides the navigation system with indices, i.e., *RI* and *SI*, representing the terrain quality for driving on quantitatively. To illustrate the application of the proposed approach, this chapter presented the implementation of the proposed technique in two UGVs' navigation applications: i) speed planning and ii) path planning. A small four wheel vehicle was considered in these simulations.

In the speed planning application, the vehicle was given a certain path to follow. The on board navigation system, with the aid of the terrain assessment module, plans the vehicle speed as per the perceived terrain quality. Two speed planning simulations were presented in this chapter. The first simulation illustrated how the vehicle changes speed as it traverses a terrain of different

roughness. The second simulation showed how the vehicle negotiates a sharp transition in elevation, i.e., bump. The second simulation showed a limitation of the proposed technique when dealing with sharp elevation transitions. General improvements were suggested.

In the path planning application a prior knowledge of the terrain profile is available. The path planning module uses this knowledge to find the optimum path between two points. The optimization criteria used in this simulation is to minimize the travel time. Three path planning simulations were presented in this chapter. The first simulation is a path planning considering a flat smooth terrain. It produced a straight line between start and destination. The second simulation considered a terrain with rough and smooth regions. The generated path negotiated rough regions by turning around and changing speed. The third simulation challenged the terrain assessment by different roughness and slopes between start and destination. The generated path negotiated the terrain by turning and changing speed to reach destination in the shortest possible time.

This chapter presented examples on implementing the proposed terrain assessment module in real life applications. However, many developments are still needed to overcome its limitations. Future work/developments are discussed in the following chapter.

Chapter Nine: Conclusions

For many years, terrain assessment for UGVs has been approached from a data processing point of view. This trend has been driven by the dramatic developments of the perception systems, e.g., [15]–[18], and digital computers, e.g., [5]–[7]. While the research in the wheeled vehicle dynamics (automotive) has hugely progressed, [64], [65], [79], [80], dynamics of the UGVs remains barely investigated, [61]–[63]. This thesis offered a trial to cross the gap between the UGV terrain assessment and the dynamics of the wheeled vehicle. This thesis should open a whole new dimension of developing UGV terrain assessment systems.

This thesis proposed a novel terrain assessment technique that is based on an analytical analysis of the vehicle/terrain dynamic interaction. Only geometric characteristics: roughness and slope, of the terrain were addressed in this thesis. Two indices were developed in this thesis to assess the traversability of the terrain quantitatively: Roughness index (*RI*) and Stability Index (*SI*). Bothe indices are functions of: i) the terrain geometry, and ii) the vehicle properties. For example, a terrain region could be too rough for a sport car with a low ground clearance and soft suspension; the same terrain region could be smooth for an SUV with high ground clearance and tough suspension.

The thesis is divided into four parts.

1. Understanding the components of the vehicle and its characteristics (Chapter Four).
2. Roughness Index development and its applications (Chapters Five and Six).
3. Stability Index development and its applications (Chapter Seven).
4. Tests and simulations of the proposed terrain assessment system (Chapter Eight).

9.1 The Vehicle

The UGV, from a control system perspective, consists of:

1. Control system (i.e., the vehicle mass, structure, and actuators),
2. Controller, and
3. Sensors

The controller (i.e., computer) is out of the scope of this thesis. The thesis addressed: the sensor (sensing system) and the vehicle dynamic model.

It is vital to calculate the required resolution. Too much data will require more computational power to process. Too little data will provide insufficient information about the geometry of the terrain. The terrain assessment perceived the terrain as a cloud of points. This cloud of points can be obtained from stereo camera or range finder. The terrain profile was assumed a uniformly distributed 2D random function. So, theoretically, the terrain profile consists of the summation of an infinite number of harmonic components of the same amplitude and of frequencies ranges from zero to infinity. However, due to the finite size of the vehicle wheels, the vehicle will respond only to the components below certain frequency. To avoid aliasing, twice this frequency was considered a cut of frequency for terrain sensing. For simplification, the wheel diameter was considered equal to the vehicle ground clearance. The required perception resolution was analytically driven as a function of the vehicle ground clearance.

Understanding the dynamics of the vehicle is a key issue that was employed in the work presented through the thesis. The thesis presented a derivation of a simplified dynamic model of the vehicle. The amount of transmitted forces to the vehicle's structure was analytically driven as function of the terrain geometric profile and the vehicle characteristics. The vehicle dynamic model was used to calculate the vehicle's Eigen values (natural frequency) and Eigen vectors (mode shapes). The

expression of the transmitted forces was used to correlate the terrain roughness and the transmitted force analytically.

9.2 The Roughness Index (*RI*)

The *RI* concept is based on existing Geophysics techniques [69]. This thesis crosses the bridge between two different disciplines (i.e., Geophysics and UGV high speed navigations) to develop a novel terrain roughness index (*RI*). The terrain was perceived as a cloud of points collected via a 3D infrared camera. Only the elevation component of the points was used to calculate the *RI*. The *RI* expression was developed as a function of the followings.

1. The standard deviation of the points' elevation components of the points from the mean terrain level.
2. The vehicle characteristics.

Considering a small 4 wheels platform, the *RI* was calculated for several experimental terrain scans, asphalt, grass, and rocky terrains. The results showed consistency, where *RI* for smooth terrain (i.e., asphalt) was high, and for rough terrain, i.e., rocky, was low.

The thesis presented a derivation of the forces and moments transmitted to the frame of the vehicle due to a random excitation generated by the terrain roughness and speed of the vehicle. A closed form expression of the maximum allowable vehicle speed was developed. The core of this analysis is to limit the probability of exceeding a maximum allowable transmitted forces and moment to a certain level. Two applications of the proposed technique were presented:

1. The effect of a dramatic change of the terrain roughness (*RI*).
2. The effect of changing the vehicle's number of wheels on the vehicle maximum allowable speed.

Results showed that the proposed technique enabled the vehicle to detect terrain roughness transitions before it reached it. However, some limitations apply. Direct application to *RI* to traverse terrain roughness transitions leads to less than ideal speed profile. Limitations are left to be evaluated and adjusted for each application accordingly.

The proposed technique was applied on a real vehicle (military tank LEOPARD 1) to study the effects of the number of wheels. The results showed significant improvement of the vehicle capability of traversing rough terrain as the number of wheels increased. However, this improvement is limited by geometric constraints (limited space for wheels) and the vehicle maximum road speed. Results were consistent and reliable. The proposed technique can be used to optimize the number of wheels and type of suspension for off road vehicles.

9.3 The Stability Index (*SI*)

Vehicle stability is function of the following factors.

1. The terrain geometry.
2. Vehicle's characteristics.
3. Vehicle's state (e.g., speed and radius of turn).

Instead of assessing the slope of the terrain, the proposed technique assessed the stability of the vehicle. The advantage of this approach is taking into consideration the state of the vehicle. For example, a vehicle can roll over on a perfectly levelled terrain if it makes a very sharp turn at high speed. This thesis proposed a new index, Stability Index (*SI*), to represent the vehicle stability on a scale from zero (unstable vehicle) to one (perfectly stable vehicle). A closed form expression of *SI* was driven analytically. The *SI* expression was developed in a dimensionless form to generalize its application to any vehicle.

A small 4 wheeled vehicle was considered for simulation. The vehicle parameters (e.g., mass, elevation of centre of mass, geometry of platform, etc.) were assumed as known for a particular vehicle. The slope of the vehicle was obtained from the cloud of points representing the terrain by finding the best fitting plane. The state of the vehicle can be obtained from its sensors. Simulation results proved consistency of *SI* application results.

9.4 Terrain Assessment

The big picture is to put the proposed *RI* and *SI* into a terrain assessment module. Terrain assessment module shall provide the navigation system with the maximum allowable speed at a particular terrain. It perceives the terrain, and assesses its traversability quantitatively in terms of indices (i.e., RI and SI). Two UGVs' navigation applications were presented as examples of the possible implementations of the proposed system:

1. Speed planning, online.
2. Path planning, offline.

The applications were presented for demonstration only. Implementation of the proposed terrain assessment technique can widely vary according to the application. A small four wheel vehicle was considered in these simulations.

In the speed planning application, the navigation system is supposed to plane a speed profile along a pre-planned path. The terrain assessment module perceived the terrain as the vehicle progress on the path and planed the speed of the vehicle. Two speed planning simulations were presented. The first simulation illustrated how the vehicle changes speed as it traverses a terrain of different roughness transitions. The second simulation showed how the vehicle negotiates sharp transition in elevation, i.e., pump. It also showed that the proposed terrain assessment technique predicts the elevation transition. However the suggested speed profile was less than ideal. General

improvements were suggested; though the application should dictate the implementation of the proposed technique.

In the path planning application a prior knowledge of the terrain profile was available. The path planning module suggested the optimum path and speed profile based on the available information about the terrain and the vehicle. Path planning application is an example of offline implementations. The optimization criteria used in this simulation is to minimize the travel time. Three path planning simulations were presented.

Suggested optimum path between two points on a perfectly flat and smooth terrain were a straight line from start to destination. The second simulation assumed a terrain with rough and smooth regions. The suggested optimum path negotiated rough regions by turning around and changing speed. The third simulation was challenging a terrain of varying roughness and slopes between start and destination. The path negotiated the terrain by turning and changing speed to reach destination in the shortest possible time.

Presented applications showed consistent performance of the proposed terrain assessment module. Nevertheless, a lot of developments still needed depending on the application of the system.

9.5 Conclusion

The main component of the UGV system is the vehicle, which is a mechanical equipment that is automated via sensors, computers and actuators. The effect of the dynamics of this equipment on the performance of the UGV system has been remotely investigated in the literature. This thesis crossed the gap between UGV and automotive research fields and proposed a pioneer perspective of the UGV navigation and terrain assessment. The thesis proposed a novel terrain assessment technique that is generic, modular, and considers the vehicle characteristics as well as terrain geometric properties. Yet, the thesis did not offer a ready-to-use system. A lot of development is

still needed before the proposed system can be commercially/industrially applicable. The following are examples of the topics that need to be investigated, future work:

1. The thesis presented a simplified dynamic model for the vehicle. More sophisticated vehicle/suspension models can be imported from the automotive development literature. Integrating active/smart suspension systems and the proposed terrain assessment should be studied.
2. More terrain features and characteristics should be considered, e.g., terrain hardness, traction, etc.
3. In order to develop an applicable terrain assessment module, the proposed system should be integrated with other modules developed in the literature, e.g., obstacle avoidance, water hazards detection, etc.

References

[1] K. Demirli and M. Khoshnejad, "Autonomous parallel parking of a car-like mobile robot by a neuro-fuzzy sensor-based controller," *Fuzzy Sets Syst.*, vol. 160, no. 19, pp. 2876–2891, 2009.

[2] "Google tests driverless car," *Technol. Sci. - CBC News*, 2010.

[3] M. Holehouse, "Google's driverless cars to be allowed on roads after ministers rewrite Highway Code." [Online]. Available: http://www.telegraph.co.uk/motoring/news/10885236/Googles-driverless-cars-to-be-allowed-on-roads-after-ministers-rewrite-Highway-Code.html. [Accessed: 28-Jun-2014].

[4] J. Markoff, "Google Cars Drive Themselves, in Traffic," *New York Times*, 2010.

[5] D. F. Wolf, G. S. Sukhatme, D. Fox, and W. Burgard, "Autonomous terrain mapping and classification using hidden markov models," in *ICRA 2005. Proceedings of the 2005 IEEE International Conference on Robotics and Automation*, 2005, pp. 2026–2031.

[6] K. K. Gifford and R. R. Murphy, "Incorporating terrain uncertainties in autonomous vehicle path planning," 1996, vol. 3, pp. 1134–1140 vol. 3.

[7] N. Vandapel, D. F. Huber, A. Kapuria, and M. Hebert, "Natural terrain classification using 3-d ladar data," in *IEEE International Conference on Robotics and Automation*, 2004, vol. 5, pp. 5117–5122.

[8] Q. Zhuang, J. E. Gayko, and M. Kreutz, "Optimization of a fuzzy controller for a driver assistant system," *Fuzzy-Neuro Syst. 98-Computational Intell.*, p. 376, 1998.

[9] D. Kim, S. M. Oh, and J. M. Rehg, "Traversability classification for ugv navigation: A comparison of patch and superpixel representations," in *Proc. Int. Conf. Intelligent Robots and Systems*, 2007.

[10] D. Langer, J. K. Rosenblatt, and M. Hebert, "A behavior-based system for off-road navigation," *IEEE Trans. Robot. Autom.*, vol. 10, no. 6, pp. 776–783, 1994.

[11] K.-H. Chen and W.-H. Tsai, "Vision-based obstacle detection and avoidance for autonomous land vehicle navigation in outdoor roads," *Autom. Constr.*, vol. 10, no. 1, pp. 1–25, 2000.

[12] Y. Yoon, J. Shin, H. J. Kim, Y. Park, and S. Sastry, "Model-predictive active steering and obstacle avoidance for autonomous ground vehicles," *Control Eng. Pract.*, vol. 17, no. 7, pp. 741–750, 2009.

[13] A. Kelly and A. Stentz, “Rough terrain autonomous mobility—part 2: An active vision, predictive control approach,” *Auton. Robots*, vol. 5, no. 2, pp. 163–198, 1998.

[14] Y. Niwa, S. Yukita, and H. Hanaizumi, “Depthmap-based obstacle avoidance on rough terrain,” in *2004 IEEE/RSJ International Conference on Intelligent Robots and Systems (IROS) (IEEE Cat. No.04CH37566)*, vol. 2, pp. 1612–1617.

[15] I. R. Nourbakhsh, D. Andre, C. Tomasi, and M. R. Genesereth, “Mobile robot obstacle avoidance via depth from focus,” *Rob. Auton. Syst.*, vol. 22, no. 2, pp. 151–158, 1997.

[16] A. Huertas, L. Matthies, and A. Rankin, “Stereo-based tree traversability analysis for autonomous off-road navigation,” in *2005 Seventh IEEE Workshops on Applications of Computer Vision (WACV/MOTION’05)*, 2005, vol. vol.1, p. 8 pp.

[17] Y.-D. T. Yang Cong, Jun-Jian Peng, Jing Sun, Lin-Lin Zhu, “V-disparity Based UGV Obstacle Detection in Rough Outdoor Terrain,” *Acta Autom. Sin.*, vol. 36, no. 5, pp. 673–667, 2010.

[18] M. . Larson, Jacoby, “Off-road Obstacle Classification and Traversability Analysis in the Presence of Negative Obstacles,” vol. MAI 49/06, Dec. 2011.

[19] L. Matthies, P. Bellutta, and M. McHenry, “Detecting water hazards for autonomous off-road navigation,” in *Proceedings of the SPIE - The International Society for Optical Engineering*, 2003, 1st ed., vol. 5083, pp. 231–242.

[20] A. Angelova, L. Matthies, D. Helmick, and P. Perona, “Learning and prediction of slip from visual information,” *J. F. Robot.*, vol. 24, no. 3, pp. 205–231, 2007.

[21] O. Khatib, “Real-time obstacle avoidance for manipulators and mobile robots,” *Int. J. Rob. Res.*, vol. 5, no. 1, p. 90, 1986.

[22] H. Haddad, M. Khatib, S. Lacroix, and R. Chatila, “Reactive navigation in outdoor environments using potential fields,” 1998, vol. 2, pp. 1232–1237 vol. 2.

[23] Z.-Q. Ma and Z.-R. Yuan, “Real-time navigation and obstacle avoidance based on grids method for fast mobile robots,” *Eng. Appl. Artif. Intell.*, vol. 8, no. 1, pp. 91–95, 1995.

[24] P. Reignier, “Fuzzy logic techniques for mobile robot obstacle avoidance,” *Rob. Auton. Syst.*, vol. 12, no. 3–4, pp. 143–153, 1994.

[25] S. Thrun, M. Montemerlo, H. Dahlkamp, D. Stavens, A. Aron, J. Diebel, P. Fong, J. Gale, M. Halpenny, G. Hoffmann, K. Lau, C. Oakley, M. Palatucci, V. Pratt, P. Stang, S. Strohband, C. Dupont, L.-E. Jendrossek, C. Koelen, C. Markey, C. Rummel, J. van Niekerk, E. Jensen, P. Alessandrini, G. Bradski, B. Davies, S. Ettinger, A. Kaehler, A. Nefian, and

P. Mahoney, “Stanley: The robot that won the DARPA Grand Challenge,” *J. F. Robot.*, vol. 23, no. 9, pp. 661–692, 2006.

[26] D. M. Helmick, A. Angelova, M. Livianu, and L. H. Matthies, “Terrain adaptive navigation for Mars rovers,” in *2007 IEEE Aerospace Conference*, 2007, pp. 1–11.

[27] M. Sonka, V. Hlavac, and R. Boyle, *Image Processing, Analysis, and Machine Vision*, vol. 3. PWS Publishing, 2007, p. 800.

[28] M. Hebert, N. Vandapel, S. Keller, and R. R. Donamukkala, “Evaluation and comparison of terrain classification techniques from LADAR data for autonomous navigation,” in *23rd Army Science Conference*, 2002.

[29] G.-Y. Sung, D.-M. Kwak, and J. Lyou, “Neural Network Based Terrain Classification Using Wavelet Features,” *J. Intell. Robot. Syst.*, vol. 59, no. 3–4, pp. 269–281, Feb. 2010.

[30] T. Y. Kim, G. Y. Sung, and J. Lyou, “Robust terrain classification by introducing environmental sensors,” in *2010 IEEE Safety Security and Rescue Robotics*, 2010, pp. 1–6.

[31] A. Rankin, A. Huertas, L. Matthies, M. Bajracharya, C. Assad, S. Brennan, P. Bellutta, O. G. Drive, and G. W. Sherwin, “Unmanned ground vehicle perception using thermal infrared cameras,” *SPIE*, vol. 8045, no. 818, 2011.

[32] D. Sadhukhan, C. Moore, and E. Collins, “Terrain estimation using internal sensors,” in *Proceedings of the IASTED International Conference on Robotics and Applications*, 2004, pp. 195–199.

[33] E. M. DuPont, R. G. Roberts, M. F. Selekwa, C. A. Moore, and E. G. Collins, “Online terrain classification for mobile robots,” 2005.

[34] A. Angelova, L. Matthias, D. Helmick, G. Sibley, and P. Perona, “Learning to predict slip for ground robots,” 2006, vol. 2006, pp. 3324–3331.

[35] A. Angelova, L. Matthies, D. Helmick, and P. Perona, “Dimensionality reduction using automatic supervision for vision-based terrain learning,” *Proc. Robot. Sci. Syst. (RSS), Atlanta, GA (p29). Cambridge, MA MIT Press*, 2007.

[36] R. Manduchi, A. Castano, A. Talukder, and L. Matthies, “Obstacle detection and terrain classification for autonomous off-road navigation,” *Auton. Robots*, vol. 18, no. 1, pp. 81–102, 2005.

[37] H. Seraji, “Traversability index: a new concept for planetary rovers,” in *Proceedings 1999 IEEE International Conference on Robotics and Automation (Cat. No.99CH36288C)*, 1999, vol. vol.3, pp. 2006–2013.

[38] A. Howard and H. Seraji, “Real-time assessment of terrain traversability for autonomous rover navigation,” in *IEEE International Conference on Intelligent Robots and Systems*, 2000, vol. 1, pp. 58–63.

[39] A. Howard and H. Seraji, “Vision-based terrain characterization and traversability assessment,” *J. Robot. Syst.*, vol. 18, no. 10, pp. 577–587, 2001.

[40] A. Howard, H. Seraji, and E. Tunstel, “A rule-based fuzzy traversability index for mobile robot navigation,” in *Proceedings 2001 ICRA. IEEE International Conference on Robotics and Automation (Cat. No.01CH37164)*, 2001, vol. vol.3, pp. 3067–3071.

[41] H. Seraji and A. Howard, “Behavior-based robot navigation on challenging terrain: A fuzzy logic approach,” *IEEE Trans. Robot. Autom.*, vol. 18, no. 3, pp. 308–321, 2002.

[42] E. Tunstel, A. Howard, and H. Seraji, “Fuzzy rule-based reasoning for rover safety and survivability,” in *Proceedings 2001 ICRA. IEEE International Conference on Robotics and Automation (Cat. No.01CH37164)*, 2001, vol. vol.2, pp. 1413–1420.

[43] M. Tarokh, “Hybrid intelligent path planning for articulated rovers in rough terrain,” *Fuzzy Sets Syst.*, vol. 159, no. 21, pp. 2927–2937, 2008.

[44] K. Iagnemma, H. Shibly, and S. Dubowsky, “On-line terrain parameter estimation for planetary rovers,” 2002, vol. vol.3, pp. 3142–3147.

[45] P. F. Muir and C. P. Neuman, “Kinematic modeling of wheeled mobile robots,” *J. Robot. Syst.*, vol. 4, no. 2, pp. 281–340, Apr. 1987.

[46] N. Sarkar and V. Kumar, “Control of Mechanical Systems With Rolling Constraints: Application to Dynamic Control of Mobile Robots,” *Int. J. Rob. Res.*, vol. 13, no. 1, pp. 55–69, Feb. 1994.

[47] J. P. Laumond, *Robot motion planning and control*. Springer, 1998.

[48] A. G. O. Mutambara and H. E. Durrant-Whyte, “Estimation and control for a modular wheeled mobile robot,” *IEEE Trans. Control Syst. Technol.*, vol. 8, no. 1, pp. 35–46, 2000.

[49] C. Milesi-Bellier, C. Laugier, and B. Faverjon, “A kinematic simulator for motion planning of a mobile robot on a terrain,” *Proc. 1993 IEEE/RSJ Int. Conf. Intell. Robot. Syst. (IROS ’93)*, vol. 1, no. C, pp. 339–344, 1993.

[50] S. V. Sreenivasan and K. J. Waldron, “Displacement Analysis of an Actively Articulated Wheeled Vehicle Configuration With Extensions to Motion Planning on Uneven Terrain,” *J. Mech. Des.*, vol. 118, no. 2, pp. 312–317, Jun. 1996.

[51] S. V. Sreenivasan and P. Nanua, “Kinematic Geometry of Wheeled Vehicle Systems,” *J. Mech. Des.*, vol. 121, no. 1, pp. 50–56, Mar. 1999.

[52] B. L. Gajjar and R. W. Johnson, “Kinematic modeling of terrain adapting wheeled mobile robot for Mars exploration,” 2002, pp. 291–296.

[53] V. Kumar and K. J. Waldron, “Actively coordinated vehicle systems,” *J. Mech. Transm. Autom. Des.*, vol. 111, no. 2, pp. 223–231, 1989.

[54] V. Kumar and K. J. Waldron, “Force distribution in walking vehicles,” *J. Mech. Des.*, vol. 112, p. 90, 1990.

[55] K. Iagnemma and S. Dubowsky, *Mobile robots in rough terrain*. Springer, 2004.

[56] J. E. Chottiner, “Simulation of a six wheeled martian rover called the rocker bogie,” 1992.

[57] A. El-Kabbany and A. Ramirez-Serrano, “TERRAIN ROUGHNESS ASSESSMENT FOR HIGH SPEED UGV NAVIGATION IN UNKNOWN HETEROGENEOUS TERRAINS,” *Int. J. Inf. Acquis.*, vol. 7, no. 2, pp. 165–176, 2010.

[58] A. Talukder, R. Manduchi, R. Castano, K. Owens, L. Matthies, A. Castano, and R. Hogg, “Autonomous terrain characterisation and modelling for dynamic control of unmanned vehicles,” 2002, pp. 708–713.

[59] K. Iagnemma and S. Dubowsky, “Terrain estimation for high-speed rough-terrain autonomous vehicle navigation,” 2002, vol. 4715, pp. 256–266.

[60] K. Iagnemma, C. Brooks, and S. Dubowsky, “Visual, tactile, and vibration-based terrain analysis for planetary rovers,” 2004, vol. 2.

[61] C. Brooks, K. Iagnemma, and S. Dubowsky, “Vibration-based terrain analysis for mobile robots,” 2005, vol. 2005, pp. 3415–3420.

[62] E. G. Collins and E. J. Coyle, “Vibration-based terrain classification using surface profile input frequency responses,” in *IEEE International Conference on Robotics and Automation, 2008. ICRA 2008*, 2008, pp. 3276–3283.

[63] E. Coyle, E. G. Collins Jr., E. DuPont, D. Dan, W. Hongwu, R. A. Cooper, and G. Grindle, “Vibration-based terrain classification for electric powered wheelchairs,” 2008, pp. 139–144.

[64] K. Singal and R. Rajamani, “Simulation Study of a Novel Self-Powered Active Suspension System for Automobiles,” in *2011 American Control Conference*, 2011, pp. 3332–3337.

[65] L. Wang, W. Zhang, G. Cao, T. Chen, and X. Wang, "A Study of EPS Control Strategy Based on Multibody Dynamics," *Adv. Sci. Lett.*, vol. 4, pp. 2911–2915, 2011.

[66] N. J. Nilsson, "Shakey the Robot," *Sci. Technol.*, no. April, p. 150, 1984.

[67] J. Y. Wong, *Theory of ground vehicles*. Wiley-Interscience, 2001.

[68] W. Thomson, *Theory of Vibration with Applications*. Taylor & Francis, 2004, p. 560.

[69] M. K. Shepard, B. A. Campbell, M. H. Bulmer, T. G. Farr, L. R. Gaddis, and J. J. Plaut, "The roughness of natural terrain: A planetary and remote sensing perspective," *J. Geophys. Res.*, vol. 106, no. E12, 2001.

[70] B.-C. Chen and H. Peng, "ROLLOVER PREVENTION FOR SPORTS UTILITY VEHICLES WITH HUMAN-IN-THE-LOOP EVALUATIONS Bo-Chiuan Chen 1 , Huei Peng 2 IRul „" in *Proceedings of AVEC 2000, 5th Inernational Symposium on Advanced Vehicle Control*, 2000.

[71] T. Chou and T.-W. Chu, "An improvement in rollover detection of articulated vehicles using the grey system theory," *Veh. Syst. Dyn.*, pp. 1–25, Feb. 2014.

[72] J. Yoon, D. Kim, and K. Yi, "Design of a rollover index-based vehicle stability control scheme," *Vehicle System Dynamics*, vol. 45, no. 5. pp. 459–475, 2007.

[73] J. Y. J. Yoon and K. Y. K. Yi, "A rollover mitigation control scheme based on rollover index," *2006 Am. Control Conf.*, 2006.

[74] S. Solmaz, M. Corless, and R. Shorten, "A methodology for the design of robust rollover prevention controllers for automotive vehicles: Part 2-Active steering," *2007 Am. Control Conf.*, 2007.

[75] S. N. Sicanandam and S. N. Deepa, *Introduction to Genetic Algorithms*, 1st ed. Springer Publishing Company, 2007.

[76] G. . Wilson, "High Speed Navigation of UGVs in Rough Unknown Terrains," Master of Science Thesis. Mechanical and Manufacturing Engineering, University of Calgary, 2013.

[77] G. N. Wilson, A. Ramirez-Serrano, M. Mustafa, and K. A. Davies, "Velocity Selection for High-Speed UGVs in Rough Unknown Terrains Using Force Predictions," in *Proceedings 5th International Conference on Intelligent Robotics and Applications*, 2012, pp. 387–396.

[78] G. N. Wilson and A. Ramirez-Serrano, "Terrain Roughness Identification for High-Speed UGVs," in *Proceedings of International Conference of Control, Dynamic Systems, and Robotics*, 2013.

[79] G. Verros, S. Natsiavas, and C. Papadimitriou, “Design optimization of quarter-car models with passive and semi-active suspensions under random road excitation,” *J. Vib. Control*, vol. 11, no. 5, pp. 581–606, 2005.

[80] N. Al-Holou, J. M. Weaver, T. Lahdhiri, and F. Al-Abbas, “Nonlinear modeling of vehicle suspension system,” in *Proceedings of the 2000 American Control Conference. ACC (IEEE Cat. No.00CH36334)*, vol. 1, pp. 115–119.

Appendix A: Matlab code to calculate vehicle desired speed profile

```
function [x CRI v v1 TimeRatio Prb, Prb1] = SpeedPlanning(c,dt)
%% SpeedPlanning
% Generates a desired speed profile pf the UGV as the vehicle traverse the
% terrain.

%% Syntax
% [RI v] = SpeedPlanning(c, w, l, v_max, N, dt)

%% Description
% [RI v] = SpeedPlanning(T, c, VAR, v_max, dt) returns an n length vector
% RI (Roughness Index) of each terrain region the UGV is traversing and an
% n length vector of the desired vehicle speed as it go. The input
% arguments are:
% T, the terrain points.
% c, the UGV ground clearance.
% VAR, the Vehicle Aspect Ratio.
% v_max, the vehicle maximum speed.
% dt, the sampling period.

%% Simulation
load terrain;
T = Terrain;
R = 1.27; Fall = 50; P = 0.9999;
x(1) = 0; i = 1;
while x<=max(T(1,:))-1
    PT = T(:, find(T(1,:)>=x(i) & T(1,:)<=x(i)+1));
    index = randperm(length(PT));
    PT1 = PT(:,index(1:10));
    CT = T(:, find(T(1,:)>=floor(x(i)/2)*2 &
T(1,:)<=ceil((x(i)+0.001)/2)*2));
    CRI(i) = 1-2*std(CT(3,:)/c);
    tic
    PRI(i) = 1-2*std(PT(3,:)/c);
    t(i) = toc;
    tic
    PRI1(i)= 1-2*std(PT1(3,:)/c);
    t1(i) = toc;
    v(i) = sqrt(3/R^2*(2*Fall^2/(1-PRI(i))^2/erfinv(P)^2-1))*c;
    v1(i)= sqrt(3/R^2*(2*Fall^2/(1-PRI1(i))^2/erfinv(P)^2-1))*c;
    x(i+1) = x(i)+v(i)*dt;
    Var_F(i) = (1/4)*(1-CRI(i))^2*((1/3)*R^2*(v(i)/c)^2+1);
    Prb(i) = normcdf(Fall,0,sqrt(Var_F(i)))-normcdf(-Fall,0,sqrt(Var_F(i)));
    Var_F1(i) = (1/4)*(1-CRI(i))^2*((1/3)*R^2*(v1(i)/c)^2+1);
    Prb1(i) = normcdf(Fall,0,sqrt(Var_F1(i)))-normcdf(-
Fall,0,sqrt(Var_F1(i)));
    i = i+1;
end
TimeRatio = mean(t1)/mean(t);
v1 = smooth(v1);
```

Appendix B: Matlab code for path planning and Genetic Algorithm

The genetic algorithm parameters are:

1. number of generations used is 20,
2. population size is 10,
3. mutation function is “Adaptive Feasible” which randomly generates directions that are adaptive with respect to the last successful or unsuccessful generation, and
4. crossover function is “Scattered” which creates a random binary vector and selects the genes where the vector is a 1 from the first parent, and the genes where the vector is a 0 from the second parent, and combines the genes to form the child.

```
clear

%% Declaration
global Terrain V StartPoint EndPoint
%% Data
% loads a pre-constructed terrain.
[FileName,PathName] = uigetfile('*.mat','Select the terrain file');
load(FileName)

% Read vehicle data
V = ReadVehicle;

% Start and end points
StartPoint  = [7.0; 0.5];
EndPoint    = [3.0; 9.5];

%% Path planning
options = gaoptimset(@ga);
options.PopulationSize = 10;
options.PopInitRange = [1.0;9.0];
options.Generations = 30;
options.MutationFcn = @mutationadaptfeasible;
options.PlotFcns = @gaplotbestf;
[path, Time] = ga(@PathTime, 4, [], [], [], [], 1.0*ones(1,2), 9.0*ones(1,2),
[], options);

%% Terrain display

%% Path plot

% cp = [StartPoint reshape(path,2,length(path)/2) EndPoint];
% p = spcrv([cp(:,1), cp, cp(:,end)],3, 20);
```

```
% p = p(:,2:end-1);
% figure(2)
% subplot(1,2,1)
% hold on; grid on; axis([0 10 0 10]);
% plot(p(1,:), p(2,:), 'b-o', 'LineWidth', 2)
% plot(cp(1,:), cp(2,:), 'ro')
[Time v] = FinalSpeedProfile(path);
% subplot(1,2,2)
% plot(v, '-o')

PlotFlatAndSmooth
```